ERDC/GSL TR-07-24

US Army Corps
of Engineers®
Engineer Research and
Development Center

Laboratory Characterization of Solid Grade SW Brick

Erin M. Williams, Stephen A. Akers, and Paul A. Reed

August 2007

Geotechnical and Structures Laboratory

ERDC/GSL TR-07-24
August 2007

Laboratory Characterization of Solid Grade SW Brick

Erin M. Williams, Stephen A. Akers, and Paul A. Reed

Geotechnical and Structures Laboratory
U.S. Army Engineer Research and Development Center
3909 Halls Ferry Road
Vicksburg, MS 39180-6199

Final report
Approved for public release; distribution is unlimited.

Prepared for Headquarters, U.S. Army Corps of Engineers
Washington, DC 20314-1000

Under Hardened Combined Effects Penetrator Warheads Work Package
Work Unit No. OP003, Material Properties of Urban Materials

Abstract: Personnel of the Geotechnical and Structures Laboratory, U.S. Army Engineer Research and Development Center, conducted a laboratory investigation to characterize the strength and constitutive property behavior of solid Grade SW brick. A total of 37 mechanical property tests were successfully completed, consisting of two hydrostatic compression tests, four unconfined compression (UC) tests, 12 triaxial compression tests (TXC), two constant mean normal stress tests, four direct pull (DP) tests, two uniaxial strain tests, four uniaxial strain load/biaxial strain unload (UX/BX) tests, five uniaxial strain load/constant volume strain loading (UX/CV) tests, and two uniaxial strain load/constant strain path (UX/SP) tests. In addition to the mechanical property tests, nondestructive pulse-velocity measurements were performed on each specimen. Results from the TXC tests exhibited a continuous increase in principal stress difference with increasing confining stress. A compression failure surface was developed from the TXC results at six levels of confining pressure and from the results of the UC tests. The results for the DP tests were used to evaluate the tensile strength of the brick. During UX/BX tests, stress relaxation was evident during the change from uniaxial strain loading to biaxial strain unloading. Good correlations were observed between the stress paths obtained from the UX/BX, UX/CV, and UX/SP strain path tests and the failure surface developed from the TXC tests.

Contents

List of Figures

Preface

This laboratory mechanical property investigation of solid Grade SW brick was conducted by personnel of the U.S. Army Engineer Research and Development Center (ERDC). The study was conducted with funds provided by the Directorate of Military Programs, Headquarters, U.S. Army Corps of Engineers, under the Research, Development, Test, and Evaluation (RDT&E) Program. The investigation reported herein was accomplished under the Military RDT&E Work Package OP003, Hardened Combined Effects Penetrator Warheads; Work Unit, Material Properties of Urban Materials.

This study was conducted between July and August 2005 by staff members of the Impact and Explosion Effects Branch (IEEB), Engineering Systems and Materials Division (ESMD), Geotechnical and Structures Laboratory (GSL), ERDC, under the general direction of Henry S. McDevitt Jr., Chief, IEEB. At the time of report publication, Dr. Larry N. Lynch was Chief, ESMD; Dr. William P. Grogan was Deputy Directory, GSL; and Dr. David W. Pittman was Director, GSL.

The principal investigator for this project was Dr. Stephen A. Akers, IEEB. Material property data were processed and analyzed by Erin M. Williams, IEEB, co-investigator for this project. The laboratory characterization tests were performed by Paul A. Reed, IEEB, under the technical direction of Dr. Akers. Instrumentation support was provided by Johnny L. Morrow, Engineering and Informatic Systems Division, Information Technology Laboratory, ERDC. This report was prepared by Erin Williams, under the direction of Dr. Akers.

COL Richard B. Jenkins was Commander and Executive Director of ERDC. Dr. James R. Houston was Director.

1 Introduction

Background

Personnel of the Geotechnical and Structures Laboratory, U.S. Army Engineer Research and Development Center (ERDC) conducted a laboratory investigation to characterize the strength and constitutive property behavior of solid Grade SW Brick for the Material Properties of Urban Materials Work Unit of the AT40-WP-248A Hardened Combined Effects Penetrator Warheads Work Package. A total of 41 mechanical property tests were conducted, of which 37 were successfully completed. The 37 tests consisted of two hydrostatic compression tests, four unconfined compression tests, 12 triaxial compression tests, two constant mean normal stress tests, four direct pull tests, two uniaxial strain tests, four uniaxial strain load/biaxial strain unload tests, five uniaxial strain load/constant volume strain loading tests, and two uniaxial strain load/constant strain path tests. In addition to the mechanical property tests, nondestructive pulse-velocity measurements were performed on each specimen.

Purpose and Scope

The purpose of this report is to document the results from the laboratory mechanical property tests and the nondestructive pulse-velocity measurements conducted on the brick specimens. The physical and composition properties, test procedures, and test results are documented in Chapter 2. Comparative plots and analyses of the experimental results are presented in Chapter 3. A summary is provided in Chapter 4.

2 Laboratory Tests

Material Description

The test specimens used in this investigation were prepared from samples cored from solid Grade SW brick with dimensions of 64 mm by 102 mm by 203 mm. Half-scale solid Grade SW brick was manufactured by the same company and were used in penetration experiments conducted at ERDC. The material properties determined from the characterization of the material will be used in numerical simulations of the penetration tests.

Composition Property Tests

Prior to performing the mechanical property tests, the height, diameter, and weight of each test specimen were determined. These measurements were used to compute the specimen's wet, bulk, or "as-tested" density. Results from these determinations are provided in Table 1. Measurements of posttest water content[1] were conducted in accordance with procedures given in American Society for Testing and Materials (ASTM) D 2216 (ASTM 2002e). Based on the appropriate values of posttest water content, wet density, and an assumed grain density of 2.25 Mg/m^3, values of dry density, porosity, degree of saturation, and volumes of air, water, and solids were calculated (Table 1). Also listed in the table are maximum, minimum, and mean values and the standard deviation about the mean for each quantity. The brick specimens had a mean wet density of 1.987 Mg/m^3, a mean water content of 0.04 percent, and a mean dry density of 1.986 Mg/m^3.

Ultrasonic Pulse-Velocity Determinations

Prior to performing a mechanical property test, ultrasonic pulse-velocity measurements were collected on each test specimen. This involved measuring the transit distance and time for each compressional (P) or shear (S) pulse to propagate through a given specimen. The velocity was then computed by dividing the transit distance by the transit time. A matching pair of 1-MHz piezoelectric transducers was used to transmit and receive the ultrasonic P waves. A pair of 2.25-

[1] Water content is defined as the weight of water (removed during drying in a standard oven) divided by the weight of dry solids.

MHz piezoelectric transducers was used to transmit and receive the ultrasonic S waves. The transit time was measured with a 100-MHz digital oscilloscope and the transit distance with a digital micrometer. All of these wave-velocity determinations were made under atmospheric conditions, i.e., no prestress of any kind was applied to the specimens. The tests were conducted in accordance with procedures given in ASTM C 597 (ASTM 2002c).

One compressional-wave (P-wave) and one shear-wave (S-wave) velocity were determined axially through each specimen. Radial P- and S-wave velocities were determined for each specimen in the following manner. Six radial P-wave velocities were determined, i.e., two transverse to each other at elevations of 1/4, 1/2, and 3/4 of the specimen height. Two radial S-wave velocities were measured; these determinations were made transverse to each other at the mid-height of the specimen. The various P- and S-wave velocities determined for the test specimens are provided in Table 1; the radial-wave velocities listed in Table 1 are the average values.

Mechanical Property Tests

Thirty-seven mechanical property tests were successfully performed on the brick specimens to characterize the strength and constitutive properties of the material. All of the mechanical property tests were conducted quasi-statically with axial strain rates on the order of 10^{-4} to 10^{-5} per second and times to peak load on the order of 5 to 30 min. Mechanical property data were obtained under several different stress and strain paths. Undrained compressibility data were obtained during the hydrostatic loading phases of the triaxial compression (TXC) tests and from two hydrostatic compression (HC) tests. Shear and failure data were obtained from unconfined compression (UC) tests, unconsolidated-undrained TXC tests, unconsolidated-undrained constant mean normal stress (CMNS) tests, and from direct pull (DP) tests. One-dimensional compressibility data were obtained from undrained uniaxial strain (UX) tests with lateral stress measurements or K_0 tests. Three types of undrained strain-path tests were conducted during the test program. All of the strain-path tests were initially loaded under uniaxial strain boundary conditions to a prescribed level of stress or strain. At the end of the UX loading, constant axial to radial strain ratios (ARSR) of 0, -1.33, and -2.0 were applied. The ARSR = 0 path is a constant axial strain unloading path and produces a forced state of volumetric expansion; these tests will be referred to as UX/BX tests. The UX/SP tests have an ARSR = -1.33. The ARSR = -2.0 path is a constant volume strain loading path, and these paths will be referred to as UX/CV tests. The terms undrained and unconsolidated signify that no pore fluid (liquid or gas) was allowed to escape or drain from the membrane-enclosed specimens. The completed test matrix is presented in Table 2, which lists the types of tests conducted, the number of tests, the test numbers for each group, the test numbers of the specimens that had cyclic unloading/reloading, and the nominal peak radial stress applied to specimens prior to shear loading or during the HC, UX, or strain-path loading.

Specimen preparation

The mechanical property test specimens were cut from sections of brick using a diamond-bit core barrel by following the procedures provided in ASTM C 42 (ASTM 2002b). The test specimens were cut to the correct length, and the ends were ground flat and parallel to each other and perpendicular to the sides of the core in accordance with procedures in ASTM D 4543 (ASTM 2002f). Prior to testing, the prepared specimens were measured for height, diameter, and weight and were ultrasonically pulsed. This information was used to calculate the composition properties and wave velocities of the specimens. The prepared test specimens had a nominal height of 110 mm and a nominal diameter of 50 mm.

Prior to testing, each specimen was placed between hardened steel top and base caps. With the exception of the UC and DP test specimens, two 0.6-mm-thick synthetic latex membranes and an Aqua seal® membrane were placed around the specimen, and the exterior of the outside membrane was coated with a liquid synthetic rubber to inhibit deterioration caused by the confining-pressure fluid (Figure 1). The fluid was a mixture of kerosene and hydraulic oil. Finally, the specimen, along with its top cap and base cap assembly, was placed on the instrumentation stand of the test apparatus, and the instrumentation setup was initiated.

Test devices

Three different sets of test devices were used in this test program. The axial load for all of the UC tests were provided by a 3.3-MN (750,000-lb force) loader. The application of load was manually controlled with this test device. No pressure vessel was required for the UC tests; only a base, load cell, and vertical and radial deformeters were necessary.

Direct pull tests were performed by using the direct pull apparatus, in which end caps were attached to the specimens with a high-modulus high-strength epoxy. A manual hydraulic pump was used to pressurize the direct pull chamber. When the direct pull chamber was pressurized, a piston retracted and produced tensile loading on the test specimen. Measurements of the tensile loading on the specimen were recorded with an 89-KN load cell.

All of the remaining tests were conducted in a 600-MPa-capacity pressure vessel (Figure 2), and the axial load was provided by an 8.9-MN loader. With the 8.9-MN loader, the application of load, pressure, and axial displacement was regulated by a servo-controlled data acquisition system. This servo-controlled system allowed the user to program rates of load, pressure, and axial displacement in order to achieve the desired stress or strain path. Confining pressure was measured external to the pressure vessel by a pressure transducer mounted in the confining fluid line. A load cell mounted in the base of the specimen pedestal was used to measure the applied axial loads inside the pressure vessel (Figure 1).

Outputs from the various instrumentation sensors were electronically amplified and filtered, and the conditioned signals were recorded by computer-controlled 16-bit analog-to-digital converters. The data acquisition systems were

programmed to sample the data channels every 1 to 5 seconds. The data acquisition systems then convert the measured voltages to engineering units and store the data for further posttest processing.

Test instrumentation

The vertical deflection measurement system in all the test areas except the DP test area consisted of two linear variable differential transformers (LVDTs) mounted vertically on the instrumentation stands and positioned 180 degrees apart. They were oriented to measure the displacement between the top and base caps, thus providing a measure of the axial deformations of the specimen. For the confined tests, a linear potentiometer was mounted external to the pressure vessel so as to measure the displacement of the piston through which axial loads were applied. This provided a backup to the vertical LVDTs in case they exceeded their calibrated range.

Two types of radial deflection measurement systems (lateral deformeters) were used in this test program. The output of each deformeter was calibrated to the radial displacement of the two footings that were glued to the sides of the test specimen (Figure 1). These two small steel footings were mounted 180 degrees apart at the specimen's mid-height. The footing faces were machined to match the curvature of the test specimen. A threaded post extended from the outside of each footing and protruded through the membrane. The footings must be mounted to the specimen prior to placement of the membrane. Once the membranes were in place, steel caps were screwed onto the threaded posts to seal the membrane to the footing. The lateral deformeter ring was attached to these steel caps with set-screws. The completed specimen lateral deformeter setup is shown in Figure 3.

One type of lateral deformeter consisted of an LVDT mounted on a hinged ring; the LVDT measured the expansion or contraction of the ring. This lateral deformeter was used over smaller ranges of radial deformation when the greatest measurement accuracy was required. This lateral deformeter was used for all of the HC, UC, UX, and strain-path tests and for the TXC tests at confining pressures less than 100 MPa. This design is similar to the radial-deformeter design provided by Bishop and Henkel (1962). When the specimen expanded (or contracted), the hinged-deformeter ring opened up (or closed) causing a change in the electrical output of the horizontally mounted LVDT.

The second type of lateral deformeter, which was used for all of the TXC tests at confining pressures of 100 MPa and greater, consisted of two strain-gauged spring-steel arms mounted on a double-hinged ring; the strain-gauged arms deflected as the ring expanded or contracted. This lateral deformeter was used when the greatest radial deformation range was required and, therefore, was less accurate than the LVDT deformeter. With this deformeter, when the specimen expanded or contracted, the rigid deformeter ring flexed about its hinge causing a change in the electrical output of the strain-gauged spring-arm. The output of the spring-arms was calibrated to the specimen's deformation. Radial measurements were not performed during the DP tests.

Test descriptions

The UC and TXC tests were performed in accordance with ASTM C 39 (ASTM 2002a) and ASTM C 801 (ASTM 2002d), respectively. A TXC test was conducted in two phases. During the first phase, the hydrostatic compression phase, the cylindrical test specimen was subjected to an increase in hydrostatic pressure while measurements of the specimen's height and diameter changes were made. The data are typically plotted as pressure versus volumetric strain, the slope of which, assuming elastic theory, is the bulk modulus, *K*. The second phase of the TXC test, the shear phase, was conducted after the desired confining pressure was applied during the HC phase. While holding the desired confining pressure constant, axial load was increased, and measurements of the changes in the specimen's height and diameter were made. The axial (compressive) load was increased until the specimen failed. The shear data are generally plotted as principal stress difference versus axial strain, the slope of which represents Young's modulus, *E*. The peak strength of the specimen is defined as the maximum principal stress difference that a given specimen can support or the principal stress difference at 15 percent axial strain during the shear loading, whichever occurs first.

Note that the UC test is a TXC test in which no confining pressure is applied. The maximum principal stress difference observed during a UC test is defined as the unconfined compressive strength of the material.

Extension data were obtained for brick by performing four DP tests. The DP tests have no confining pressure during the tests. To conduct the DP tests, end caps are attached with epoxy to the specimen. The end caps are screwed into the direct pull apparatus, and the specimen is pulled apart axially when pressure is applied to the piston. Strain gauges are attached to the specimen to measure the axial strain until the specimen fails.

A UX test was conducted by applying an axial load and confining pressure simultaneously so that, as the cylindrical specimen shortened, its diameter remained unchanged, i.e., zero radial strain boundary conditions were maintained. The data are generally plotted as axial stress versus axial strain, the slope of which is the constrained modulus, *M*. The data are also plotted as principal stress difference versus mean normal stress, the slope of which is twice the shear modulus *G* divided by the bulk modulus *K*, i.e., *2G/K*, or, in terms of Poisson's ratio ν, $3(1-2\nu)/(1+\nu)$.

The strain-path tests in this test program were conducted in two phases. Initially, the specimen was subjected to a uniaxial-strain loading up to a desired level of mean normal, radial, or axial stress. At the end of the UX loading, constant axial-to-radial-strain ratios of 0, -1.33, or -2.0 were applied; these tests were identified earlier as UX/BX, UX/SP, and UX/CV tests, respectively. To conduct these tests, the software controlling the servo-controls had to correct the measured inputs for system compressibility and for the nonlinear calibrations of specific transducers.

Definition of stresses and strains

During the mechanical property tests, measurements were typically made of the axial and radial deformations of the specimen as confining pressure and/or axial load was applied or removed. These measurements along with the pretest measurements of the initial height and diameter of the specimen were used to convert the measured test data to true stresses and engineering strains.[1]

Axial strain, ε_a, was computed by dividing the measured axial deformation, Δh (change in height), by the original height h_o, i.e., $\varepsilon_a = \Delta h/h_o$. Similarly, radial strain, ε_r, was computed by dividing the measured radial deformation, Δd (change in diameter), by the original diameter d_o, i.e., $\varepsilon_r = \Delta d/d_o$. For this report, volumetric strain was assumed to be the sum of the axial strain and twice the radial strain, $\varepsilon_v = \varepsilon_a + 2\varepsilon_r$.

The principal stress difference, q, was calculated by dividing the axial load by the cross-sectional area of the specimen A, which is equal to the original cross-sectional area, A_o, multiplied by $(1 - \varepsilon_r)^2$. In equation form,

$$q = (\sigma_a - \sigma_r) = \frac{\text{Axial Load}}{A_o(1-\varepsilon_r)^2} \tag{1}$$

where σ_a is the axial stress and σ_r is the radial stress. The axial stress is related to the confining pressure and the principal stress difference by

$$\sigma_a = q + \sigma_r \tag{2}$$

The mean normal stress, p, is the average of the applied principal stresses. In cylindrical geometry,

$$p = \frac{(\sigma_a + 2\sigma_r)}{3} \tag{3}$$

Results

Results from all of the mechanical property tests, except from the direct pull tests, are presented in Plates 1-33. One data plate is presented for each test with reliable results. Results from the HC tests are presented on the plates in four plots, i.e., (a) mean normal stress versus volumetric strain, (b) mean normal stress versus axial strain, (c) radial versus axial strain, and (d) mean normal stress versus radial strain. Each plate for the UC, TXC, CMNS, UX, and strain-path tests displays four plots, i.e., (a) principal stress difference versus mean normal stress, (b) principal stress difference versus axial strain, (c) volumetric strain versus mean normal stress, and (d) volumetric strain versus axial strain.

[1] Compressive stresses and strains are positive in this report.

Table 1
Physical and Composition Properties of Solid Grade SW Brick Test Specimens

Test Number	Type of Test	Plate No.	Wet Density Mg/m^3	Posttest Water Content %	Dry Density Mg/m^3	Porosity %	Degree of Saturation %	Volume of Air %	Volume of Water %	Volume of Solids %	Axial P-Wave Velocity km/s	Radial P-Wave Velocity km/s	Axial S-Wave Velocity km/s	Radial S-Wave Velocity km/s
01	UC	3	1.967	0.05	1.966	12.62	0.78	12.52	0.10	87.38	3.14	3.10	2.13	2.11
02	UC	4	2.009	0.06	2.008	10.75	1.12	10.63	0.12	89.25	3.25	3.16	2.18	2.19
03	UC	5	1.991	0.06	1.989	11.58	1.03	11.46	0.12	88.42	3.01	3.06	2.06	2.11
04	UC	6	1.974	0.06	1.973	12.33	0.96	12.21	0.12	87.67	2.94	3.01	2.02	1.95
06	HC	1	1.984	0.05	1.983	11.87	0.84	11.77	0.10	88.13	3.00	3.06	2.04	2.04
07	UX	21	1.997	0.01	1.997	11.25	0.18	11.23	0.02	88.75	3.16	3.05	2.12	2.10
08	UX	22	1.985	0.03	1.985	11.79	0.51	11.73	0.06	88.21	3.03	3.10	2.05	1.97
09	TXC/10	7	1.990								3.09	3.05	2.10	2.11
10	TXC/10	8	1.978	0.05	1.977	12.12	0.82	12.02	0.10	87.88	3.01	3.00	2.04	1.91
11	TXC/20	9	1.990	0.05	1.989	11.60	0.86	11.50	0.10	88.40	3.08	3.10	2.07	2.00
12	TXC/20	10	1.985	0.05	1.984	11.81	0.84	11.71	0.10	88.19	3.07	3.11	2.09	1.95
13	TXC/50	11	1.967	0.04	1.966	12.61	0.62	12.53	0.08	87.39	2.95	2.97	2.07	2.06
14	TXC/50	12	1.990	0.05	1.989	11.58	0.86	11.48	0.10	88.42	4.26	3.11	2.11	2.06
15	TXC/200	15	1.981	0.00	1.981	11.96	0.00	11.96	0.00	88.04	3.00	2.96	2.03	2.02
16	TXC/100	13	2.000	0.03	1.999	11.14	0.54	11.08	0.06	88.86	3.10	3.08	2.11	2.03
17	TXC/100	14	1.985	0.04	1.984	11.82	0.67	11.74	0.08	88.18	3.04	3.09	2.09	1.97
18	TXC/200	16	2.002	0.01	2.002	11.02	0.18	11.00	0.02	88.98	3.10	3.05	2.09	2.00
20	TXC/300	17	1.975	0.00	1.975	12.23	0.00	12.23	0.00	87.77	2.92	2.99	2.01	2.04
22	HC	2	1.985	0.05	1.984	11.83	0.84	11.73	0.10	88.17	3.03	3.12	2.08	2.08
23	UX/BX	23	1.991	0.04	1.990	11.56	0.69	11.48	0.08	88.44	3.02	3.14	2.06	1.97
24	UX/BX	24	1.991	0.04	1.990	11.57	0.69	11.49	0.08	88.43		2.99	2.05	2.03
25	UX/BX	25	1.982	0.05	1.981	11.95	0.83	11.85	0.10	88.05	3.15	3.09	2.04	1.94
26	UX/BX	26	1.985	0.05	1.984	11.84	0.84	11.74	0.10	88.16	3.12	2.99	2.13	2.13
27	UX/CV	27	1.998	0.02	1.998	11.20	0.36	11.16	0.04	88.80	3.01	3.05	2.05	2.02

Continued

Table 1 (concluded)

Test Number	Type of Test	Plate No.	Wet Density Mg/m^3	Posttest Water Content %	Dry Density Mg/m^3	Porosity %	Degree of Saturation %	Volume of Air %	Volume of Water %	Volume of Solids %	Axial P-Wave Velocity km/s	Radial P-Wave Velocity km/s	Axial S-Wave Velocity km/s	Radial S-Wave Velocity km/s
28	UX/CV	28	1.977	0.03	1.977	12.15	0.49	12.09	0.06	87.85	3.02	3.01	2.07	2.07
29	UX/CV	29	1.978	0.03	1.977	12.12	0.49	12.06	0.06	87.88	2.86	3.02	1.99	1.91
31	UX/CV	30	1.985	0.03	1.984	11.82	0.50	11.76	0.06	88.18	3.04	2.95	2.02	2.05
32	UX/CV	31	2.004	0.02	2.004	10.93	0.37	10.89	0.04	89.07	3.11	3.07	2.09	2.13
33	UX/SP	32	2.009	0.04	2.008	10.74	0.75	10.66	0.08	89.26	3.27	3.10	2.15	2.08
34	UX/SP	33	1.983	0.04	1.983	11.88	0.67	11.80	0.08	88.12	3.11	2.93	2.08	2.05
35	TXC/300	18	1.948	0.00	1.948	13.43	0.03	13.43	0.00	86.57	2.69	2.80	1.89	1.96
36	DP	--	1.987	0.05	1.986	11.71	0.85	11.61	0.10	88.29	3.04	3.12	2.09	2.07
37	DP	--	1.988	0.05	1.987	11.71	0.85	11.61	0.10	88.29	3.06	3.03	2.06	1.93
38	DP	--	1.994	0.06	1.992	11.45	0.96	11.34	0.11	88.55	3.02	3.06	2.03	1.94
39	DP	--	1.998	0.05	1.997	11.26	0.89	11.16	0.10	88.74	3.08	3.12	2.09	2.09
40	CMNS	19	1.992	0.05	1.991	11.50	0.87	11.40	0.10	88.50	3.15	2.98	2.09	1.95
41	CMNS	20	1.988	0.05	1.987	11.68	0.85	11.58	0.10	88.32	2.98	3.08	2.05	1.89
N			37	36	36	36	36	36	36	36	36	37	37	37
Mean			1.987	0.04	1.986	11.73	0.66	11.66	0.08	88.27	3.08	3.05	2.07	2.03
Stdv			0.012	0.017	0.012	0.539	0.295	0.545	0.034	0.539	0.226	0.072	0.050	0.072
Max			2.009	0.06	2.008	13.43	1.12	13.43	0.12	89.26	4.26	3.16	2.18	2.19
Min			1.948	0.00	1.948	10.74	0.00	10.63	0.00	86.57	2.69	2.80	1.89	1.89

Table 2
Completed Solid Grade SW Brick Test Matrix

Type of Test	No. of Tests	Test Nos.	Test Nos. with Unloading/ Reloading Cycles	Nominal Peak Radial Stress, MPa
Hydrostatic Compression	2	06, 22	06	500
Triaxial Compression	4	01-04		0
	2	09, 10	10	10
	2	11, 12	12	20
	2	13, 14	14	50
	2	16, 17	17	100
	2	15, 18	18	200
	2	20, 35	35	300
UX Strain	2	07, 08	08	500
UX/BX	2	25, 26		100
	2	23, 24		200
UX/CV	2	31, 32		50
	3	27-29		100
UX/SP	2	33, 34		50
Direct Pull	4	36-39		0
CMNS	1	40		50
	1	41		100
Total No. Tests:	37			

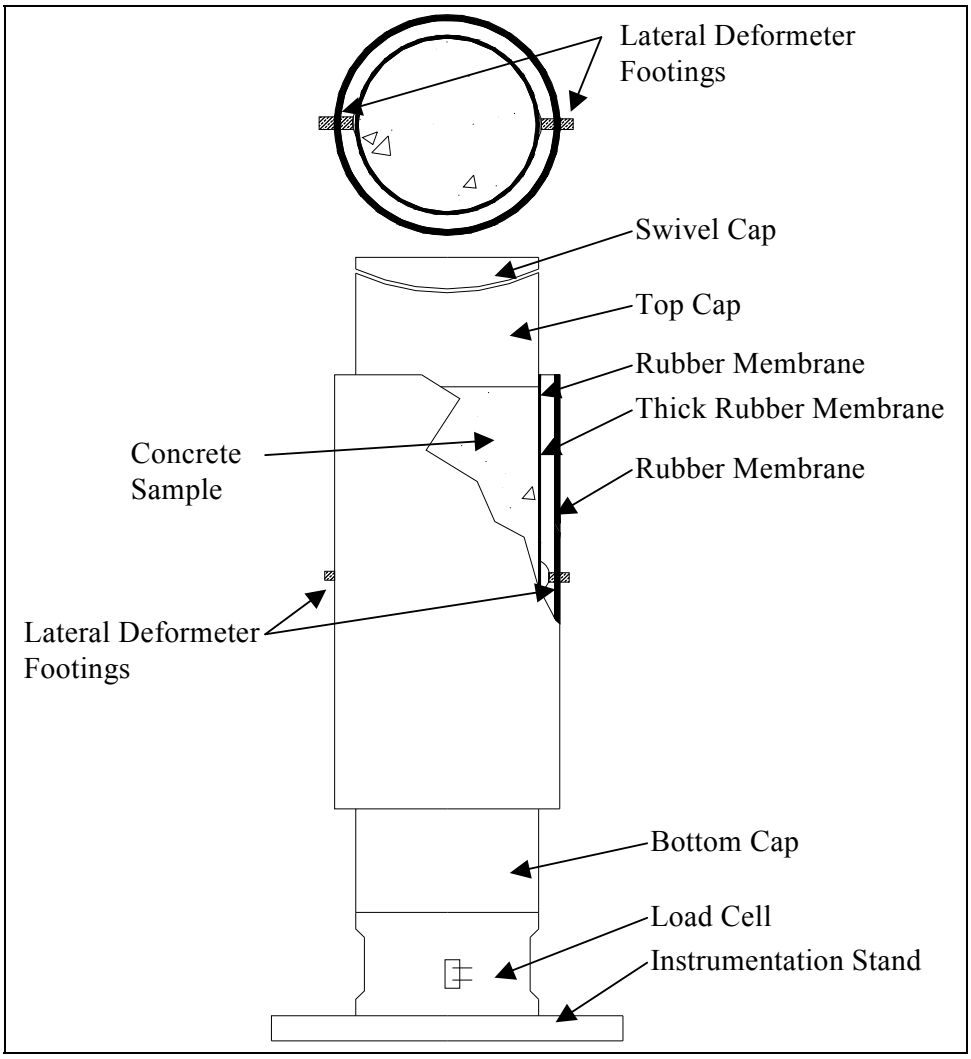

Figure 1. Typical test specimen setup

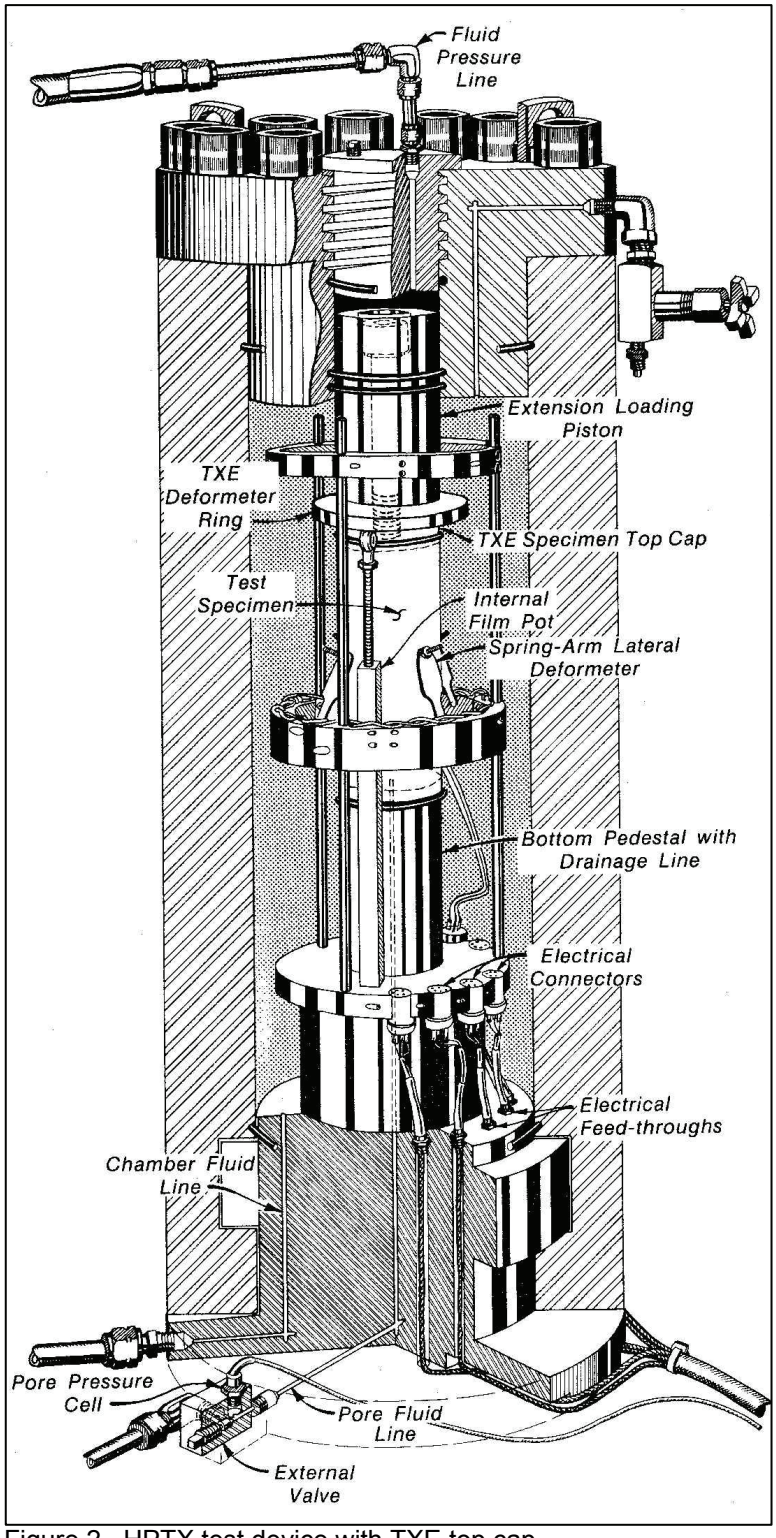

Figure 2. HPTX test device with TXE top cap

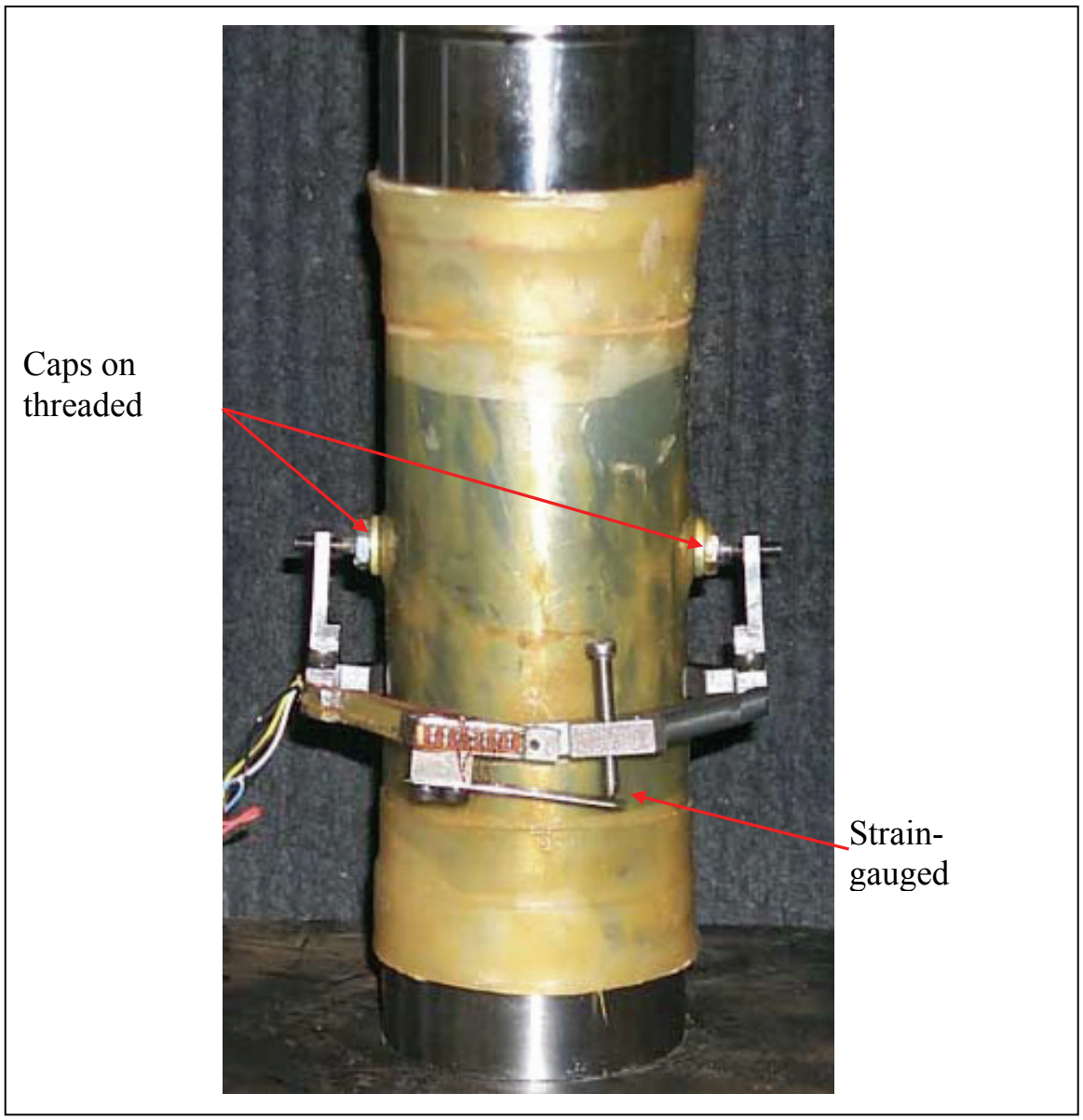

Figure 3. Spring-arm lateral deformeter mounted on test specimen

3 Analysis of Test Results

An analysis is presented in this chapter of the results from laboratory tests conducted on the solid Grade SW Brick. The purpose of this investigation was to characterize the strength and constitutive properties of the material. As described in Chapter 2, a total of 41 mechanical property tests were conducted in this investigation, and 37 tests were successfully completed. The analysis in this chapter is based on the results from the following numbers and types of tests: two HC tests, four UC tests, 12 TXC tests, two CMNS tests, four DP tests, two UX tests, four UX/BX tests, five UX/CV tests, and two UX/SP tests.

Hydrostatic Compression Test Results

Undrained compressibility data were obtained from two HC tests and during the hydrostatic loading phases of the 12 TXC tests. The pressure-volume data from the two HC tests are plotted in Figure 4. Unload-reload cycles were applied to HC test specimen 06 to obtain unload-reload data at intermediate levels of confining stress. The initial dry densities of the specimens for HC tests 06 and 22 were 1.983 and 1.984 Mg/m^3, respectively. Figure 5 presents the pressure time-histories for the HC tests. During the HC tests, the pressure was intentionally held constant for a period of time prior to the unloading cycles. During each hold in pressure, the volume strains continued to increase, indicating that brick is susceptible to creep at high pressures (Figures 4 and 5). At the peak of the first cycle for test specimen 06, the pressure was held at 253 MPa for 157 sec, during which time a volumetric strain of 0.07 percent occurred. During the second cycle, the pressure was held at 508 MPa for 414 seconds, and a volumetric strain of 0.43 percent occurred. The pressure on test specimen 22 was held at 509 MPa for 248 sec, during which time a volumetric strain of 0.34 percent occurred.

Pressure-volume data were also obtained during the hydrostatic loading phases of the TXC tests (Figures 6 and 7). The brick begins to exhibit inelastic strains at a pressure level of approximately 24 MPa and at a volumetric strain of approximately 0.45 percent. Pressure-volume data from all of the TXC tests conducted at confining pressures of 100 MPa and above and the data from Figure 4 are plotted in Figure 7. Based on the data from HC tests and the TXC tests, the initial elastic bulk modulus (K) for brick is approximately 5.3 GPa.

Triaxial Compression Test Results

Shear and failure data were successfully obtained from four unconfined compression tests and 12 unconsolidated-undrained TXC tests. Recall from Chapter 2 that the second phase of the TXC test, the shear phase, is conducted after the desired confining pressure was applied during the HC phase. The UC tests are a special type of TXC test without the application of confining pressure. Results from the UC tests are plotted in Figures 8 and 9, and results from the TXC tests are plotted in Figures 10-21. In all the figures, the axial and volumetric strains at the beginning of the shear phase were set to zero, i.e., only the strains during shear are plotted.

Stress-strain data from the four UC tests in Figures 8 and 9 are plotted as principal stress difference versus axial strain during shear and as principal stress difference versus volumetric strain during shear. Deformeters instead of strain gauges were used to measure the axial and radial strains of the UC test specimens. During the UC tests, no attempt was made to capture the post-peak (or softening) stress-strain behavior of this material. The mean unconfined strength of brick determined from specimens 01, 02, 03, and 04 was 73 MPa. The dry density of the specimens ranged from 1.966 Mg/m^3 to 2.008 Mg/m^3. The bricks with the higher dry density have higher peak strength; therefore, the dry density of the specimen affects the specimen's strength.

Figures 10-21 present the results from the TXC tests conducted at nominal confining pressures of 10, 20, 50, 100, 200, and 300 MPa. The TXC results are plotted as principal stress difference versus axial strain during shear and as principal stress difference versus volumetric strain during shear. The results are very good considering the inherent variability of the initial wet and dry densities of the specimens. The wet densities of the TXC specimens ranged from 1.948 to 2.002 Mg/m^3, the dry densities ranged from 1.948 to 2.002 Mg/m^3, and the water contents ranged from 0.00 to 0.05 percent.

A few comments should now be made concerning the unloading results. The final unloading stress-strain responses at axial strains approaching 15 percent are less reliable than the unloadings at axial strains less than 11 percent. The vertical deformeters go out of range at axial strains of approximately 11 percent. After that, an external deformeter with less resolution is used to measure axial displacement. During the initial unloadings, the creep strains are greater in magnitude than the recovered elastic strains. This behavior results in a net increase in axial strain (for example) during the initial unloading, rather than an expected decrease in axial strain.

Results of TXC tests conducted at a constant confining pressure of 10 MPa are shown in Figures 10 and 11. The initial dry density for test specimen 9 is unknown because the membrane leaked and the test specimen became saturated with the confining fluid. The initial dry density for test specimen 10 is 1.977 Mg/m^3. The volumetric response in Figure 11 indicates that the material initially compacts until just below the peak principal stress difference and then starts to dilate. Little compressive volumetric strain occurs at 10 MPa because the material is still in the elastic region, i.e., little crushing of the material bonds has occurred.

Results of TXC tests conducted at a constant confining pressure of 20 MPa are shown in Figures 12 and 13. The dry densities for specimens 11 and 12 were 1.989 and 1.984 Mg/m^3, respectively. The data exhibited few differences in peak principal stress difference (Figure 12). The post-peak data for the test specimens are not displayed because of the brittle behavior of the material. The volumetric response data in Figure 13 indicate that at 20 MPa confining pressure, the specimens experienced compressive volumetric strains before dilation occurred. At 20 MPa confining pressure, the material is still in the elastic region.

Test results for TXC tests conducted at a confining pressure of 50 MPa are shown in Figures 14 and 15. The dry densities for specimens 13 and 14 were 1.966 and 1.989 Mg/m^3, respectively. The data exhibited differences in peak principal stress difference as a result of the specimen's initial dry densities (Figure 14). A minimal amount of post-peak data was obtained for these test specimens. The volumetric response was similar to the volumetric responses of the specimens tested at 10 and 20 MPa confining pressure but with somewhat higher magnitude.

Results of TXC tests conducted at a confining pressure of 100 MPa are shown in Figures 16 and 17. The dry densities for specimens 16 and 17 were 1.999 and 1.984 Mg/m^3, respectively. Figure 16 displays a more ductile shear response. Since the tests at 50 MPa displayed brittle behavior (the material strain softens and few valid post-peak stress or strain data are acquired), the brittle-to-ductile transition is between 50 and 100 MPa. The brittle-to-ductile transition occurs when the material flows at a near constant value of principal stress difference. The volumetric response data in Figure 17 indicates that at 100 MPa confining pressure, the specimens compacted prior to reaching peak principal stress difference and then started to dilate.

Test results for TXC tests conducted at a confining pressure of 200 MPa are shown in Figures 18 and 19. The dry densities for specimens 15 and 18 were 1.981 and 2.002 Mg/m^3, respectively. The shear responses in Figure 18 were predominantly ductile. Figure 19 indicates that at 200 MPa confining pressure, the volumetric responses of the specimens compact until just below the peak principal stress difference and then dilate.

Results of TXC tests conducted at a confining pressure of 300 MPa are shown in Figures 20 and 21. The dry densities for specimens 20 and 35 were 1.975 and 1.948 Mg/m^3, respectively. The shear responses in Figure 20 were predominantly ductile. Figure 21 indicates volumetric dilation just prior to peak strength of 0.8 and 2.0 percent. After completing the TXC tests, it was determined that none of the specimens reached full saturation during the shear loading. The stress-strain data exhibited increases in principal stress difference over the entire range of increased confining stresses.

For comparison purposes, stress-strain curves from selected TXC tests for each confining pressure are plotted in Figure 22. Stress-strain data from the TXC tests in Figure 22 are plotted in Figure 23 as principal stress difference versus volumetric strain during shear. The initial loading of the TXC stress-strain curves are a function of the material's volume changes during shear and thus are dependent on the magnitude of the applied confining pressure and the position on

the material's pressure-volume response curve. Figure 22 illustrates both the brittle and ductile nature of Grade SW brick. At confining pressures of 50 MPa and below, the material behaves in a brittle manner, especially at the 10 and 20 MPa confining pressure levels. All of these test specimens developed either through-going fractures or strain localizations. At confining pressures of 100 MPa and above, the material behaves in a ductile manner, i.e., the stress-strain curves exhibit strain hardening. Between 50 and 100 MPa, the material experiences a brittle-to-ductile transition. Figure 23 shows that all of the test specimens compacted during shear loading until just prior to achieving peak strength, then began to dilate.

Results from TXC tests at confining pressures from 10 to 300 MPa are plotted in Figure 24 as radial strain during shear versus axial strain during shear. A contour of zero volumetric strain during shear is also plotted on this figure. When the instantaneous slope of a curve is shallower than the contour of zero volumetric strain, the specimen is in a state of volume compression; when steeper, the specimen is in a state of dilation or volume expansion. Data points plotting below the contour signify that a test specimen has dilated, and the current volume of the specimen is greater than the volume at the start of shear. Initially, all of the tests exhibited volumetric compression during shear.

The failure data from all of the UC and TXC tests are plotted in Figure 25 as principal stress difference versus mean normal stress; one stress path at each confining stress is also plotted. In Figure 26, a recommended failure surface is plotted through the failure points. The quality of the failure data is very good; it exhibits very little scatter. It is important to note that the failure points exhibit a continuous increase in principal stress difference with increasing values of mean normal stress. The response data from the 300 MPa TXC tests indicate that at a mean normal stress of approximately 550 MPa, the brick still has not reached void closure and is far from full saturation. Materials such as concrete and brick can continue to gain strength with increasing pressure until all of the air porosity in the specimen is crushed out, i.e., when void closure is reached. It is important to recognize that void closure can be attained during the shear loading phase of the TXC tests as well as under hydrostatic loading conditions. At levels of mean normal stress above void closure, the failure surface will have a minimal slope.

Constant Mean Normal Stress Test Results

Shear and failure data were successfully obtained from two constant mean normal stress tests. Stress-strain data from the two CMNS tests in Figures 27 and 28 are plotted as principal stress difference versus axial strain during shear and as principal stress difference versus volumetric strain during shear, respectively. The two CMNS tests were performed at a constant mean normal stress of approximately 50 and 100 MPa for test specimens 40 and 41, respectively. Figure 28 displays the volume changes due to shear for the two CMNS tests. Test specimen 40 exhibits compressive volumetric strains up to near failure then exhibits dilation while test specimen 41 exhibits the same volumetric response but abruptly changes to volumetric compaction with increasing shear strain. The stress-paths from the CMNS tests are plotted with the TXC recommended failure surface in Figure 29. The failure points from the CMNS tests plot on the TXC

recommended failure surface. The CMNS test data validates the TXC recommended failure surface between mean normal stresses of 50 and 100 MPa.

Direct Pull Test Results

Extension shear and failure data were successfully obtained from four direct pull tests. The DP tests are performed without the application of confining pressure. Results from the DP tests are plotted in Figure 30. All of the specimens fractured. Failure from the DP tests occurred at an average mean normal stress of about -2.0 MPa at approximately -6.0 MPa principal stress difference. Comparing the results of the UC tests (unconfined compression strength of 73 MPa) and the DP tests, it becomes evident that brick is able to withstand greater loads under compression.

Uniaxial Strain Test Results

One-dimensional compressibility data were obtained from two undrained uniaxial strain (UX) tests with lateral stress measurements. Data from the tests are plotted in Figures 31-33. The stress-strain data from the UX tests are plotted in Figure 31, the pressure-volume data in Figure 32, and the stress paths with the failure surface data in Figure 33. The UX responses indicate that neither test specimen reached a fully saturated state, i.e., the volume strains achieved during the tests were much less than the air porosities of the specimens.

From the UX stress-strain loading data (Figure 31), an initial constrained modulus (M) of 12.2 GPa was calculated. UX data may also be plotted as principal stress difference versus principal strain difference; the slope of an elastic material in this space is $2G$. An initial shear modulus of 5.2 GPa was calculated from the constrained modulus and the elastic bulk modulus, K (5.3 GPa) determined from the HC and TXC tests. These two values may be used to calculate any of the other elastic constants. The initial Young's modulus is 11.7 GPa, and initial Poisson's ratio is 0.13.

The stress paths from the UX tests are plotted in Figure 33. The UX stress paths almost reach the TXC recommended failure surface before the curves soften slightly. The stress paths soften after the ceramic bonds start to crush causing the data to lie below the failure surface. The stress paths from test specimens 07 and 08 display differences after nearing the failure surface, these differences are a result of the each test specimen's intrinsic properties. The dry densities for these specimens were 1.997 Mg/m^3 for test specimen 07 and 1.985 Mg/m^3 for test specimen 08. The pressure-volume responses from HC and UX tests are compared in Figure 34. HC specimen 22 and UX specimen 08 can be compared since the dry densities are similar, 1.983 and 1.985 Mg/m^3, respectively. Up to a volumetric strain of approximately three percent, the UX data for specimen 08 is somewhat stiffer than the HC data for specimen 22. This implies that the UX state of stress is not providing additional shear-induced compaction to the specimen at pressures below about 250 MPa. Above 250 MPa,

UX test specimen 08 displays a decrease in the stiffness. This decrease in stiffness is an indication of shear-induced compaction.

Strain Path Test Results

Three types of strain-path tests were conducted in this test program. UX/BX refers to tests with uniaxial strain loading followed by constant axial strain unloading. UX/CV refers to tests with uniaxial strain loading followed by constant volumetric strain loading. UX/SP refers to tests with uniaxial strain loading then continued loading along a constant ratio of radial strain to axial strain of -1.33.

Two UX/BX tests were conducted to a peak axial stress of approximately 370 MPa, and the other two tests were conducted to a peak axial stress of approximately 575 MPa. Data from the tests are plotted in Figures 35-38. The stress-strain data from the UX/BX tests are plotted in Figure 35, the pressure-volume data in Figure 36, the stress paths with the failure surface data in Figure 37, and the strain paths in Figure 38. The stress-strain response of the material (Figure 35) displays variations during the UX loading that are a function of the test specimens' initial material properties. In addition, the stress-strain curves illustrate that the specimens were allowed to creep under zero-radial-strain boundary conditions prior to initiating the BX unloading.

The pressure-volume data presented in Figure 36 illustrate the large amount of volume recovery that occurs during the BX unloading. Most of the specimens recover all of their peak compressive volumetric strain and continue to dilate an additional 1.5 to 3 percent. The stress-paths plotted in Figure 37 display some stress relaxation occurred at the end of the UX loading and prior to the BX unloading; hence the slight unload just after peak stress. During the unloading, the stress-paths show a significant decrease in principal stress difference with decreasing mean normal stress. This unloading appears to follow a limiting surface, which is normally the material's failure relation (the TXC recommend failure surface in most cases). The stress paths in Figure 37 confirm that the limiting surface for the UX/BX tests is similar to the TXC recommend failure surface. Figure 38 displays the strain paths for the four UX/BX test specimens.

Results from five UX/CV tests conducted at two peak levels of axial stress during the initial UX phase are shown in Figures 39-42. The stress-strain data from the UX/CV tests are plotted in Figure 39, the pressure-volume data in Figure 40, the stress-paths with the failure surface data in Figure 41, and the strain paths in Figure 42. The CV portions of the stress path data in Figure 41 initially exhibit an increase in stress difference with a slight decrease in mean normal stress followed by an increase of both the stress difference and the mean normal stress. During most of the CV loading, the data follow closely to the failure surface developed from the TXC tests.

Data were obtained from two UX/SP tests that were loaded to approximately the same nominal peak axial stress during the initial UX phase. Data from the tests are plotted in Figures 43-46. The stress-strain data from the UX/SP tests are plotted in Figure 43, the pressure-volume data in Figure 44, the stress paths with the failure surface in Figure 45, and the strain paths in Figure 46. The compressibility data from the UX/SP tests 33 and 34 have small differences, a result of the

slight difference of the dry densities for the test specimens, 2.008 and 1.983 Mg/m^3, respectively. The plotted stress paths (Figure 45) demonstrate increasing values of principal stress difference and decreasing values of mean normal stress after the SP loading initiates. After reaching the material's limiting surface, both stress difference and mean normal stress increase. The stress paths in Figure 45 confirm that the limiting surface for the UX/SP tests is similar to the material's recommended TXC failure surface.

Comparison plots of the results of selected UX, UX/BX, UX/CV, and UX/SP are plotted in Figures 47-50. The stress-strain data are plotted in Figure 47, the pressure-volume data are plotted in Figure 48, the stress-paths with the failure surface are plotted in Figure 49, and the strain-paths are plotted in Figure 50. The following statements provide an interpretation of the measured pressure-volume data during the strain paths. When loading along the constant volume strain path, the specimens want to increase in volume due to the material's inherent shear-induced dilation characteristics. Increasing levels of pressure are required to maintain constant volume boundary conditions (Figure 48). The material's behavior while loading along a constant SP displays a gradual increase in pressure and with decreasing volumetric strain. The SP specimen does not want to expand faster than the boundary conditions permit unlike the specimens loaded along the constant-volume strain path. To maintain the boundary conditions during the UX/SP tests, the pressure is gradually increased. The boundary conditions applied during the BX unloading require significant amounts of volume expansion. To maintain the boundary conditions, pressure must be reduced. In Figure 49, one stress path for each of the different strain path tests and the TXC failure surface are overlaid to illustrate the merger of the data in the vicinity of the failure surface. The convergence of the data from the UX/BX tests, UX/CV tests, and the UX/SP tests validates both the TXC failure data and the strain-path data.

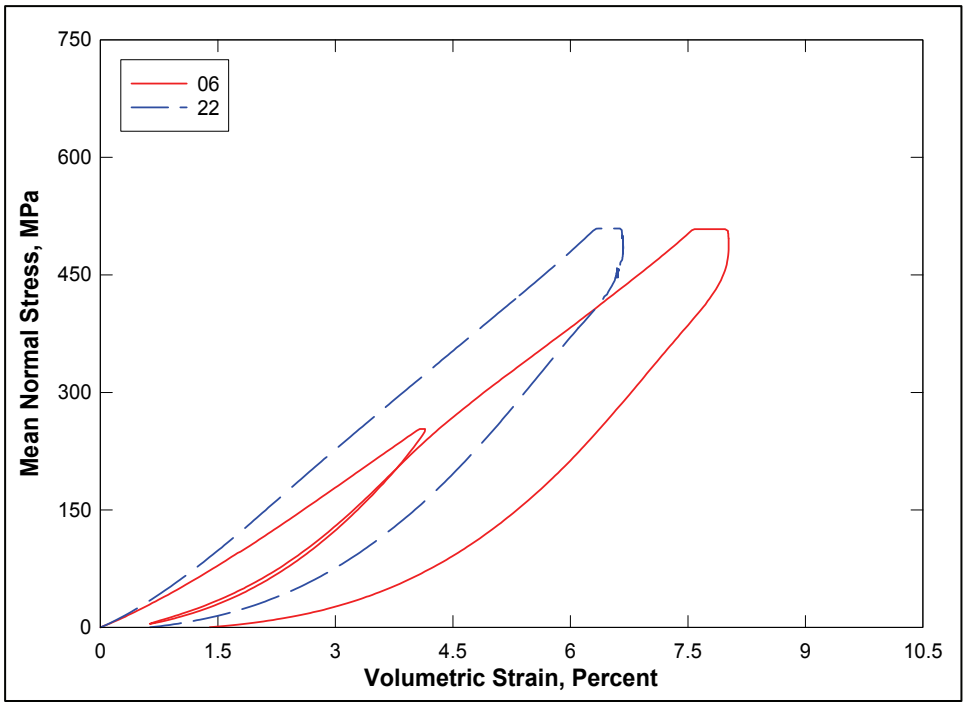

Figure 4. Pressure-volume responses from the HC tests

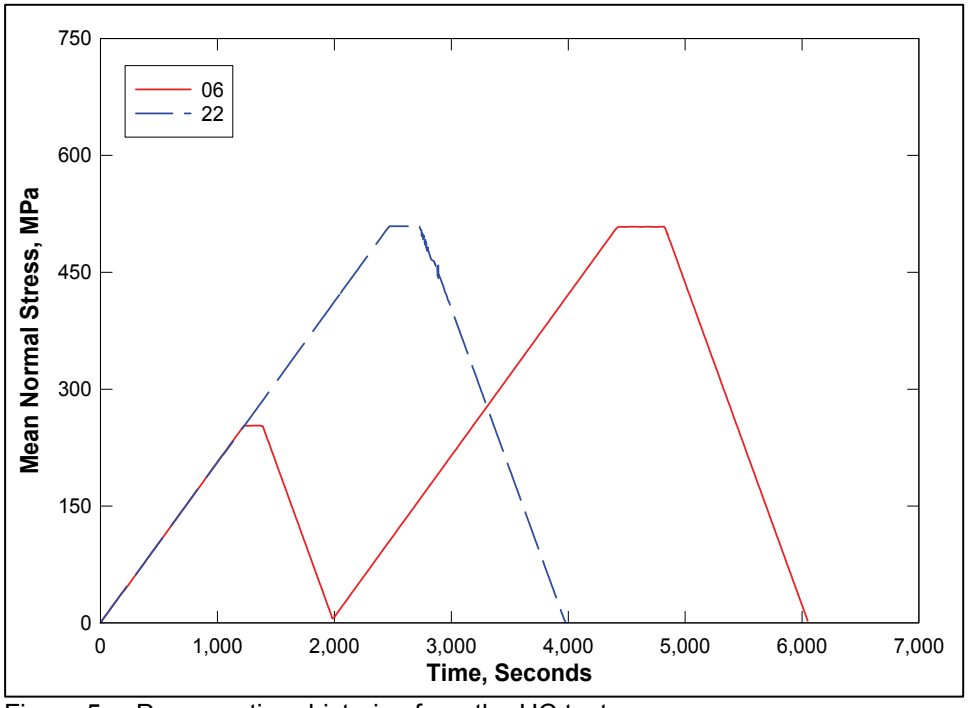

Figure 5. Pressure time-histories from the HC tests

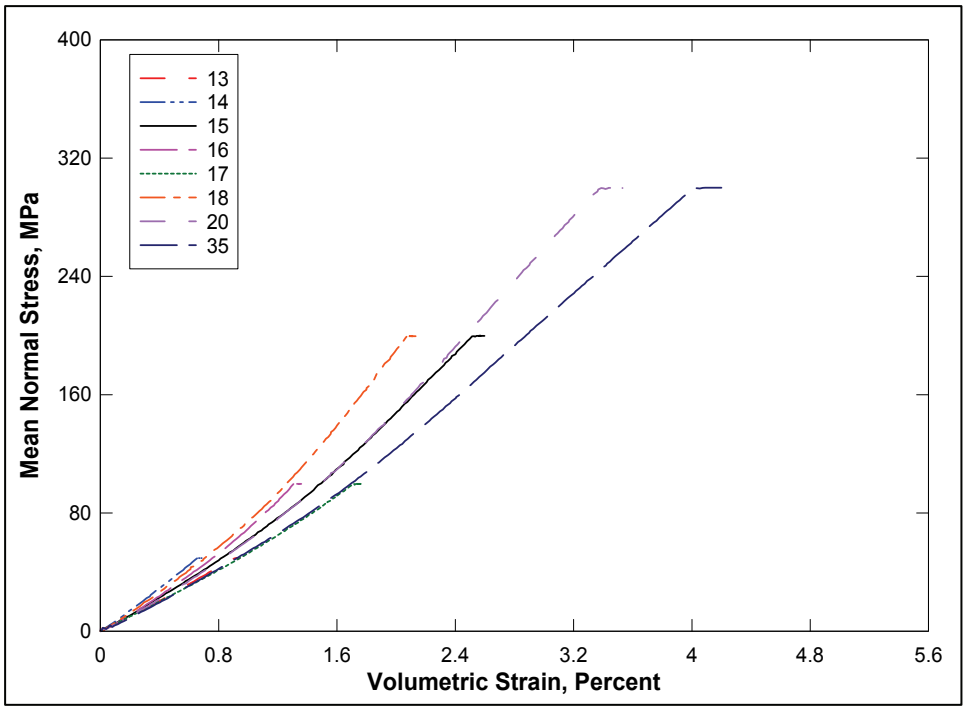

Figure 6. Pressure-volume responses during the HC phase of selected TXC tests

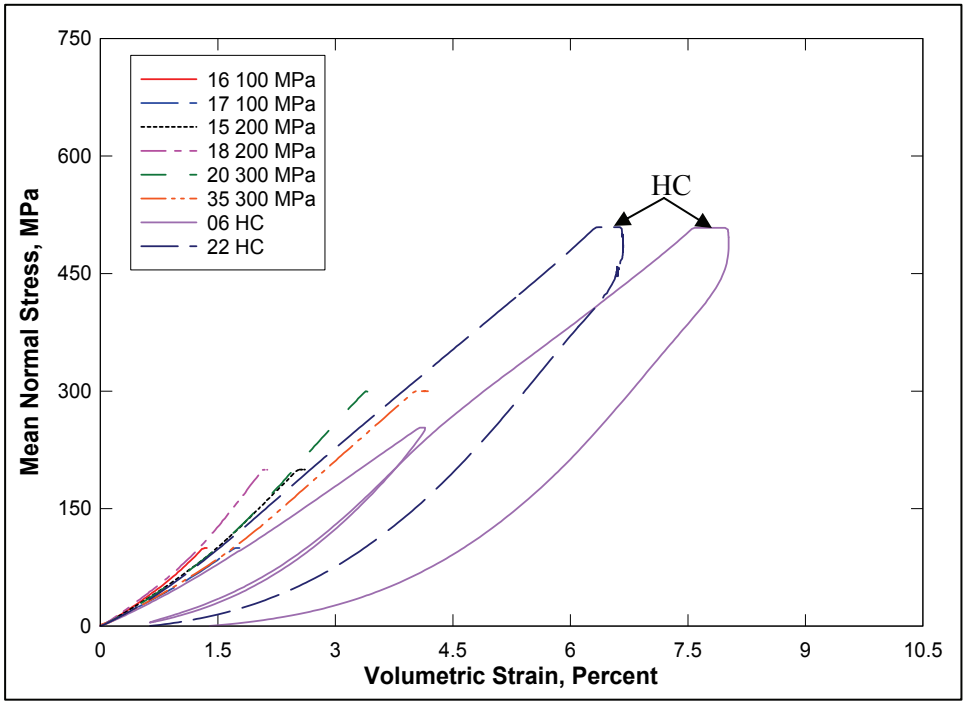

Figure 7. Pressure-volume responses from HC and TXC tests

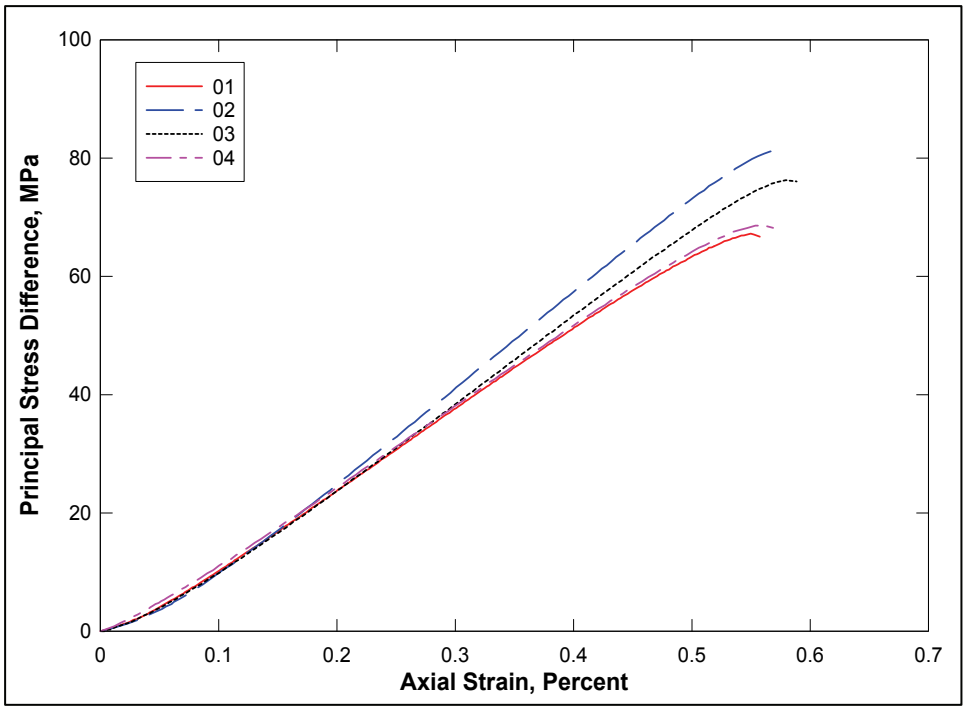

Figure 8. Stress-strain curves from UC tests

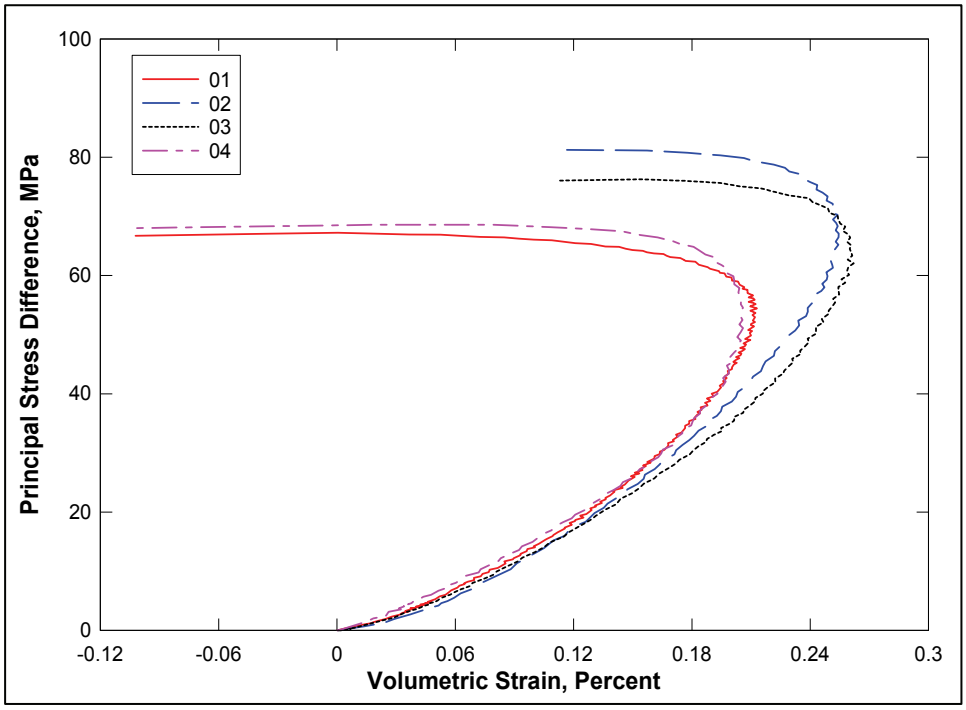

Figure 9. Stress difference-volume strain during shear from UC tests

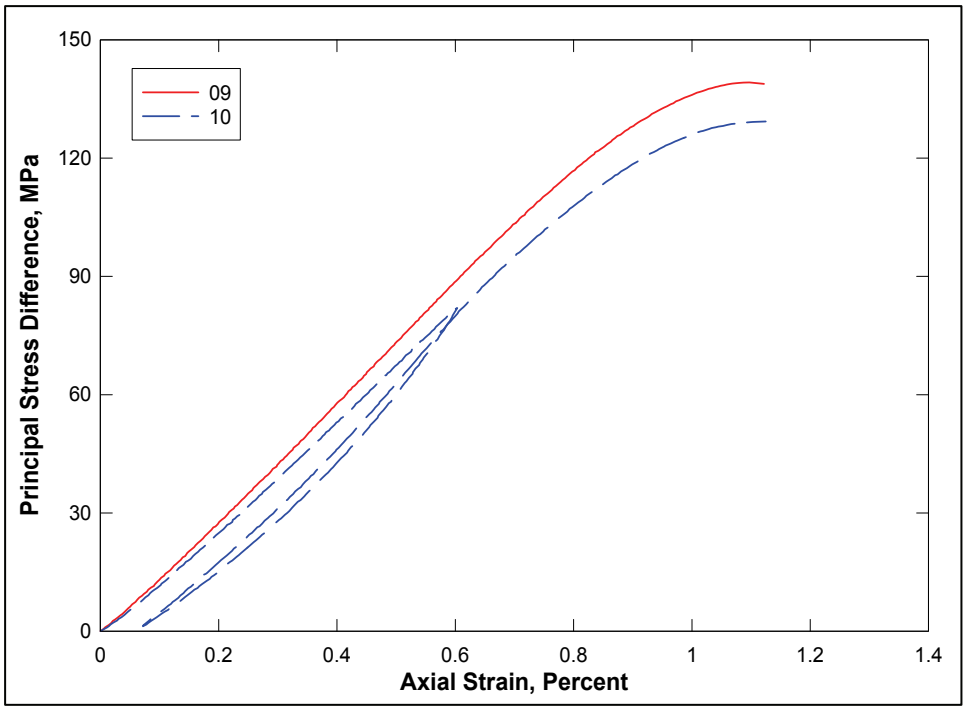

Figure 10. Stress-strain curves from TXC tests at a confining pressure of 10 MPa

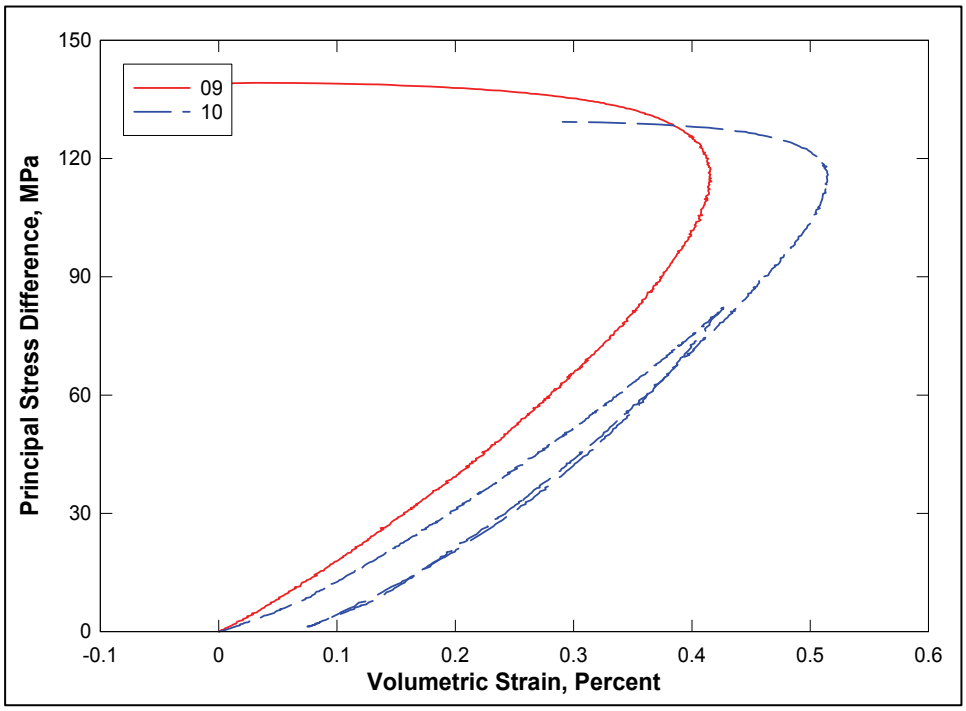

Figure 11. Stress difference-volume strain during shear from TXC tests at a confining pressure of 10 MPa

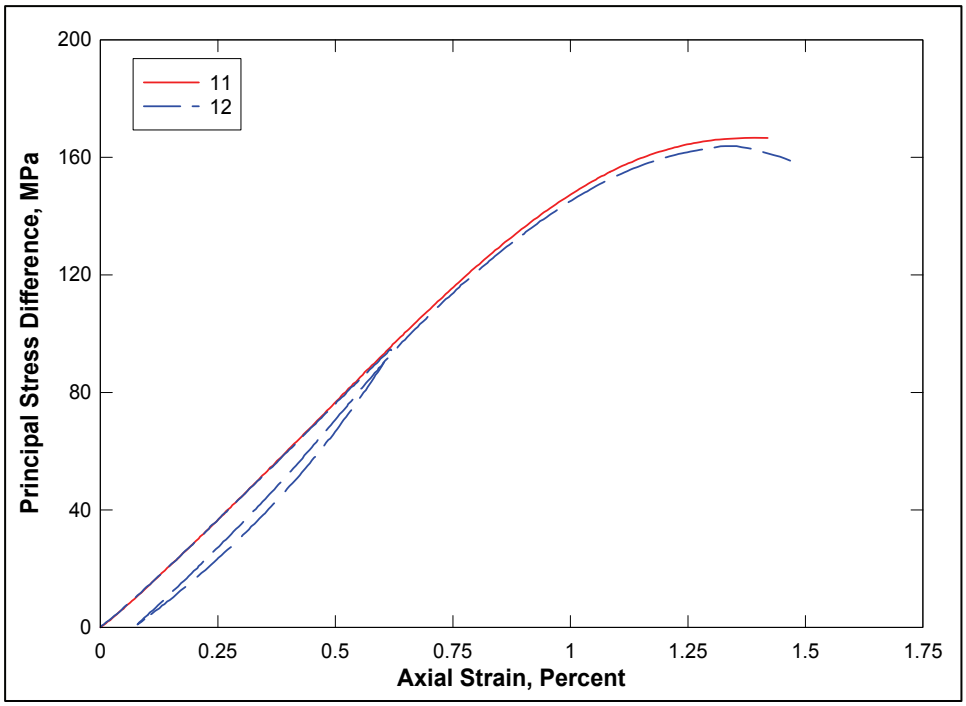

Figure 12. Stress-strain curves from TXC tests at a confining pressure of 20 MPa

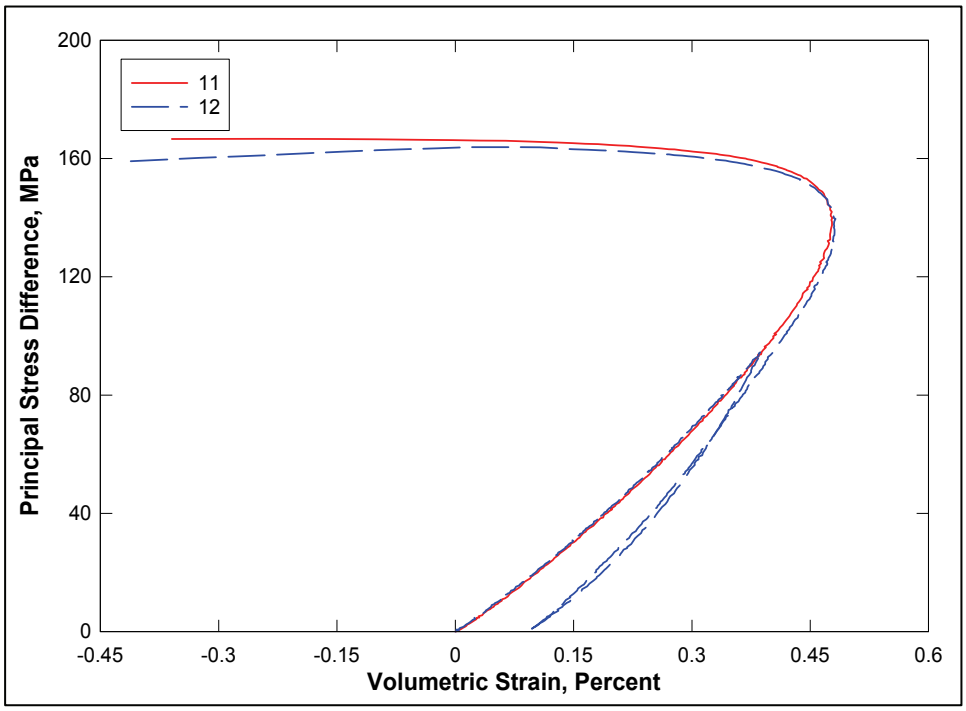

Figure 13. Stress difference-volume strain during shear from TXC tests at a confining pressure of 20 MPa

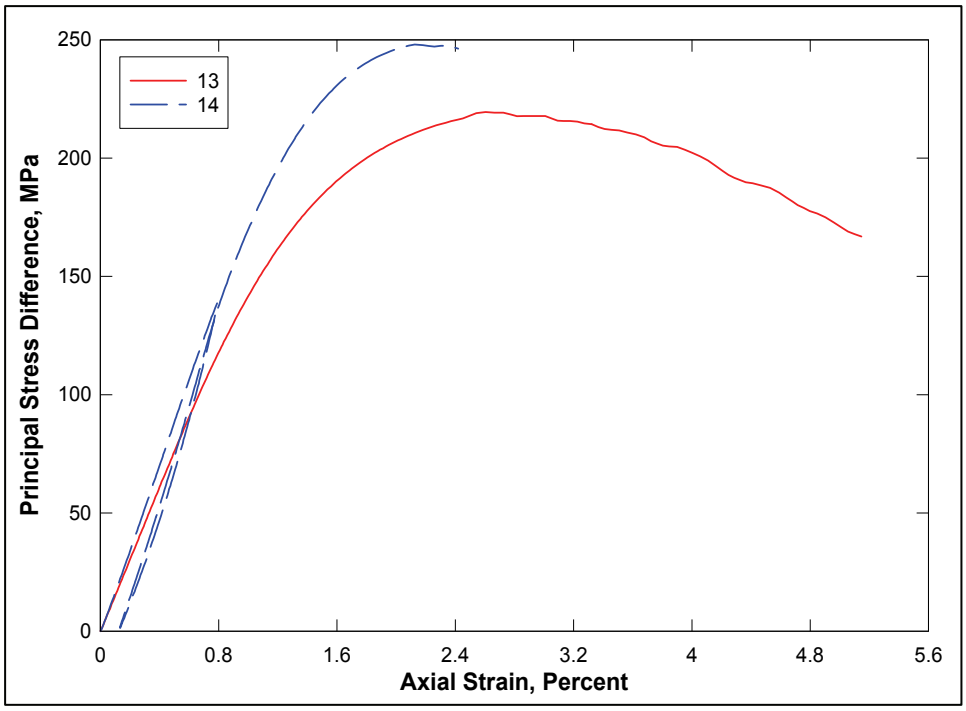

Figure 14. Stress-strain curves from TXC tests at a confining pressure of 50 MPa

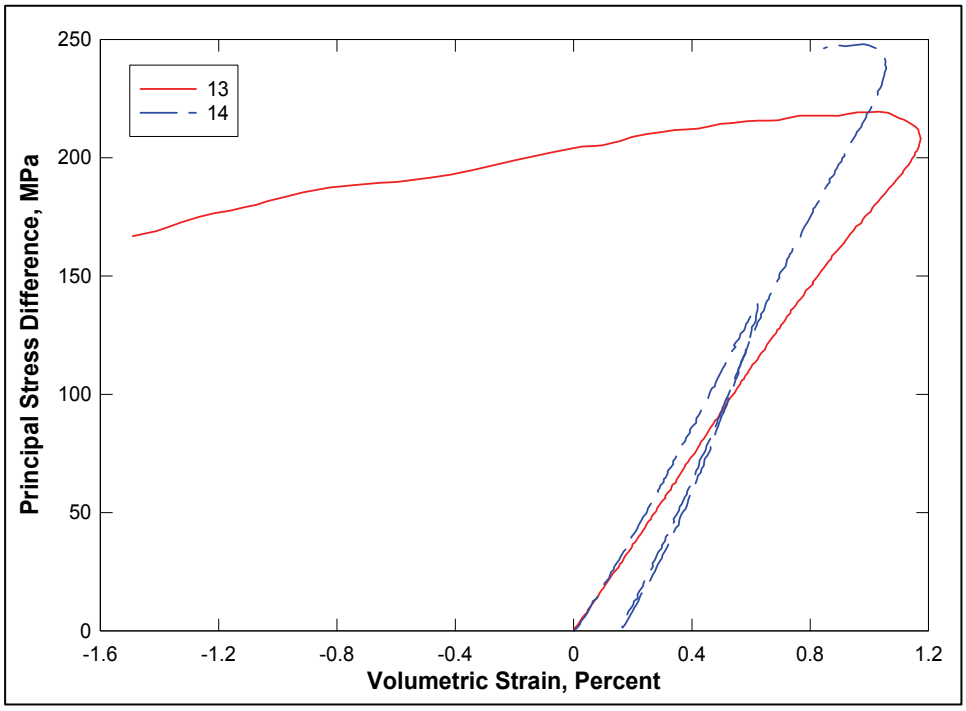

Figure 15. Stress difference-volume strain during shear from TXC tests at a confining pressure of 50 MPa

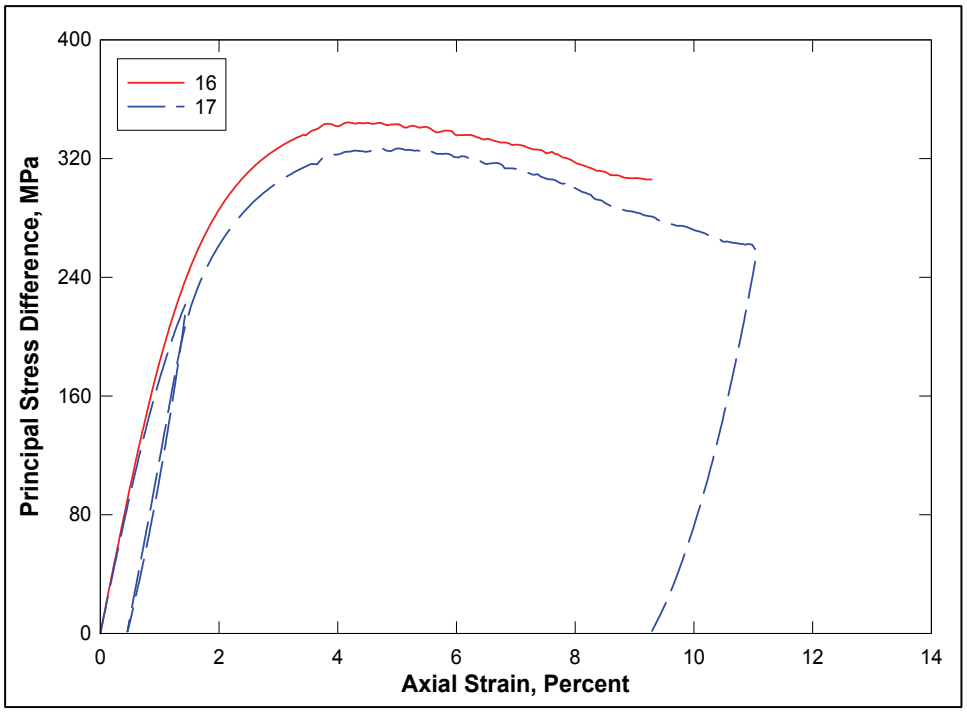

Figure 16. Stress-strain curves from TXC tests at a confining pressure of 100 MPa

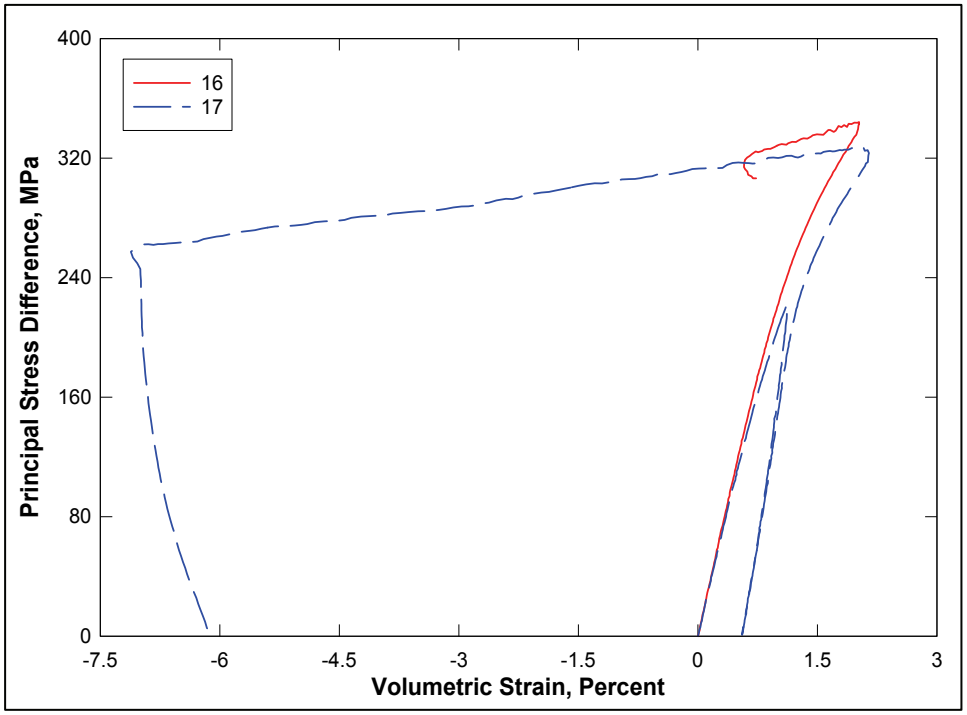

Figure 17. Stress difference-volume strain during shear from TXC tests at a confining pressure of 100 MPa

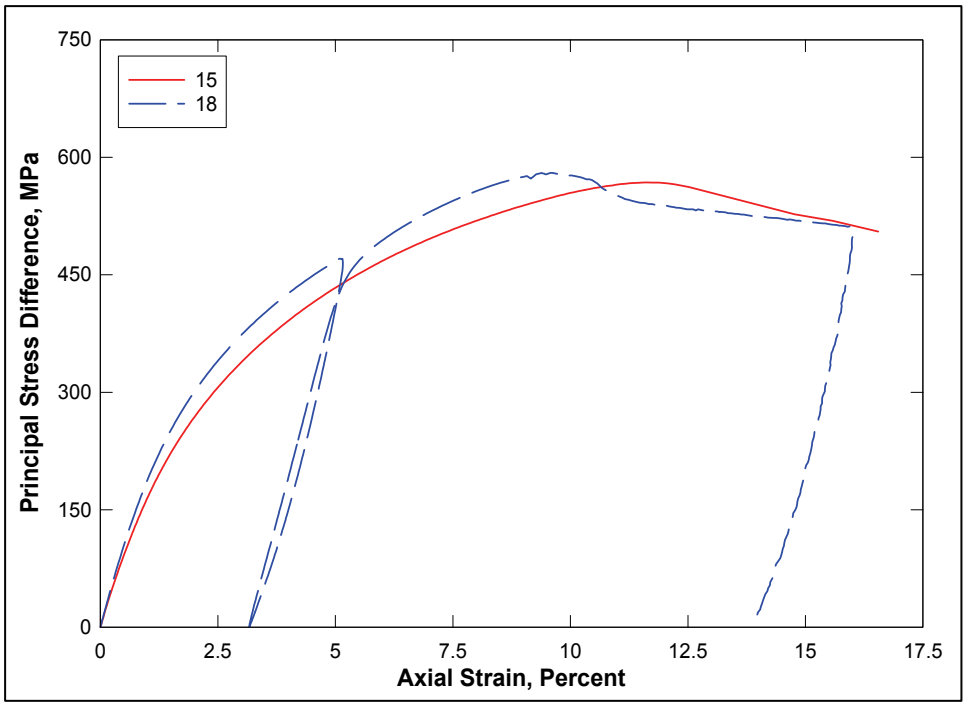

Figure 18. Stress-strain curves from TXC tests at a confining pressure of 200 MPa

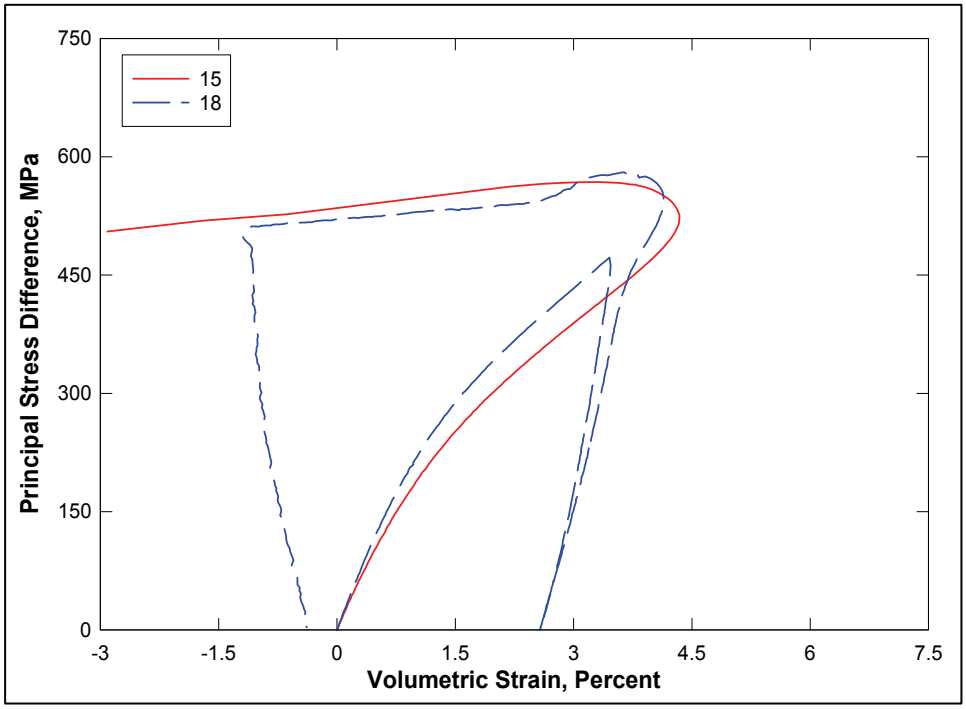

Figure 19. Stress difference-volume strain during shear from TXC tests at a confining pressure of 200 MPa

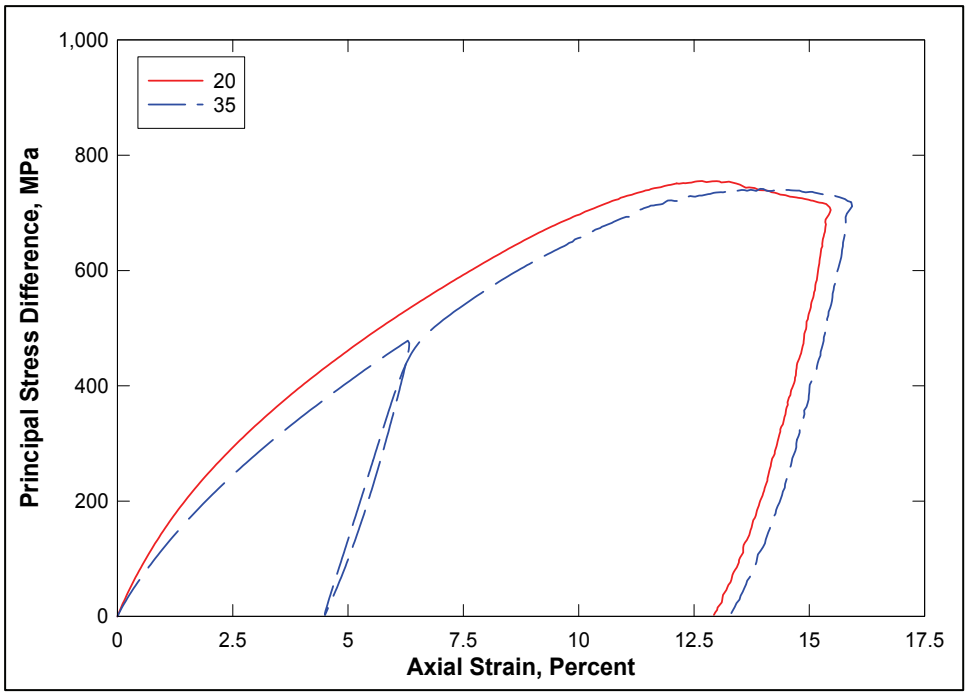

Figure 20. Stress-strain curves from TXC tests at a confining pressure of 300 MPa

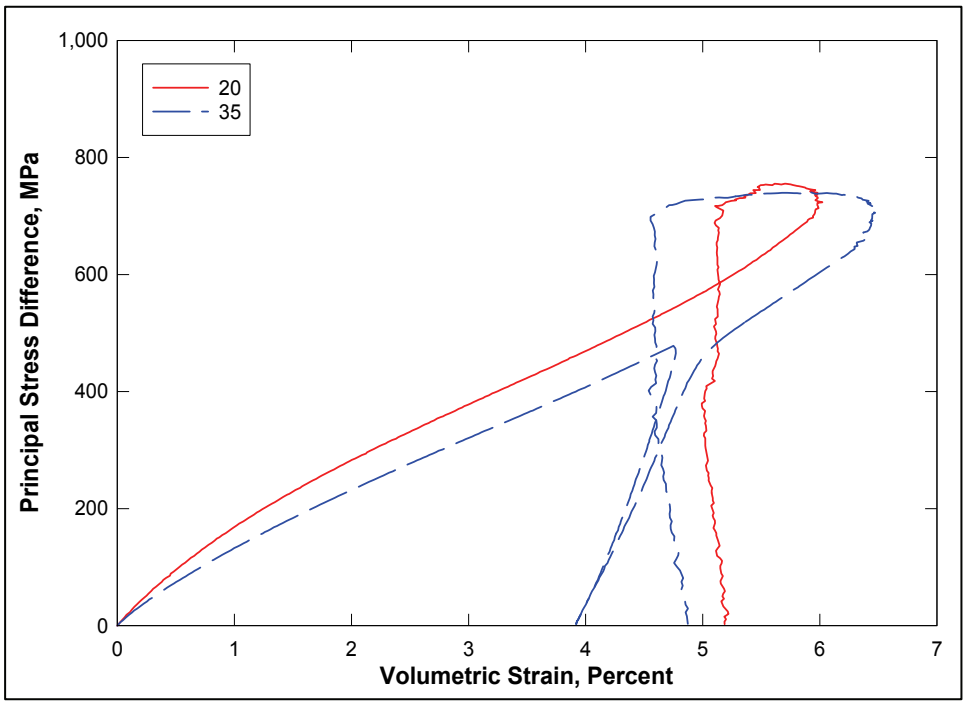

Figure 21. Stress difference-volume strain during shear from TXC tests at a confining pressure of 300 MPa

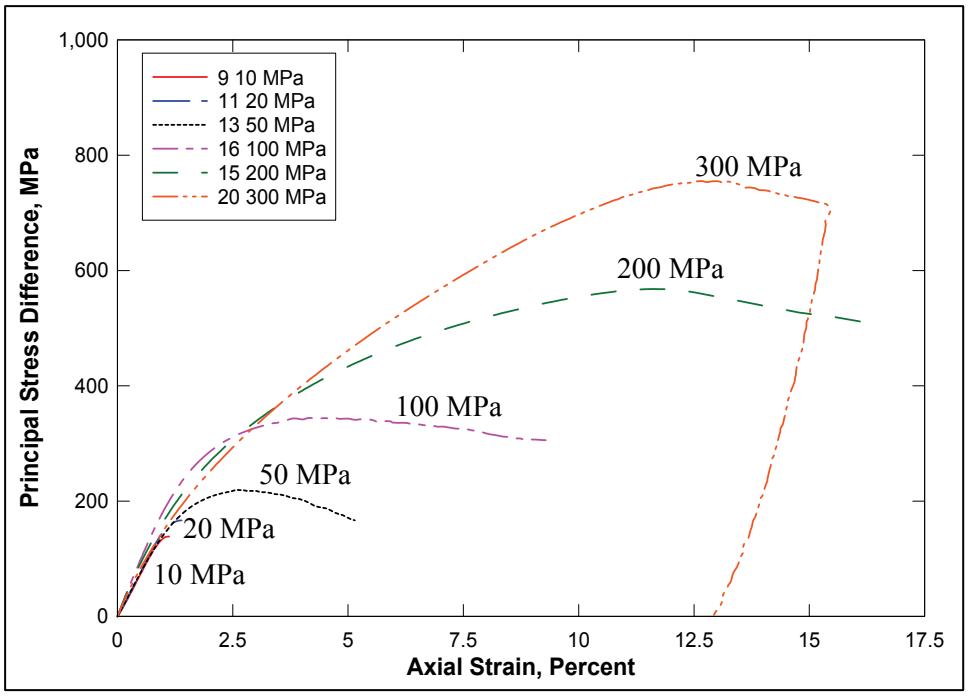

Figure 22. Stress-strain data from TXC non-cyclic tests at confining pressures between 10 and 300 MPa

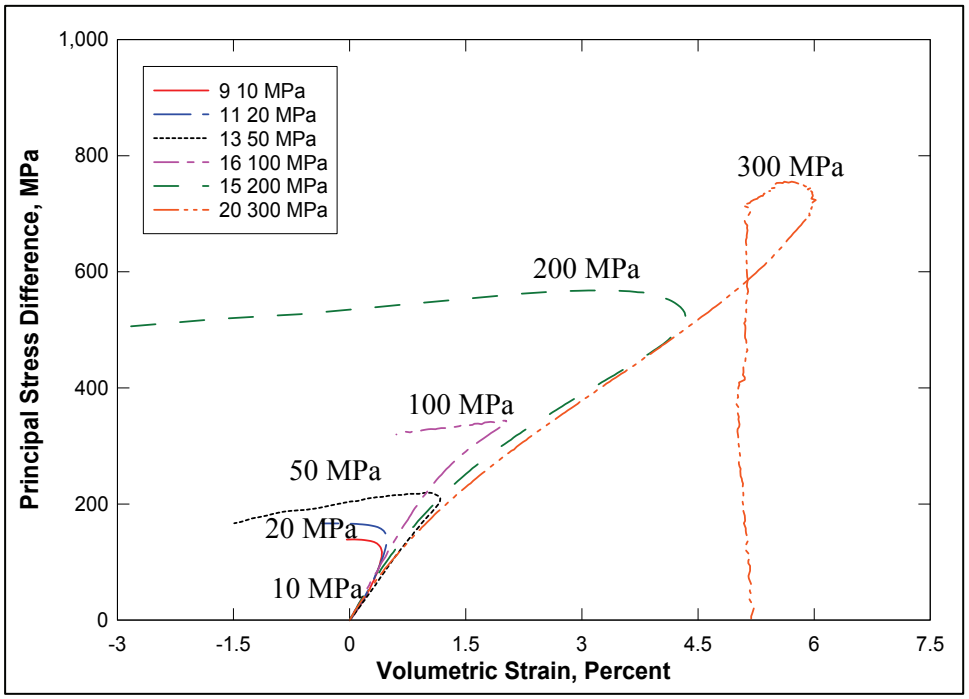

Figure 23. Stress difference-volume strain during shear from TXC non-cyclic tests at confining pressures between 10 and 300 MPa

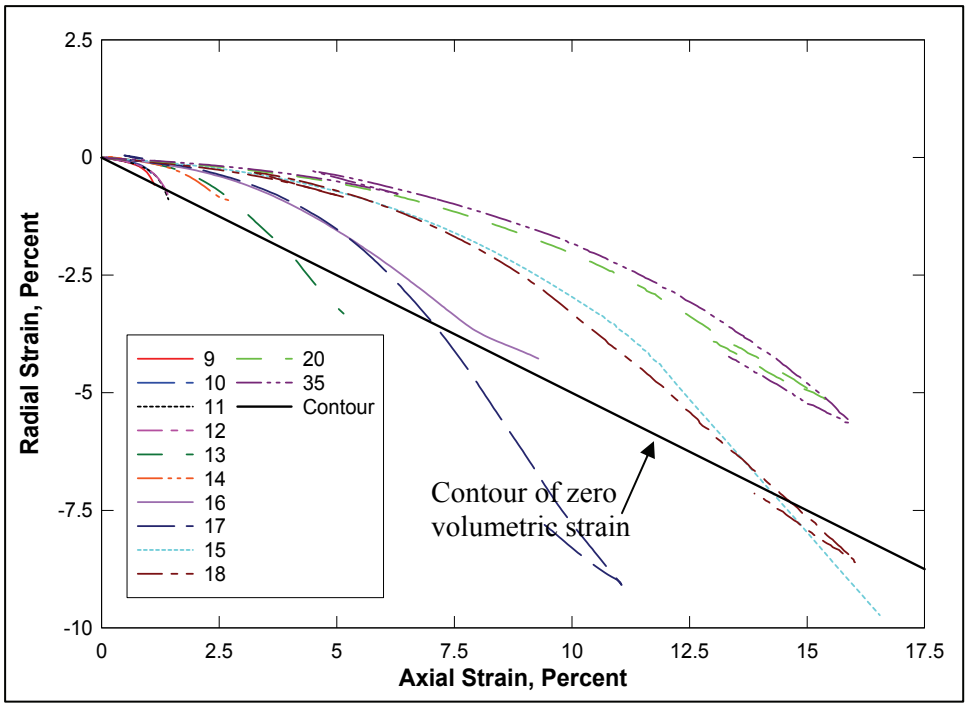

Figure 24. Radial strain-axial strain data during shear from TXC tests at confining pressures between 10 and 300 MPa

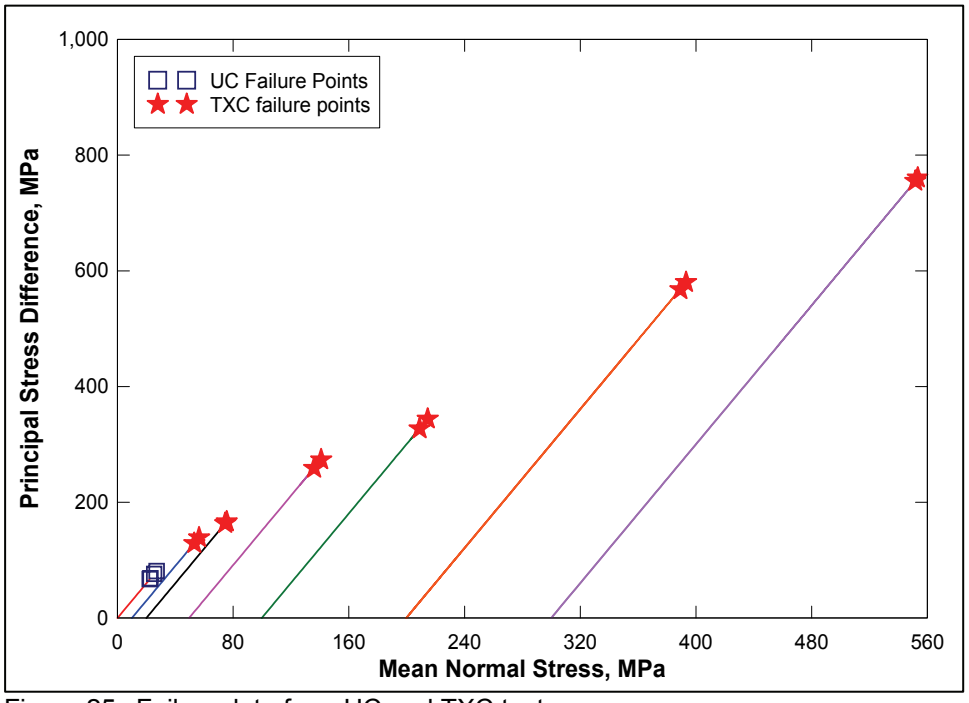

Figure 25. Failure data from UC and TXC tests

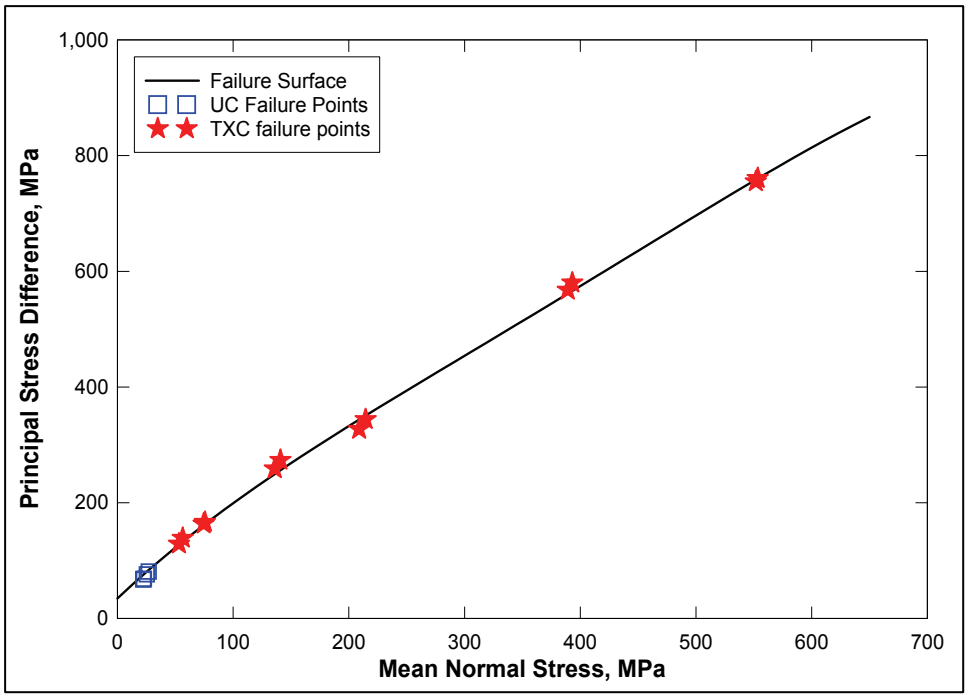

Figure 26. Failure data from UC and TXC tests and recommended failure surface

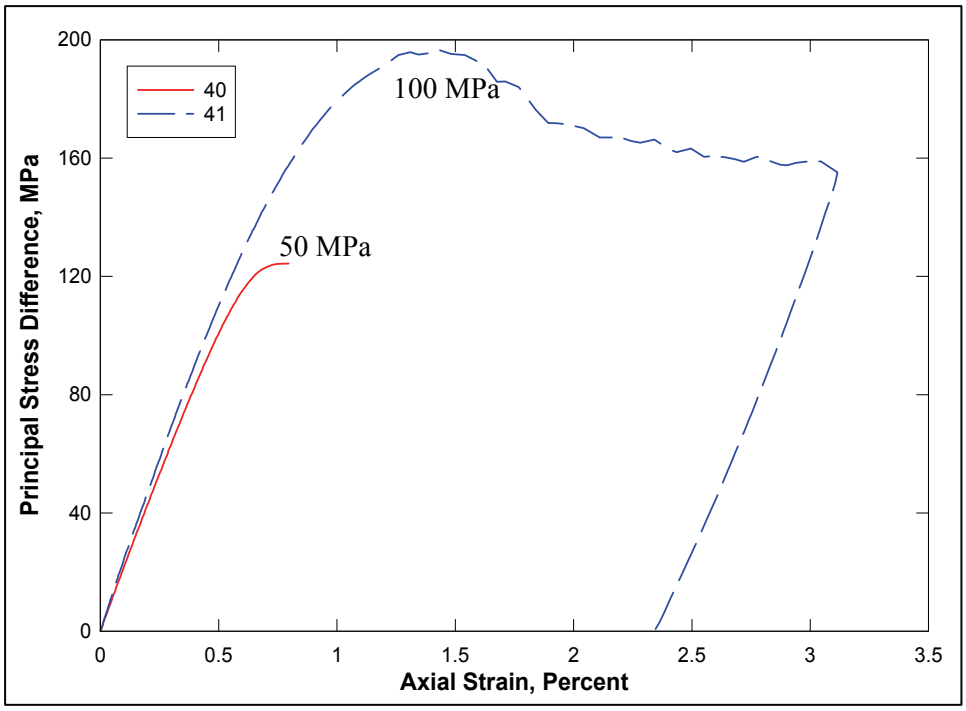

Figure 27. Stress-strain curves from CMNS tests at confining pressures of 50 and 100 MPa

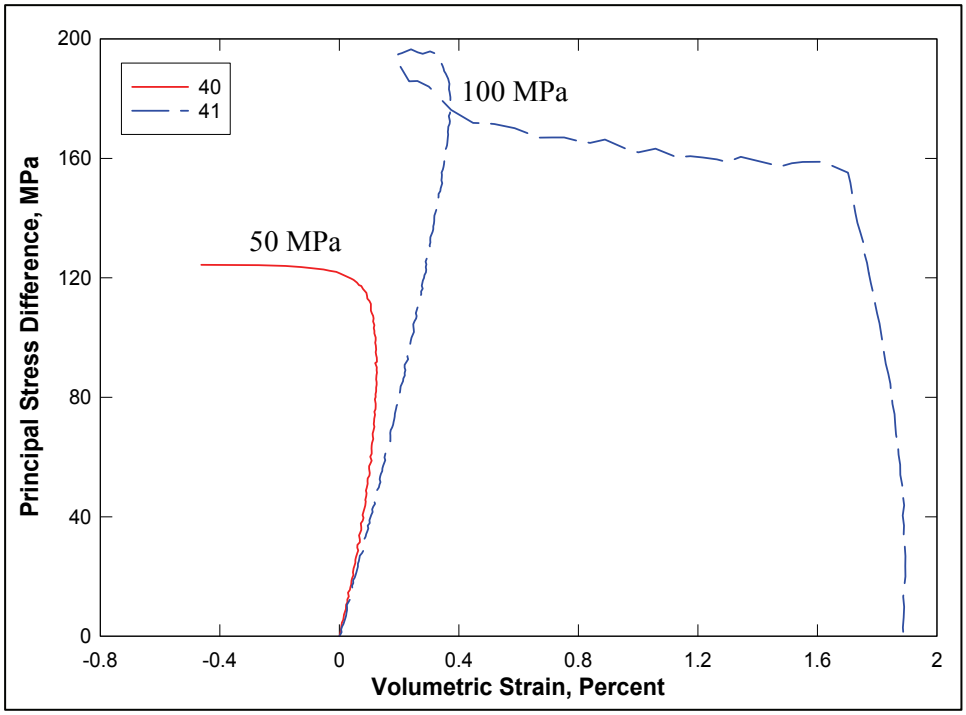

Figure 28. Stress difference-volume strain during shear from CMNS tests at confining pressures of 50 and 100 MPa

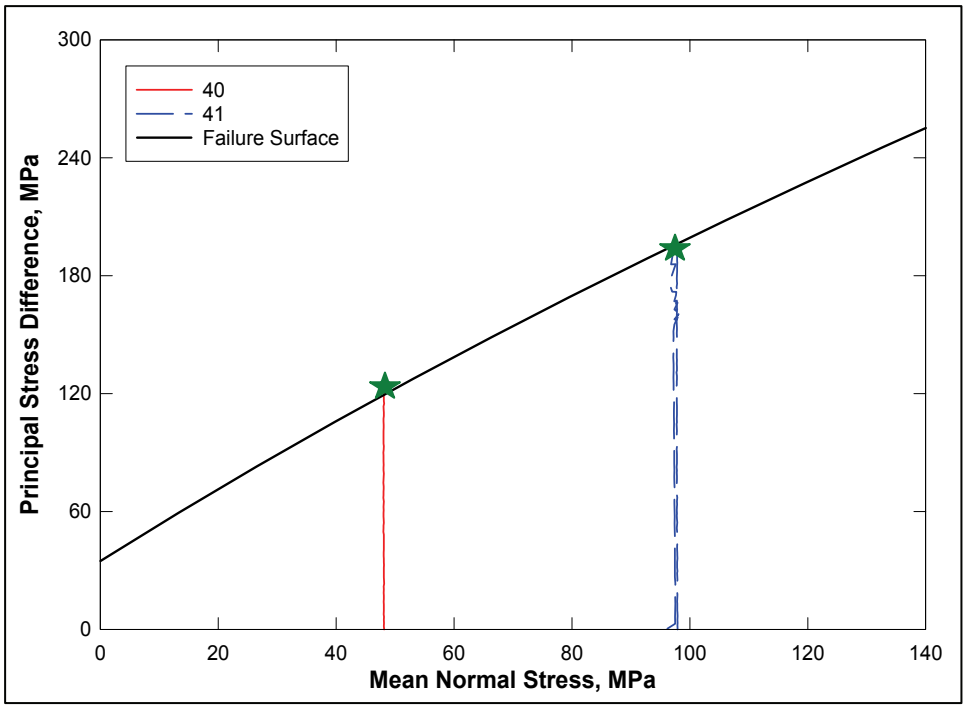

Figure 29. CMNS stress paths and failure data and the TXC recommended failure surface

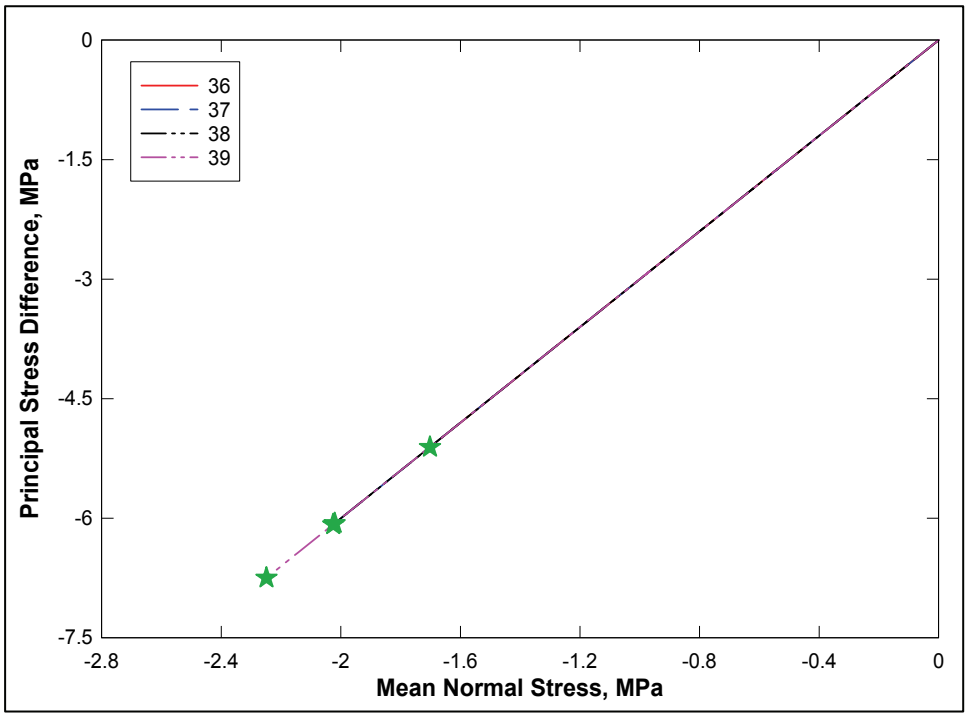

Figure 30. Stress paths and failure data from DP tests

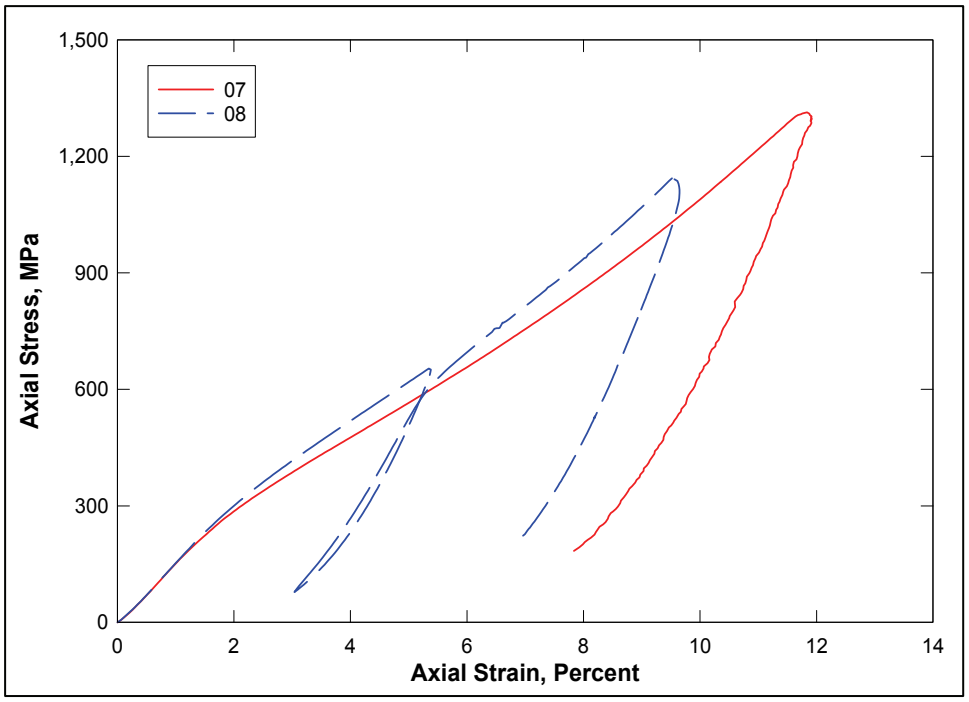

Figure 31. Stress-strain curves from UX tests

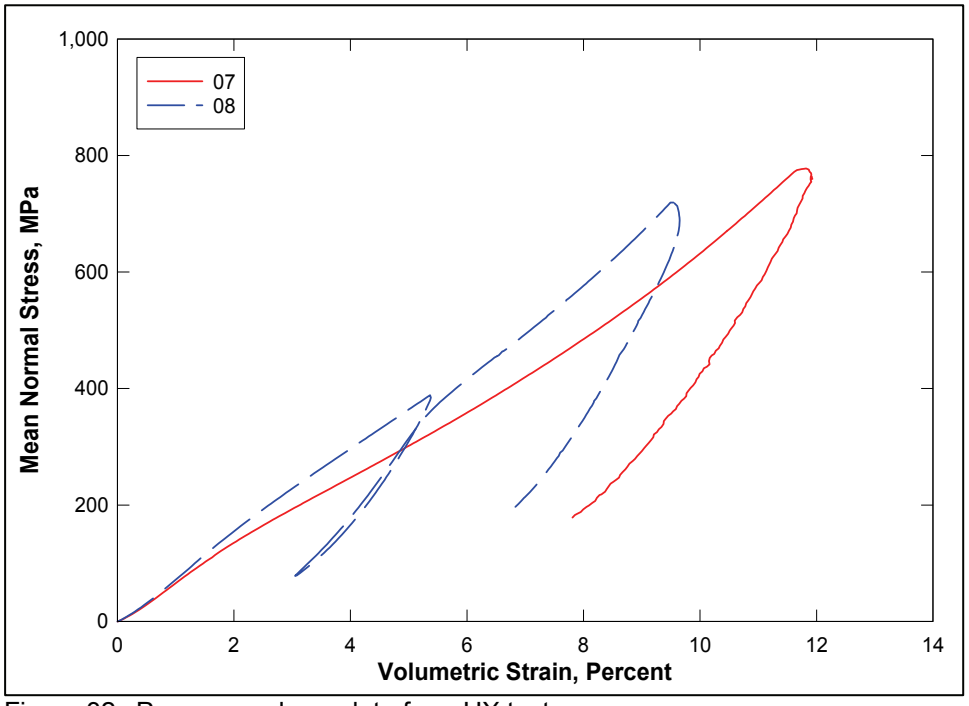

Figure 32. Pressure-volume data from UX tests

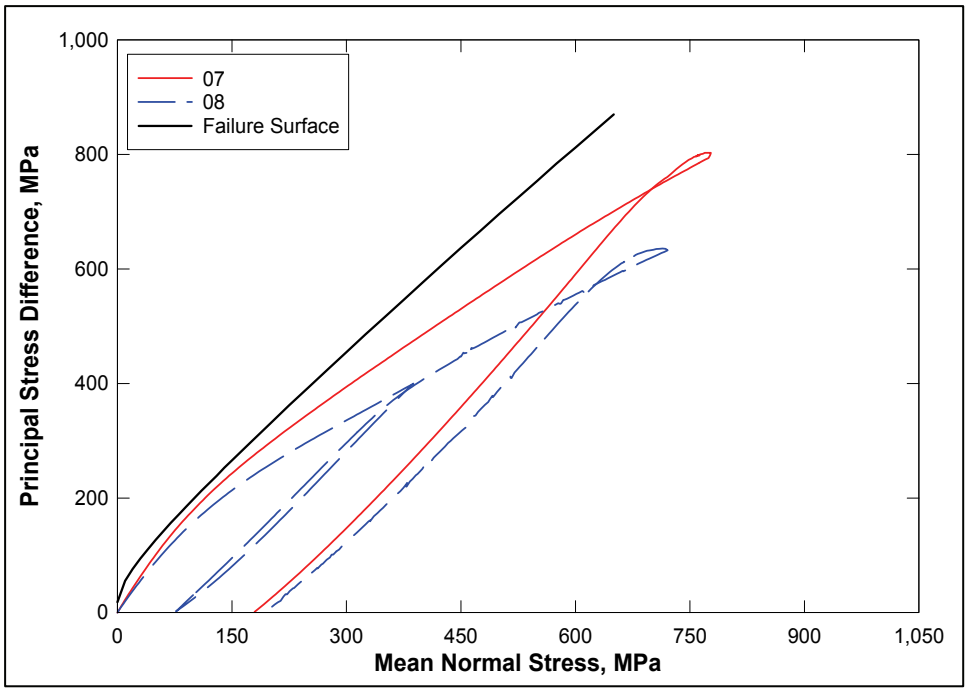

Figure 33. Stress paths from UX tests and failure surface from TXC tests

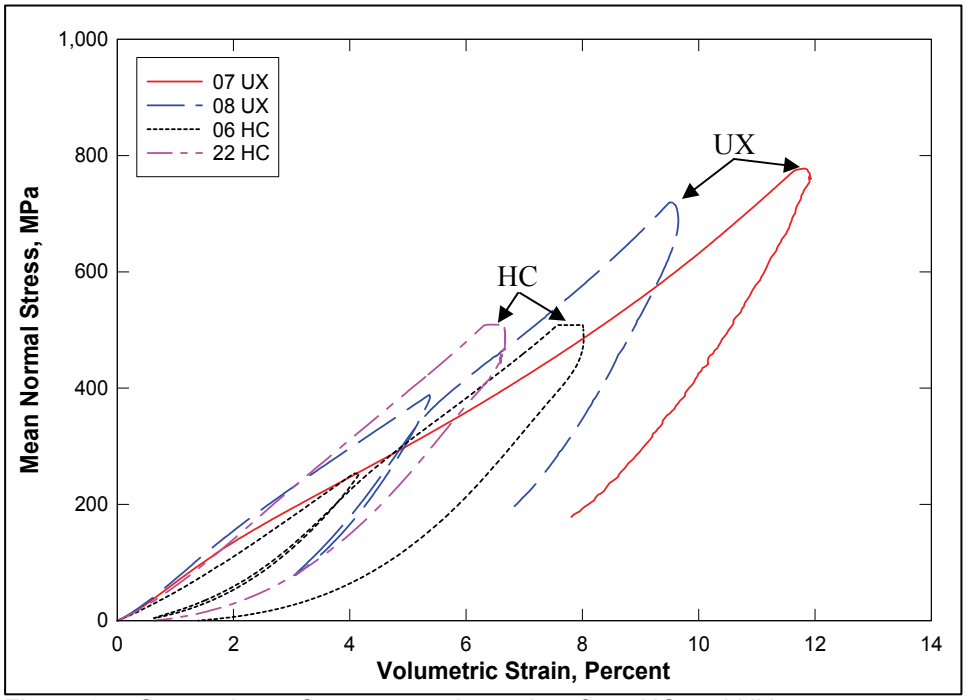

Figure 34. Comparison of pressure-volume data from HC and UX tests

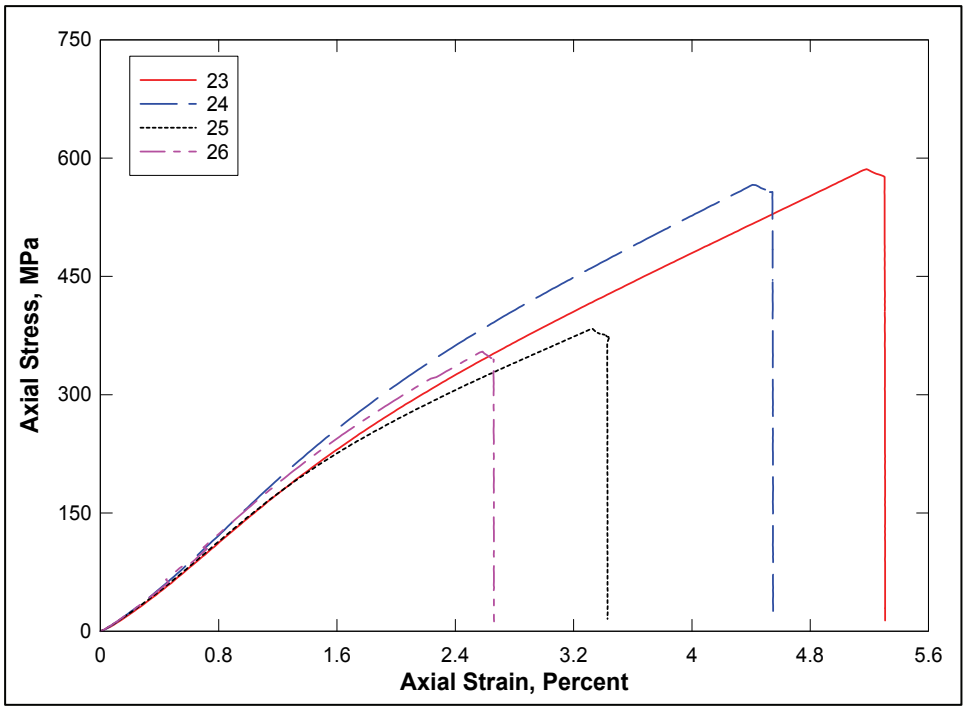

Figure 35. Stress-strain curves from UX/BX tests

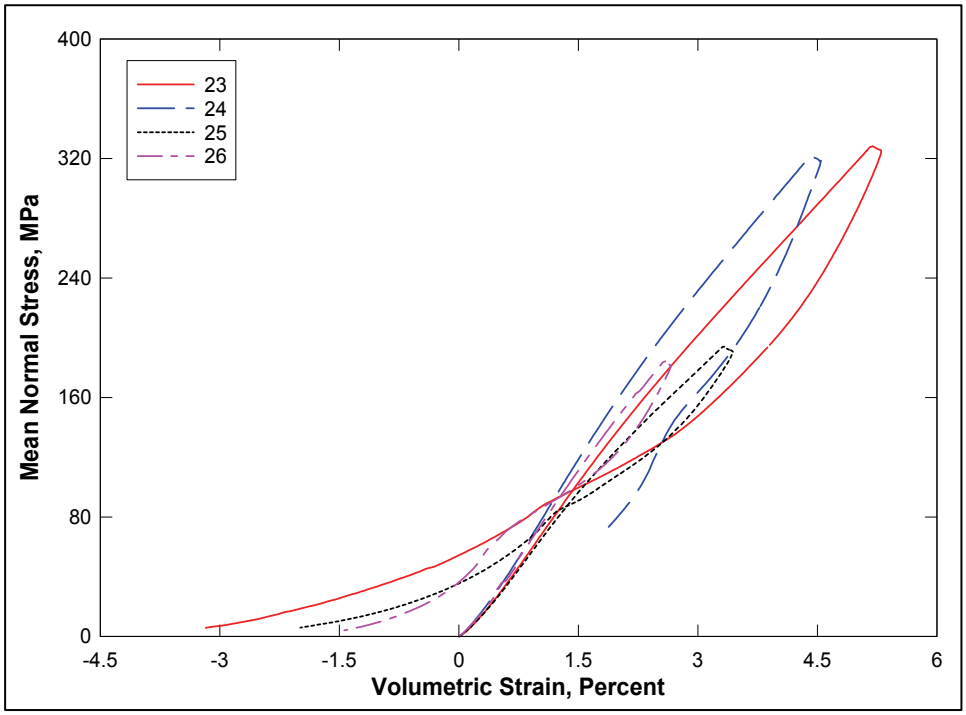

Figure 36. Pressure-volume data from UX/BX tests

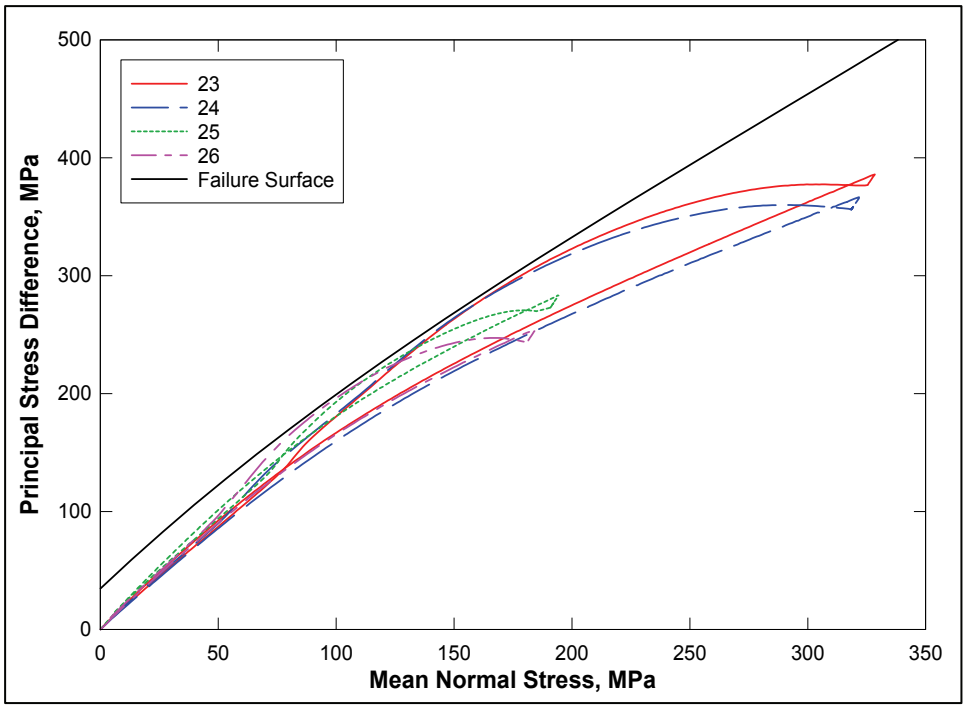

Figure 37. Stress paths from UX/BX tests and failure surface from TXC tests

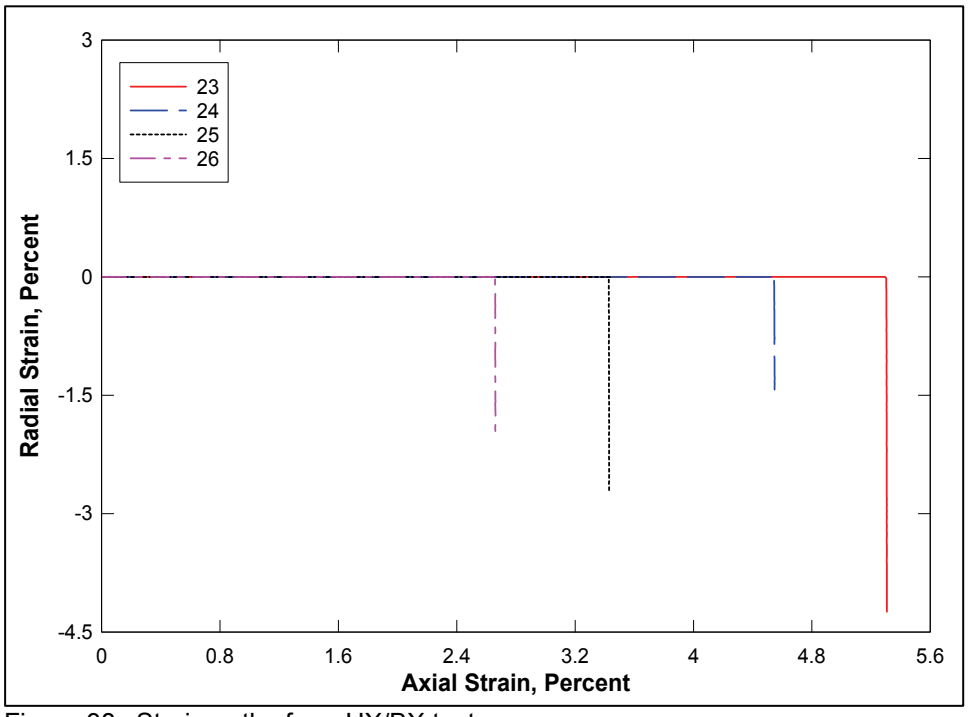

Figure 38. Strain paths from UX/BX tests

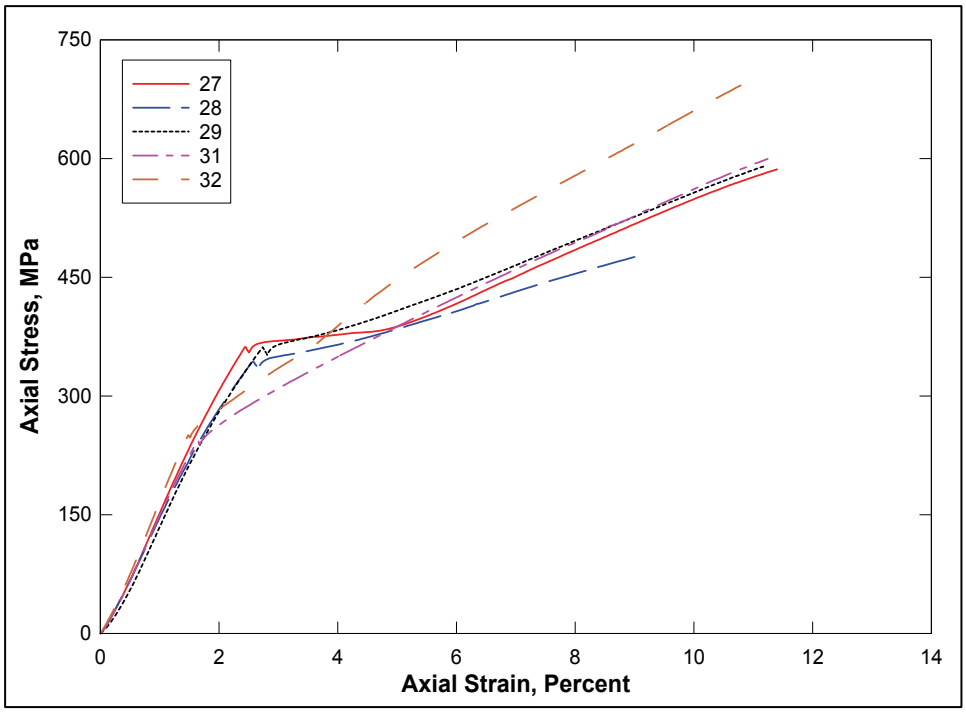

Figure 39. Stress-strain curves from UX/CV tests

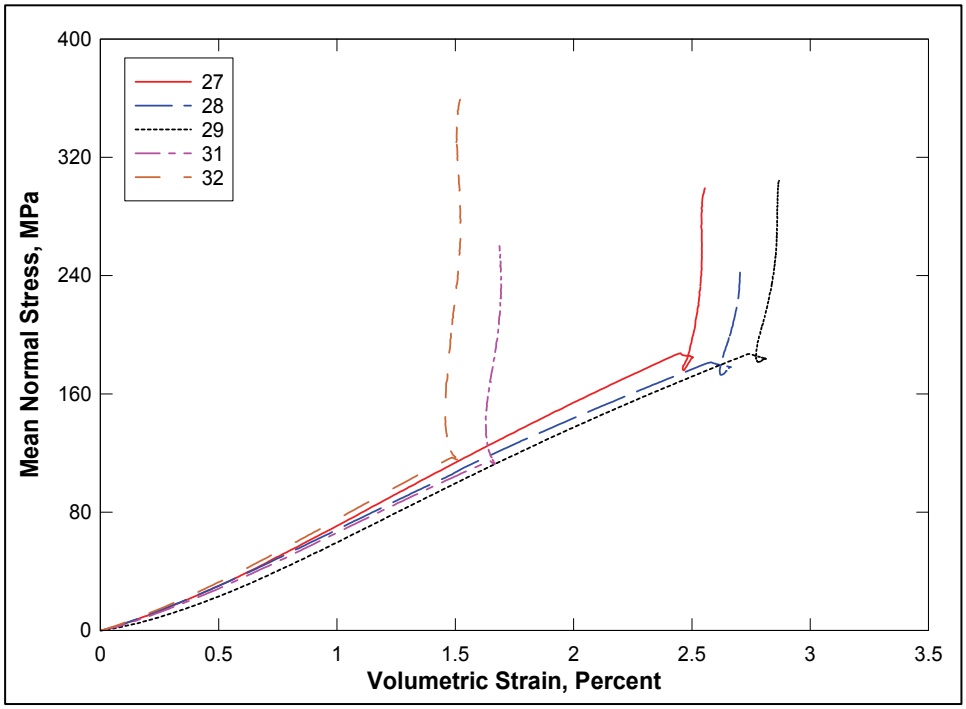

Figure 40. Pressure-volume data from UX/CV tests

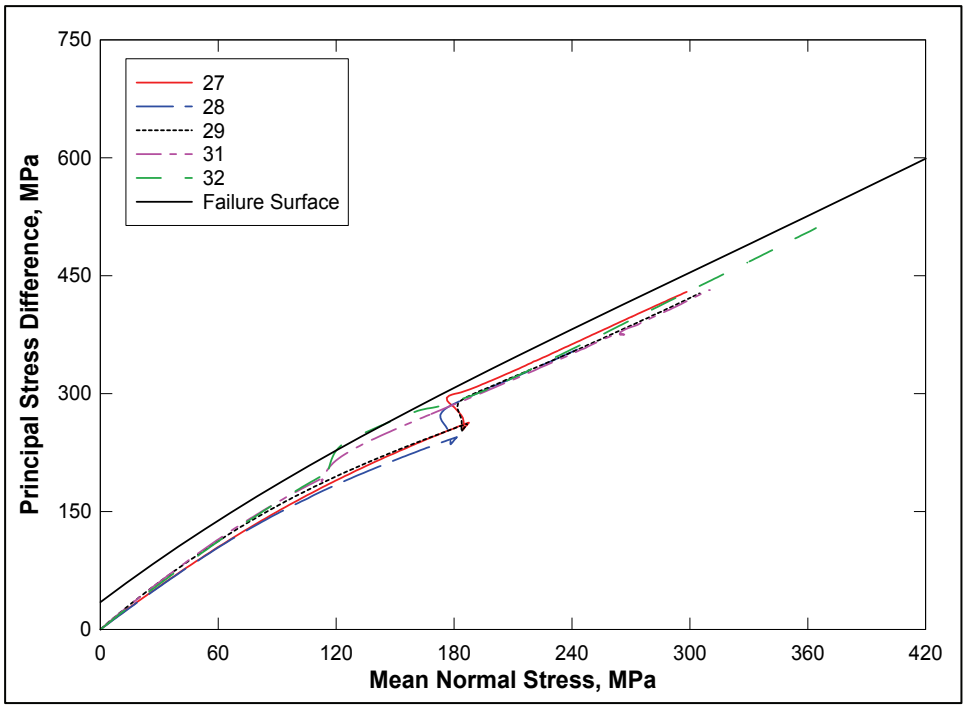

Figure 41. Stress paths from UX/CV tests and failure surface from TXC tests

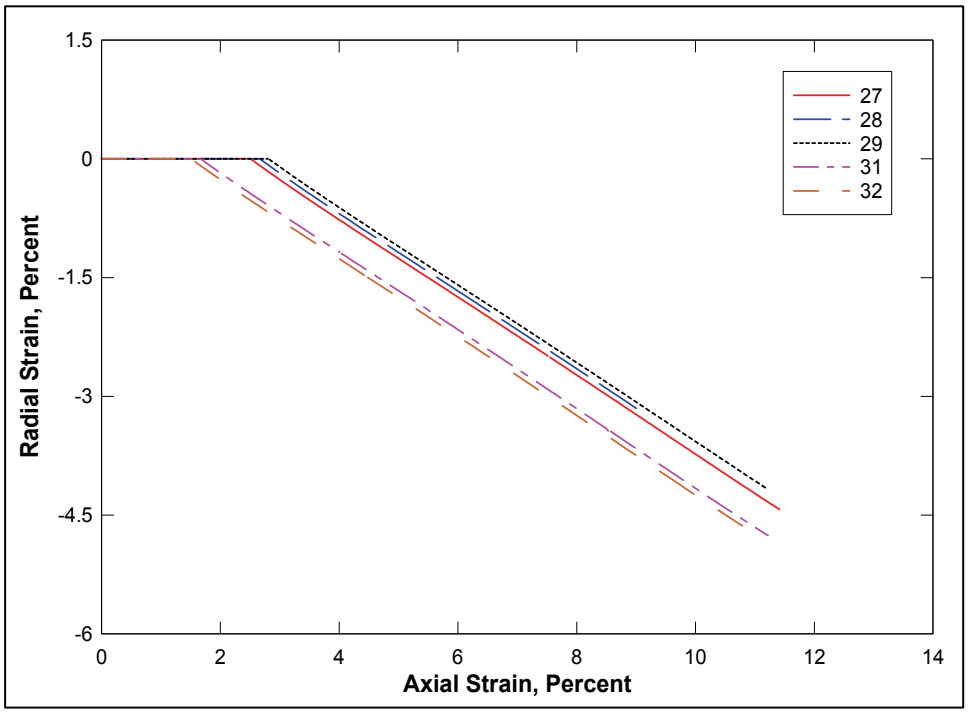

Figure 42. Strain paths from UX/CV tests

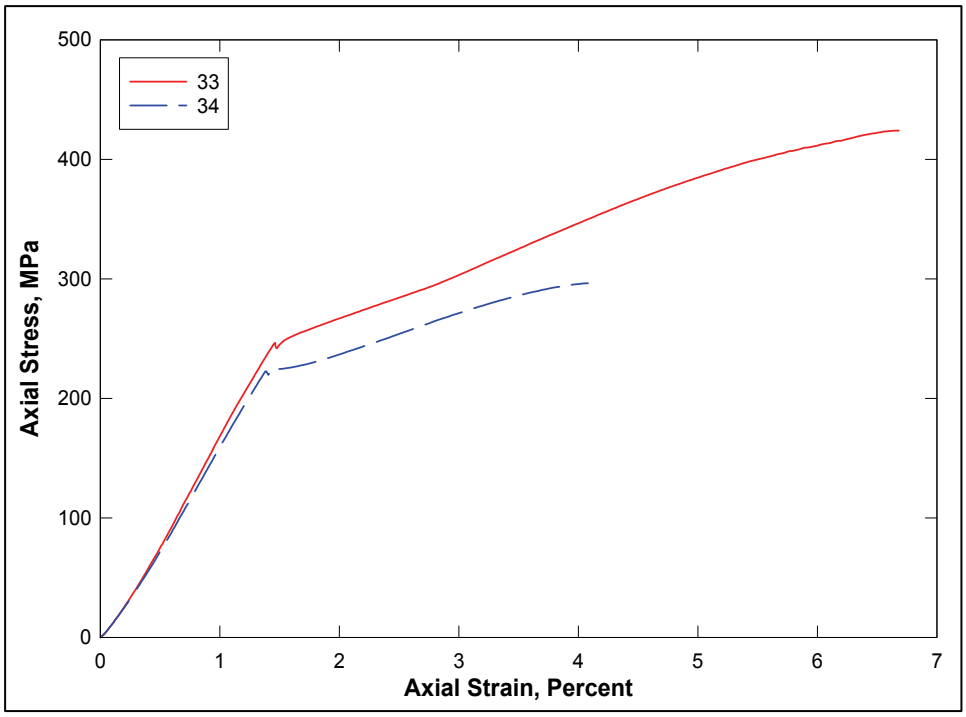

Figure 43. Stress-strain curves from UX/SP tests

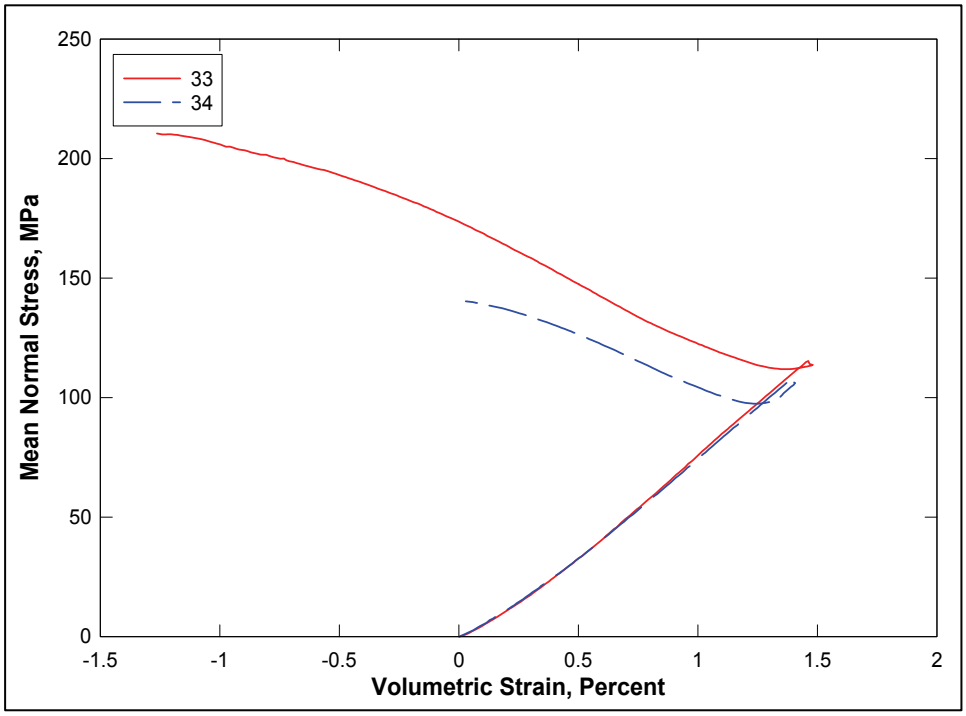

Figure 44. Pressure-volume data from UX/SP tests

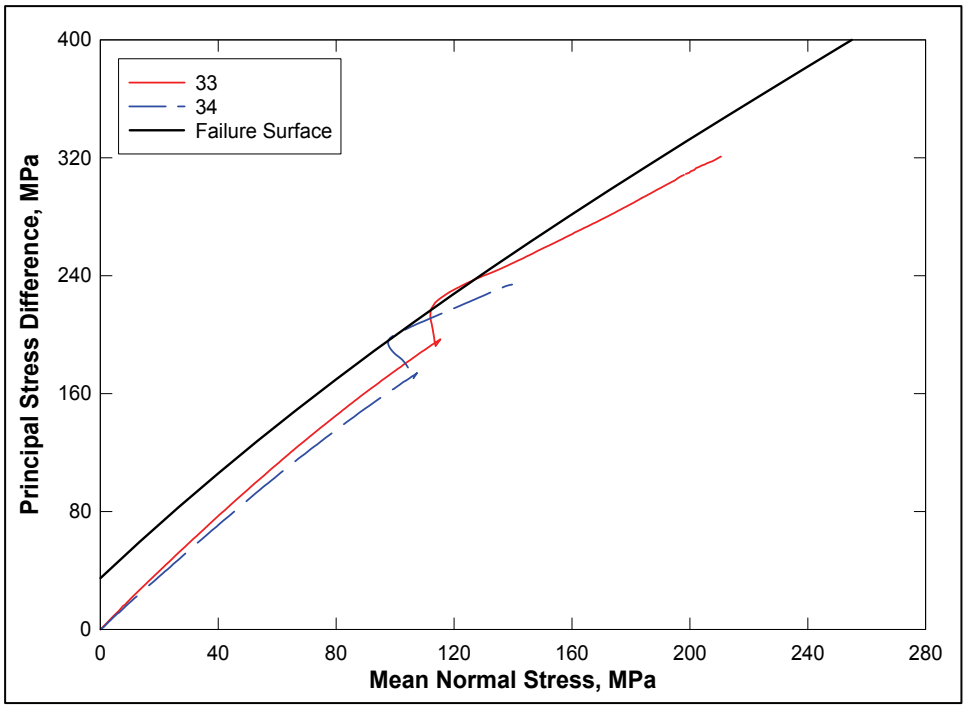

Figure 45. Stress paths from UX/SP tests and failure surface from TXC tests

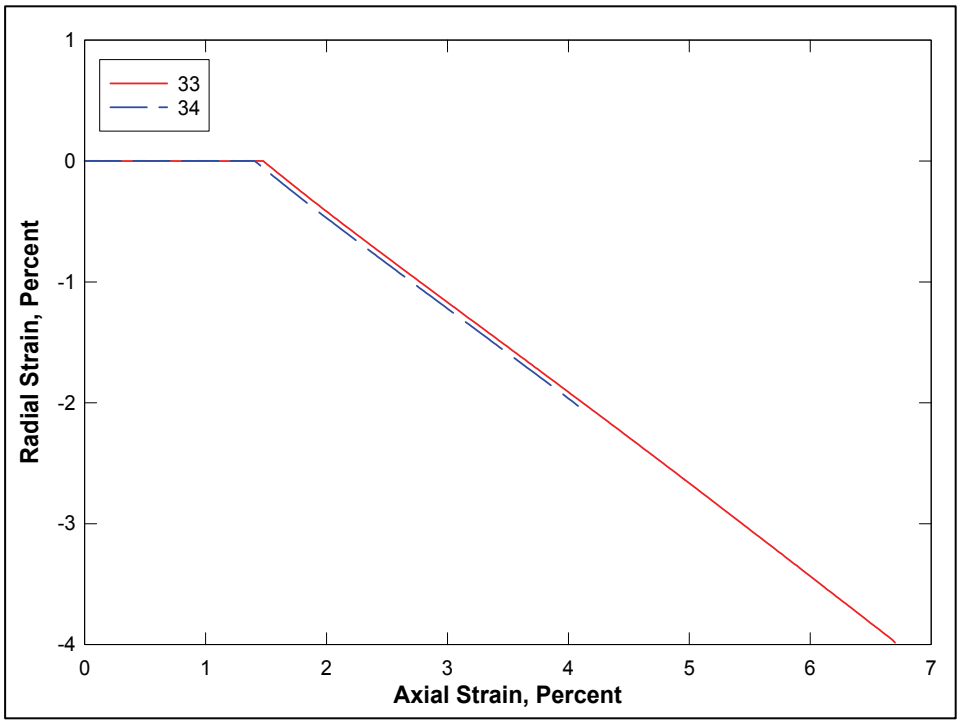

Figure 46. Strain paths from UX/SP tests

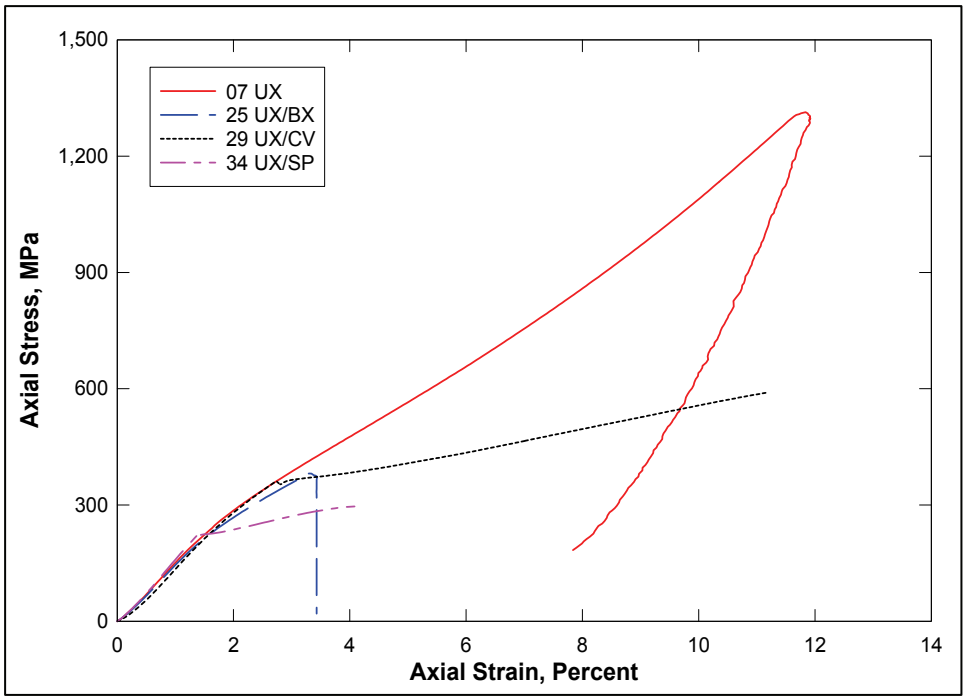

Figure 47. Stress-strain curves from selected UX, UX/BX, UX/CV, and UX/SP tests

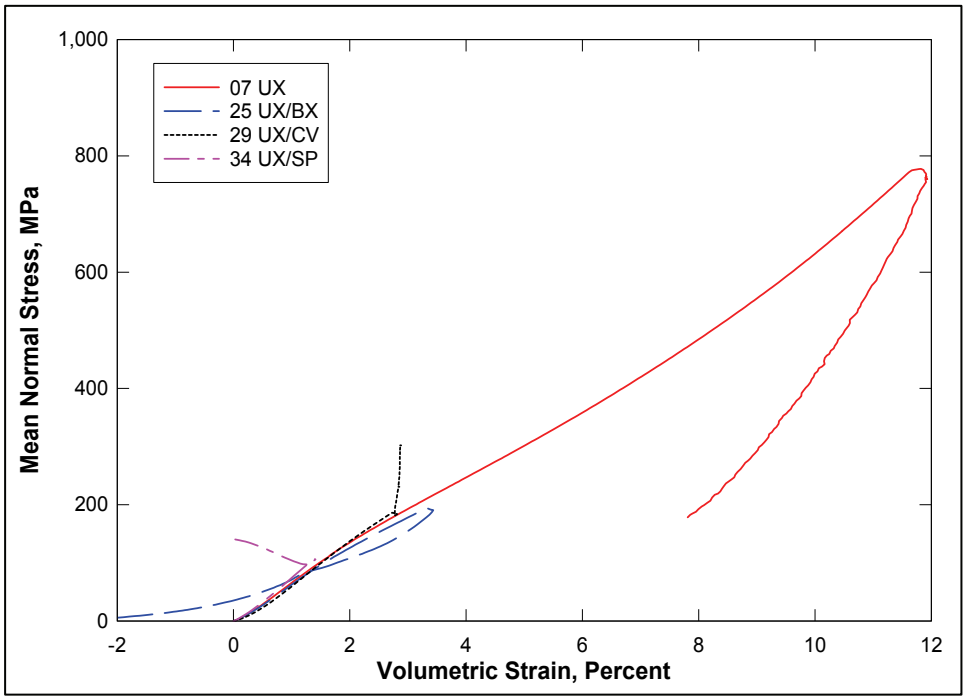

Figure 48. Pressure-volume data from selected UX, UX/BX, UX/CV, and UX/SP tests

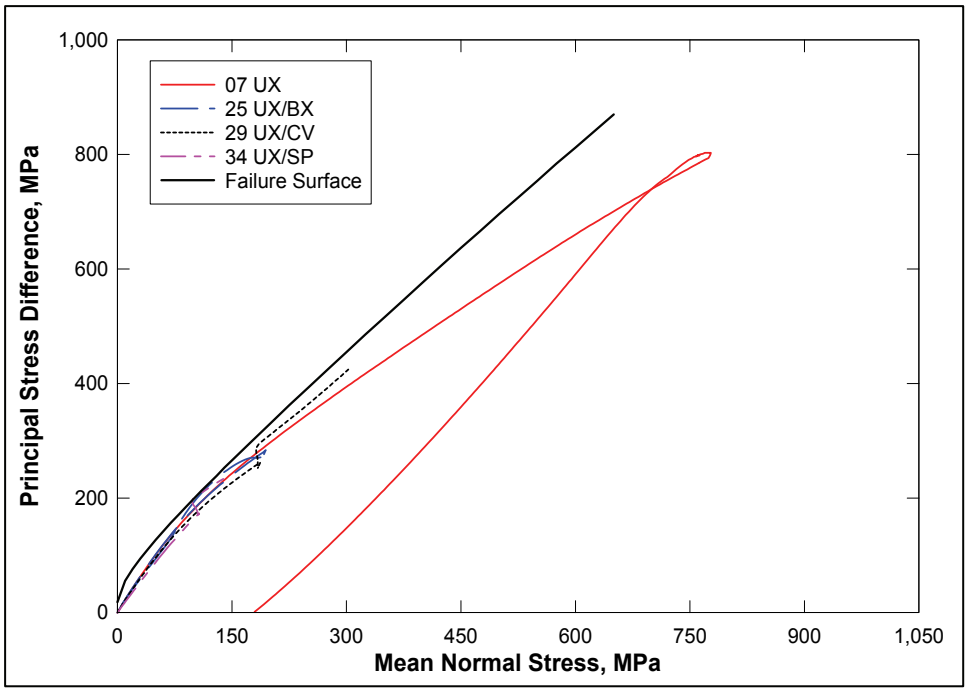

Figure 49. Stress paths from selected UX, UX/BX, UX/CV, and UX/SP tests and failure surface from TXC tests

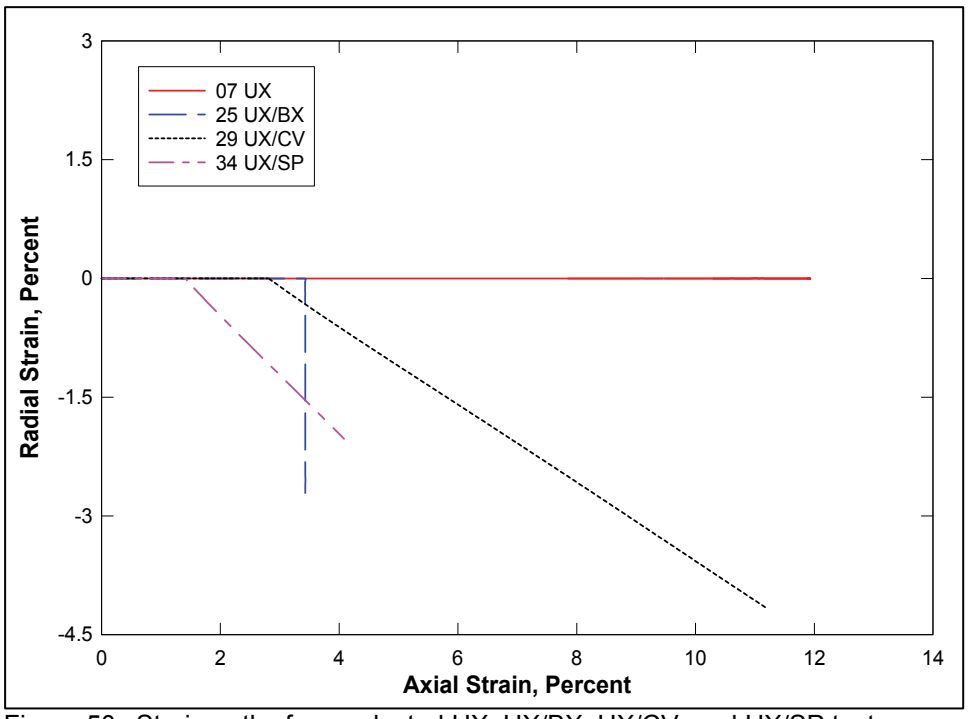

Figure 50. Strain paths from selected UX, UX/BX, UX/CV, and UX/SP tests

4 Summary

Personnel in the Geotechnical and Structures Laboratory of the U.S. Army Engineer Research and Development Center conducted a laboratory investigation to characterize the strength and constitutive property behavior of solid Grade SW brick. ERDC conducted 37 successful mechanical property tests consisting of two hydrostatic compression tests, four unconfined compression tests, 12 triaxial compression tests, two constant mean normal stress tests, four direct pull tests, two uniaxial strain tests, four uniaxial strain load/biaxial strain unload tests, five uniaxial strain load/constant volume strain loading tests, and two uniaxial strain load/constant strain path strain tests. In addition to the mechanical property tests, nondestructive pulse-velocity measurements were performed on each specimen.

The overall quality of the test data was very good; limited scatter was observed in the data over repeated loading paths. Comparisons of the volumetric responses from the HC and UX tests showed that the brick material exhibited increased compaction under shear-induced loading from the UX tests when compared with results from HC tests in which no shear-induced loading occurred. Creep was observed during the HC tests. Results from the TXC tests exhibited a continuous increase in principal stress difference with increasing confining stress. A compression failure surface was developed from the TXC results at six levels of confining pressure and from the results of the UC tests. The results for the DP tests were used to evaluate the tensile strength of the brick. During UX/BX tests, stress relaxation was evident during the change from uniaxial strain loading to biaxial strain unloading. Good correlations were observed between the stress paths obtained from the UX/BX, UX/CV, and UX/SP strain path tests and the failure surface from the TXC tests.

References

American Society for Testing and Materials. (2002). *2002 annual book of ASTM standards*, Philadelphia, PA.

a. Designation C 39-01. "Standard test method for compressive strength of concrete specimens."
b. Designation C 42-99. "Standard test method for obtaining and testing drilled cores and sawed beams of concrete."
c. Designation C 597-97. "Standard test method for pulse velocity through concrete."
d. Designation C 801-98. "Standard test method for determining the mechanical properties of hardened concrete under triaxial loads."
e. Designation D 2216-98. "Standard test method for laboratory determination of water (moisture) content of soil and rock by mass."
f. Designation D 4543-01. "Standard test method for preparing rock core specimens and determining dimensional and shape tolerances."

Bishop, A. W., and Henkel, D. J. (1962). *The measurement of soil properties in the triaxial test*, Edward Arnold, LTD, London, pp 72-74.

Solid Grade SW Brick
Test No. 06

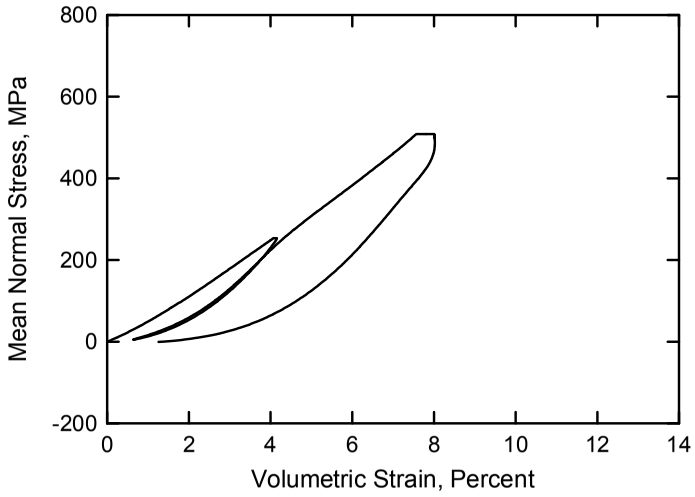

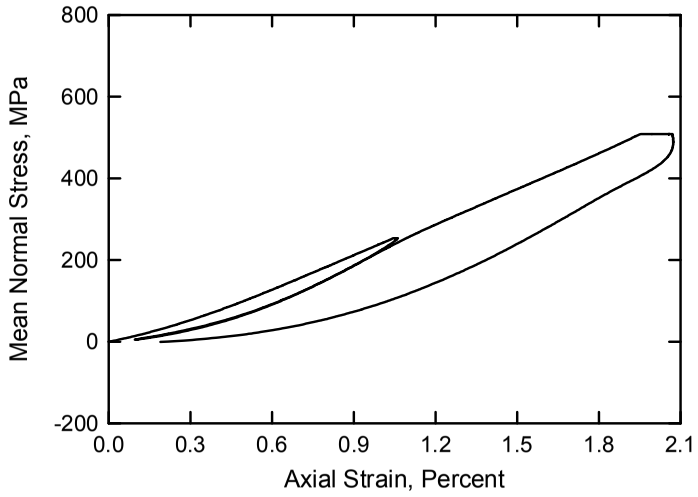

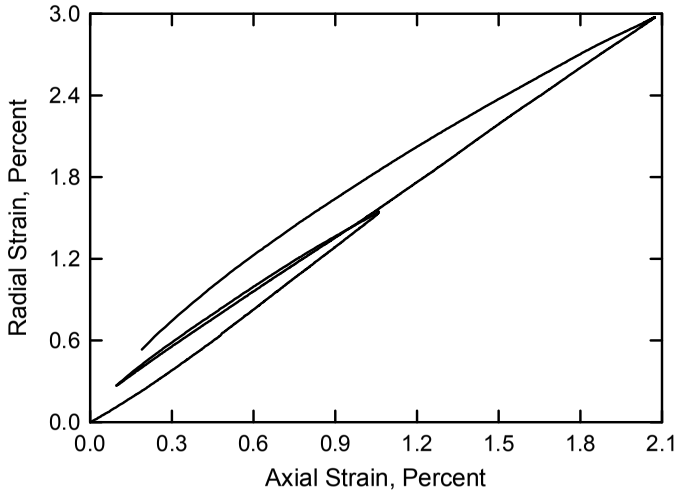

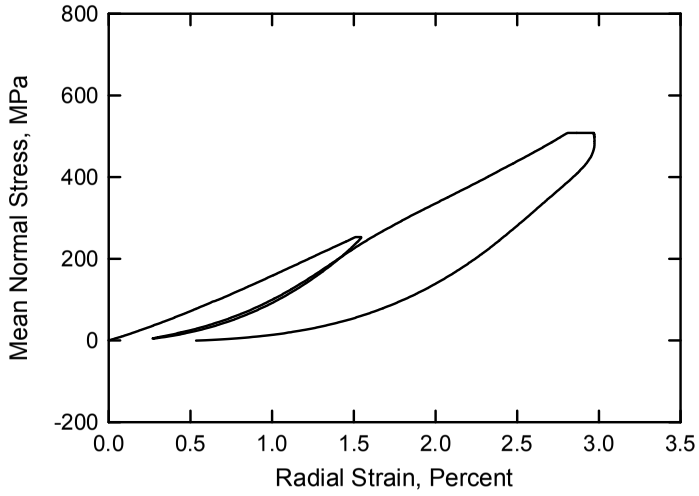

Plate 1

Solid Grade SW Brick
Test No. 22

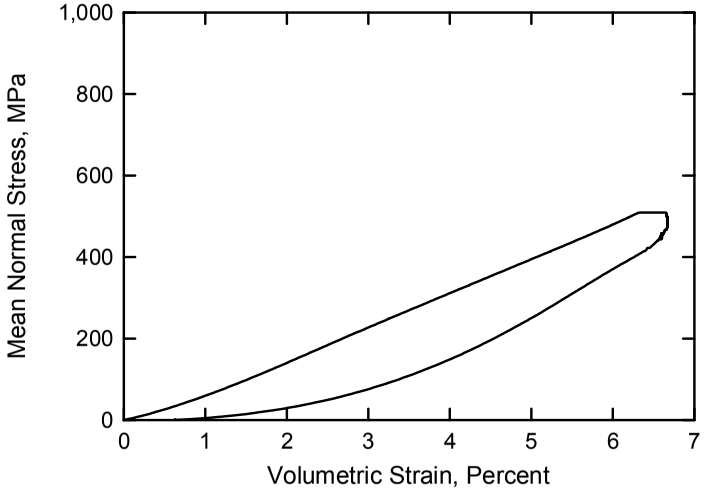

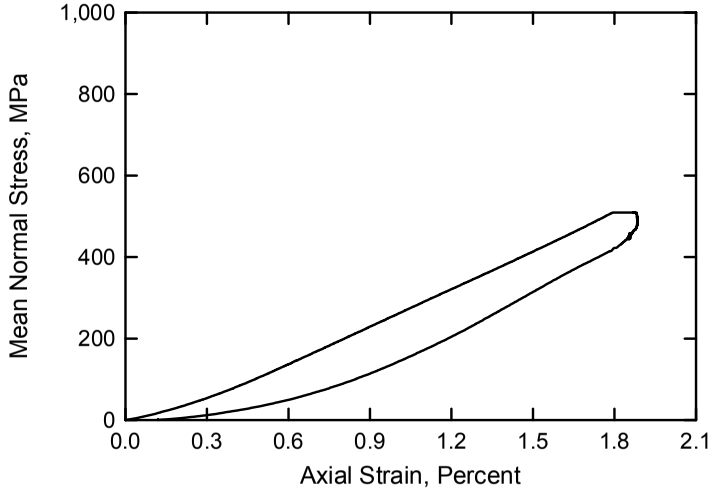

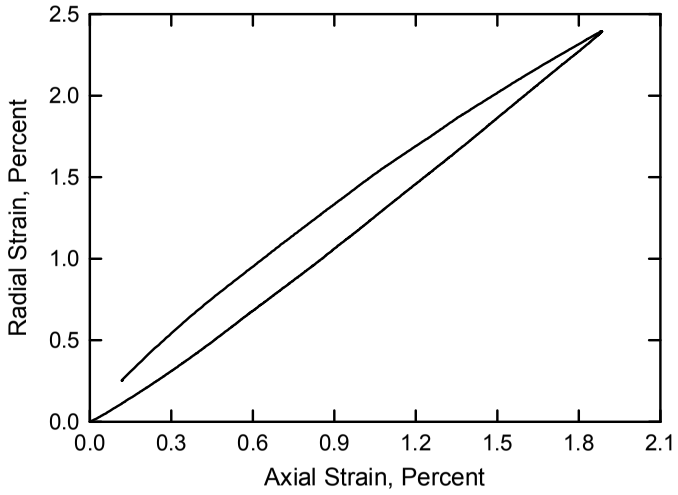

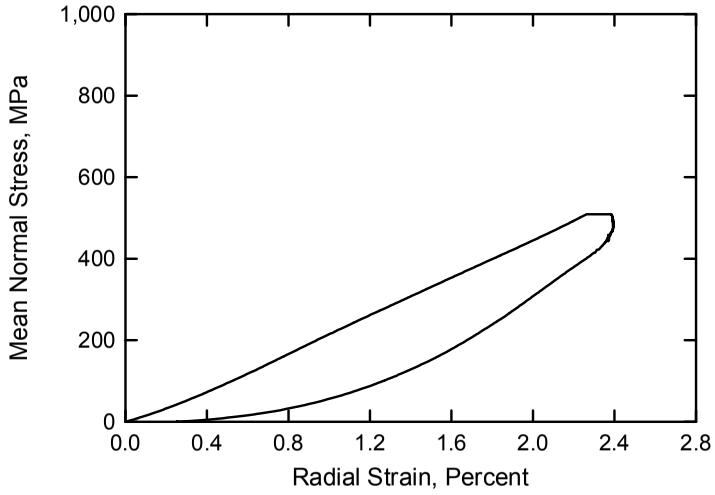

Plate 2

Solid Grade SW Brick
Test No. 01

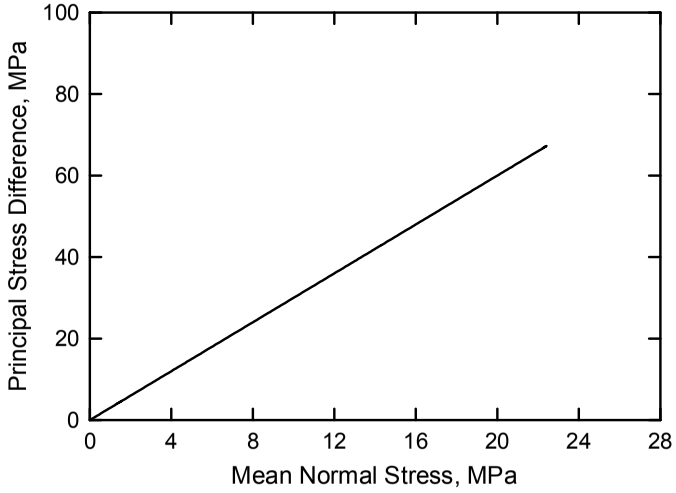

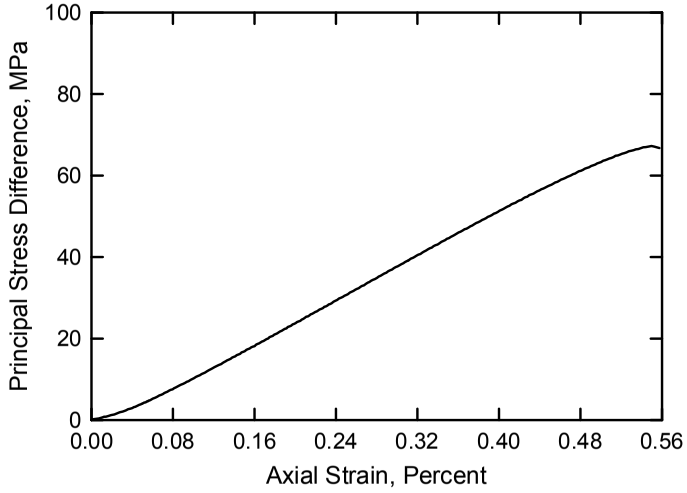

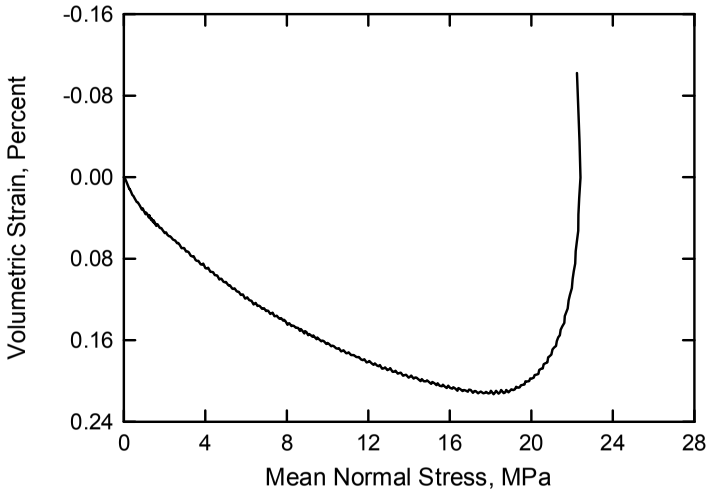

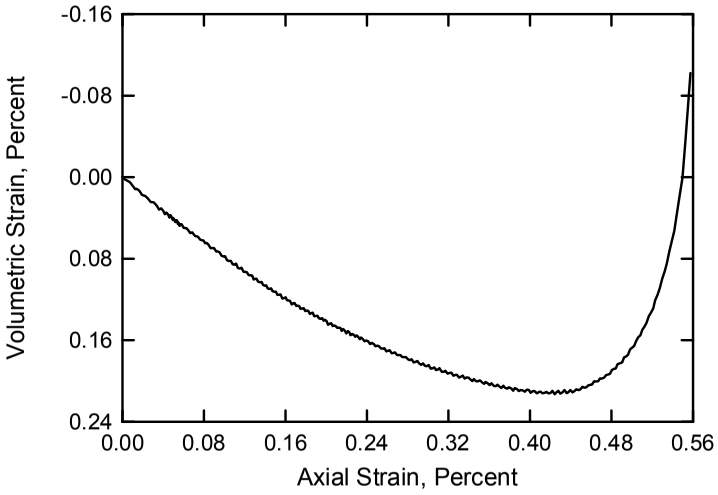

Solid Grade SW Brick
Test No. 02

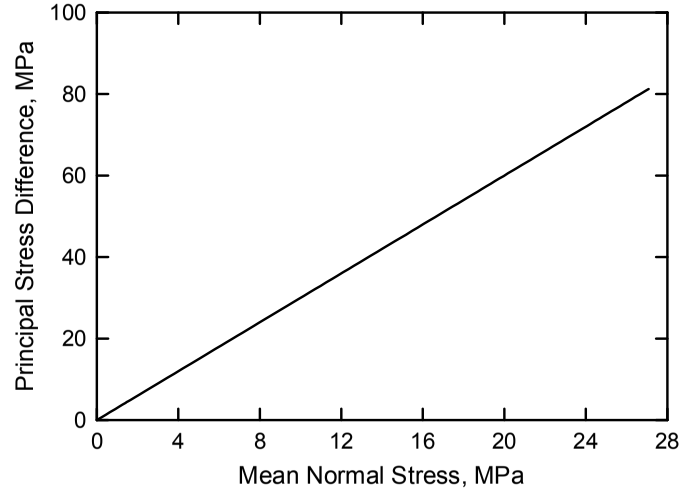

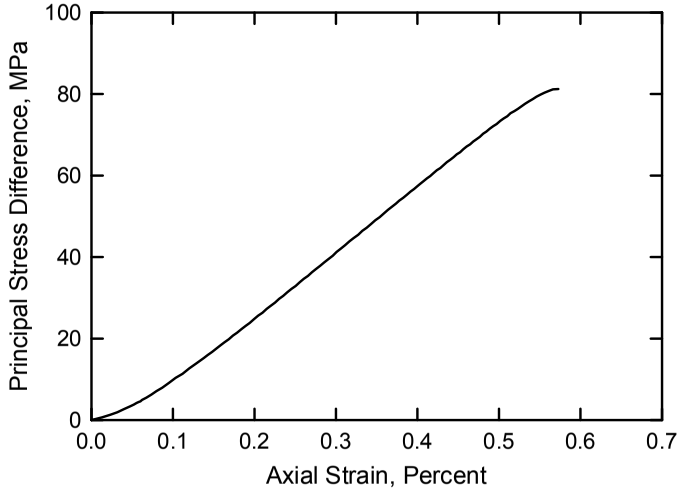

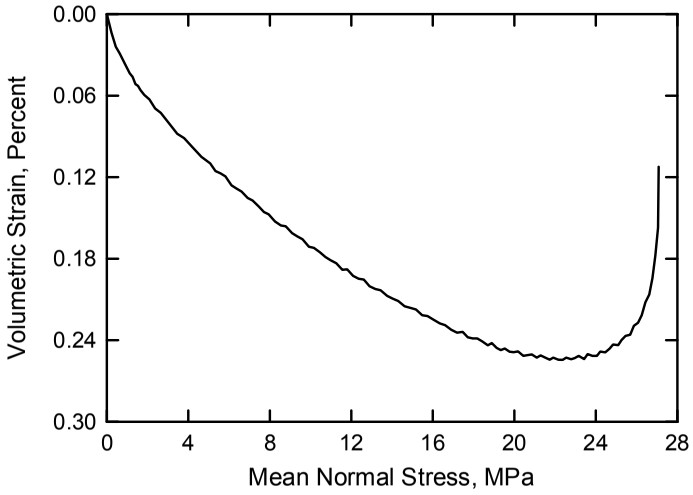

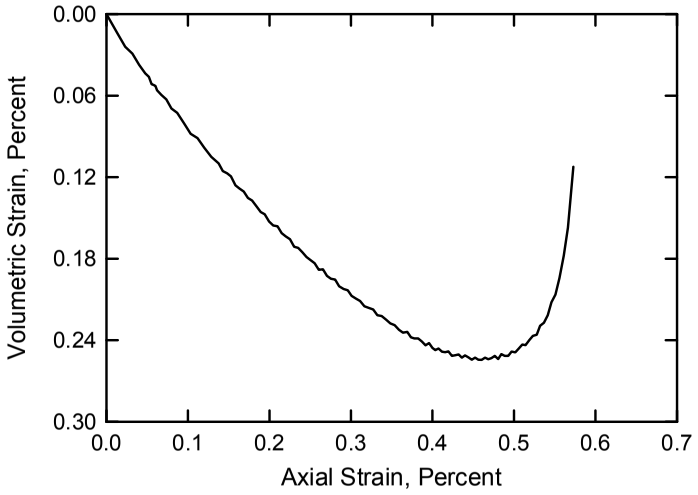

Solid Grade SW Brick
Test No. 03

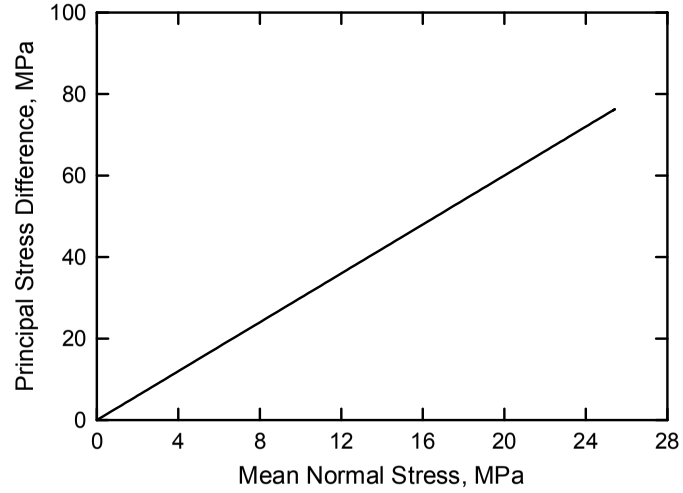

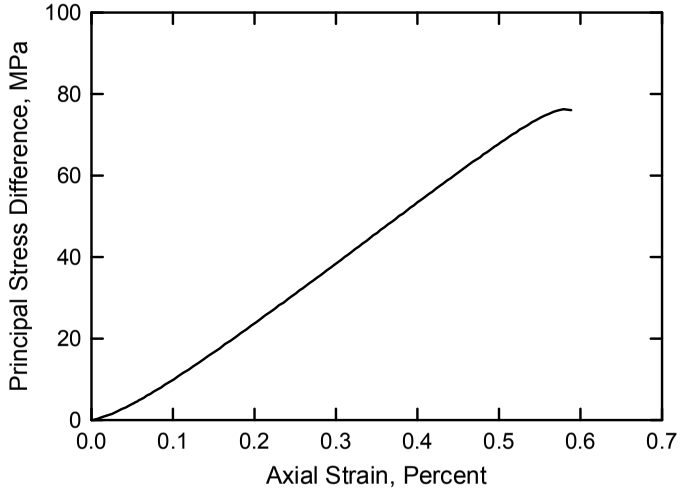

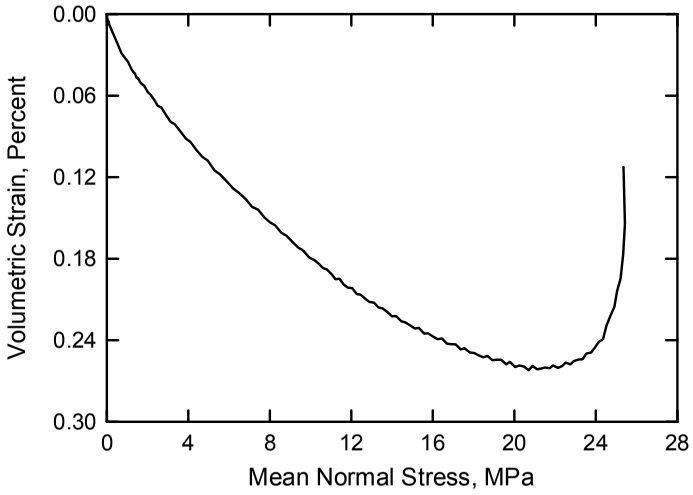

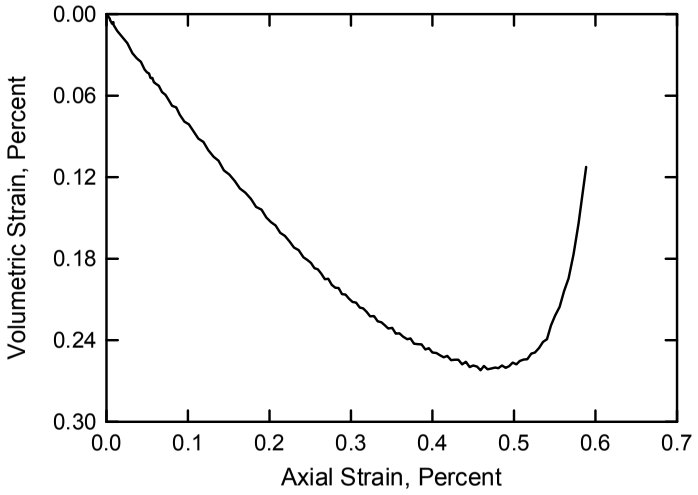

Solid Grade SW Brick
Test No. 04

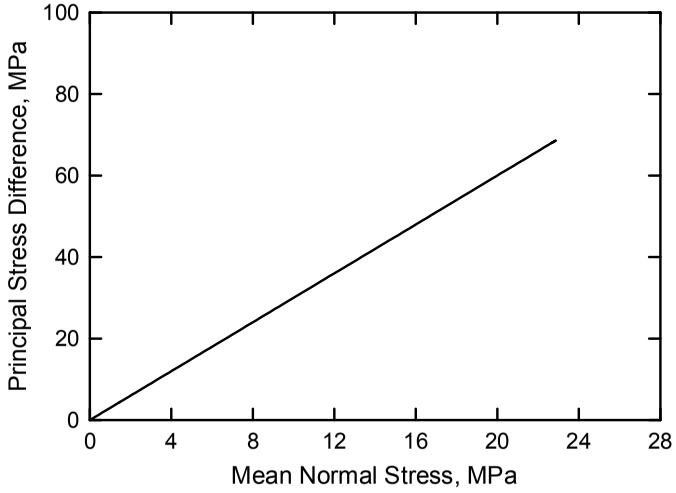

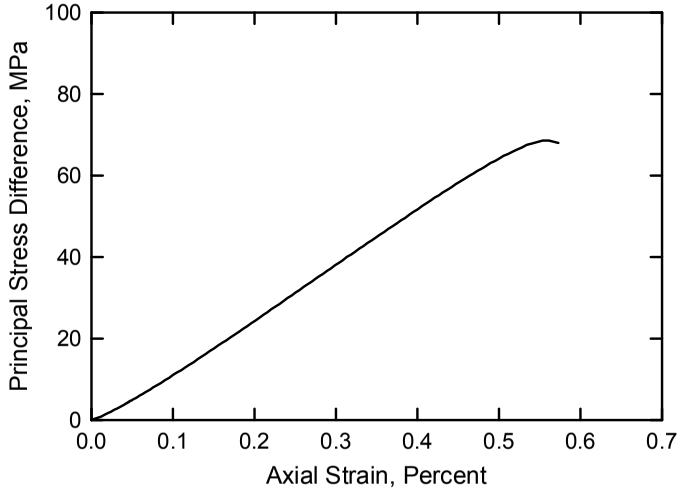

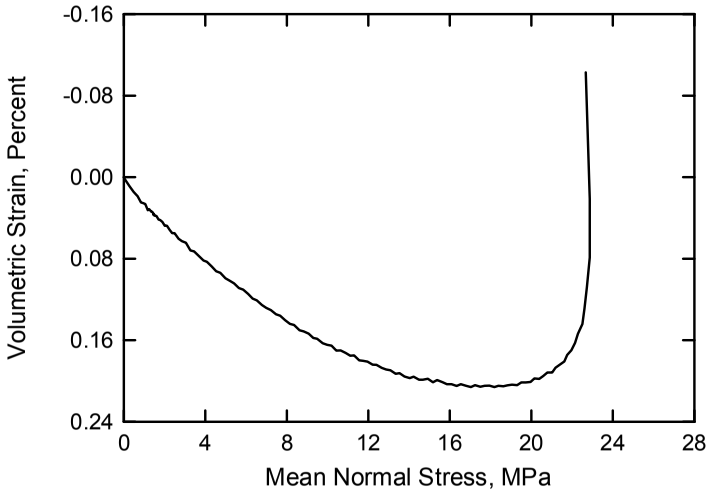

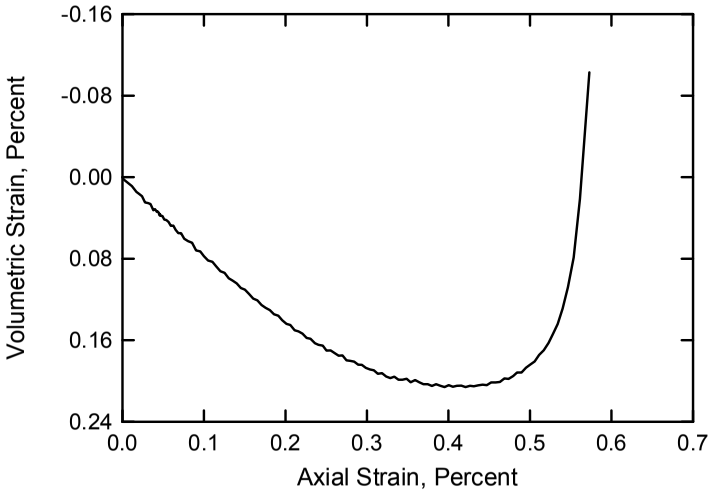

Plate 6

Solid Grade SW Brick
Test No. 9

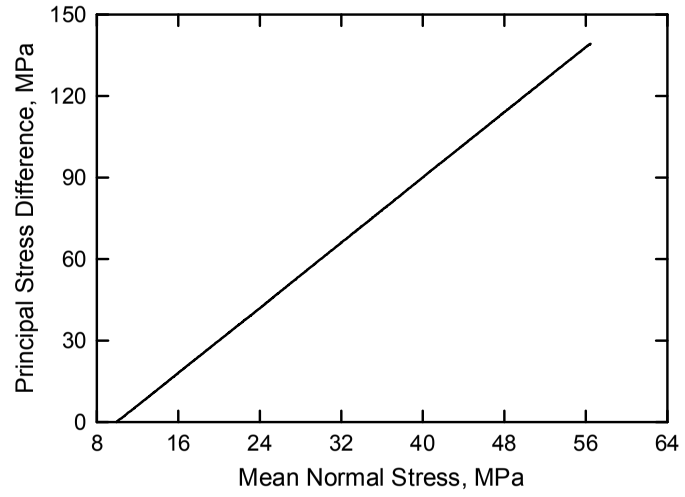

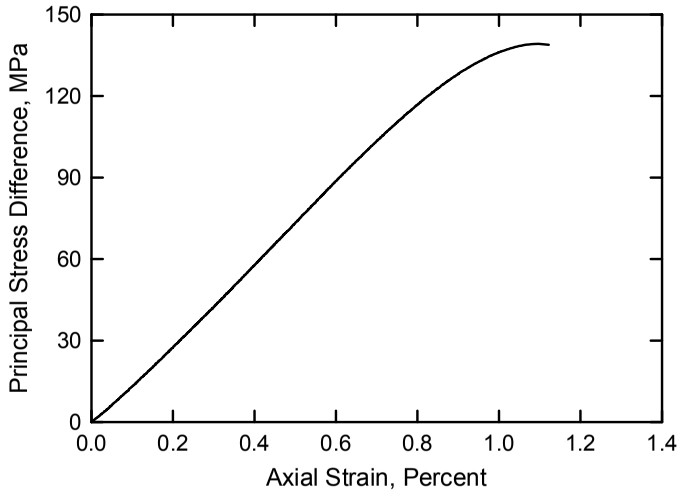

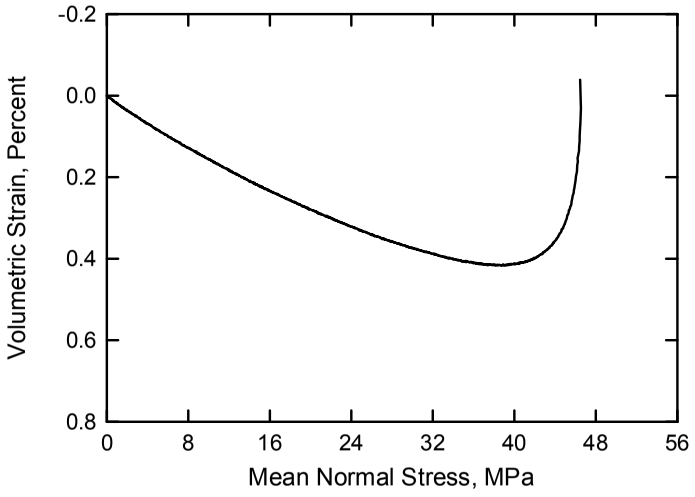

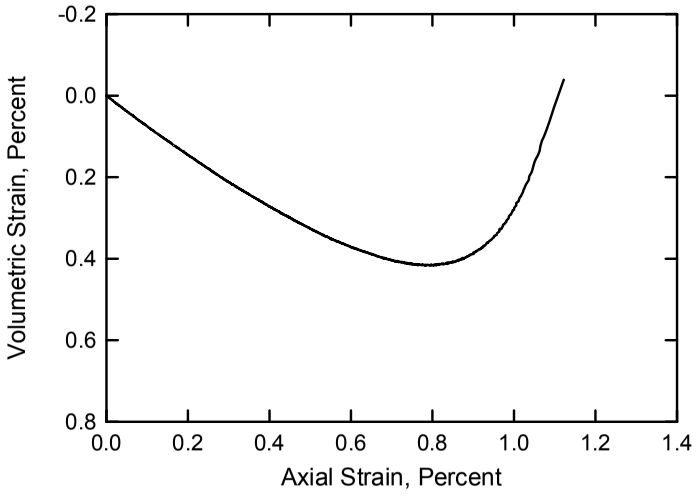

Solid Grade SW Brick
Test No. 10

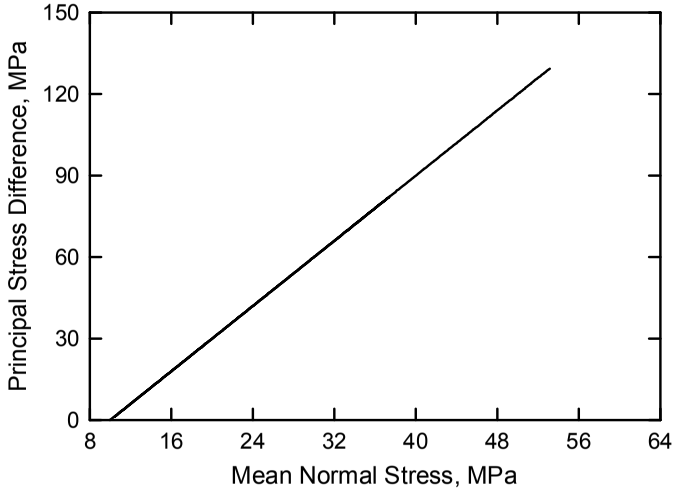

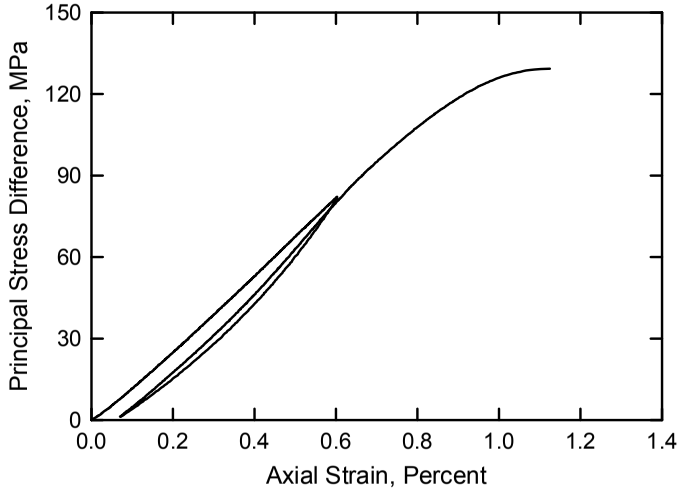

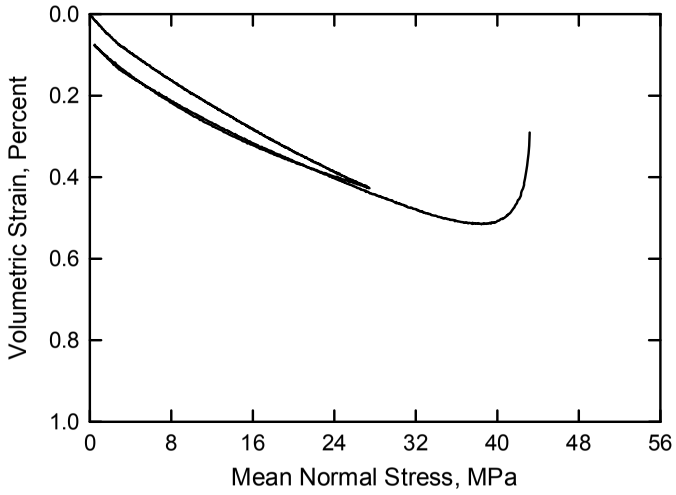

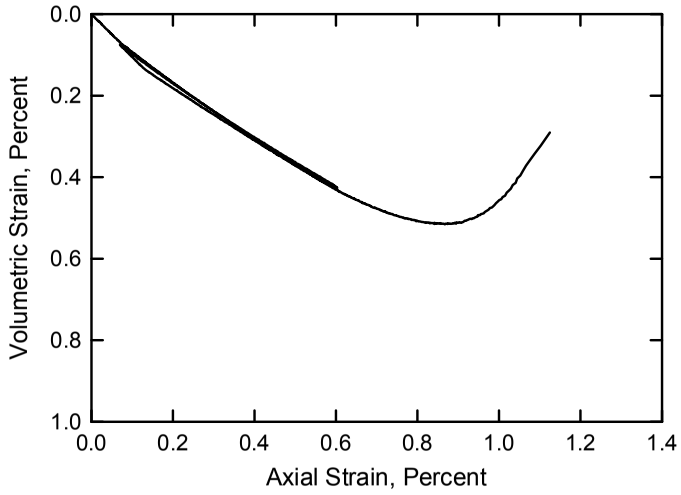

Solid Grade SW Brick
Test No. 11

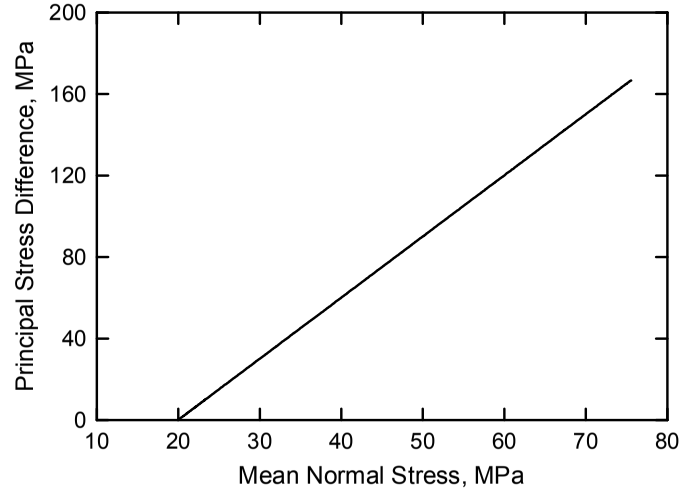

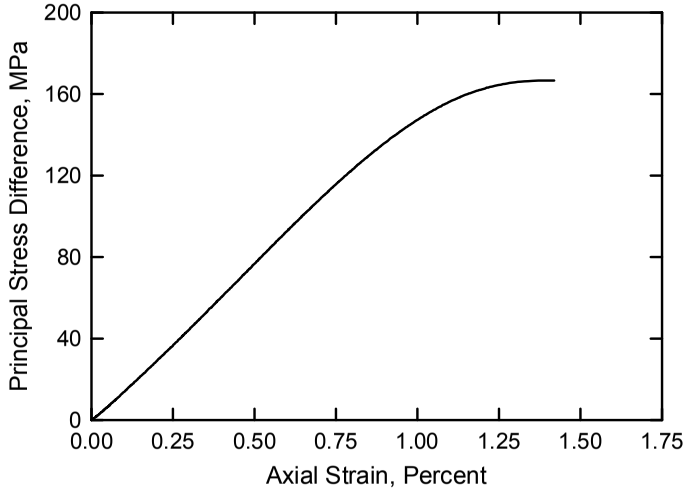

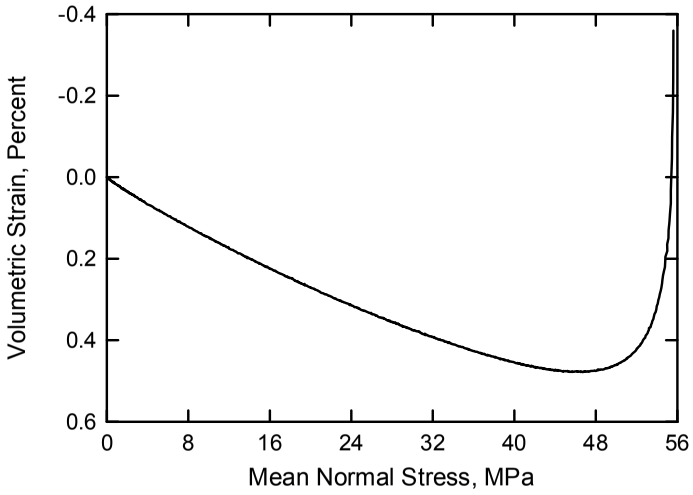

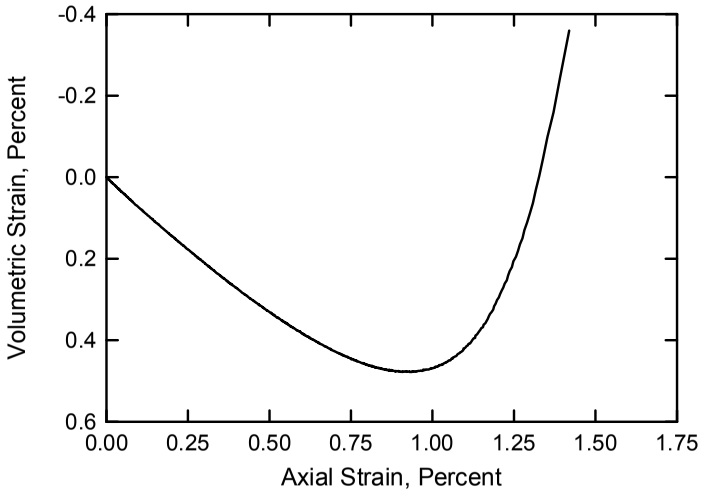

Solid Grade SW Brick
Test No. 12

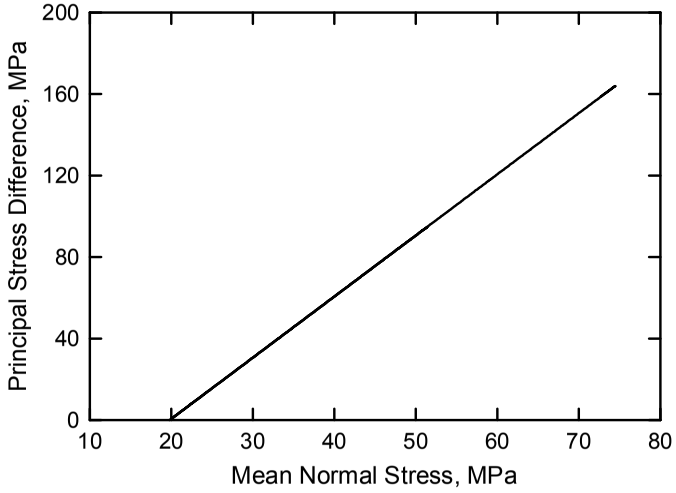

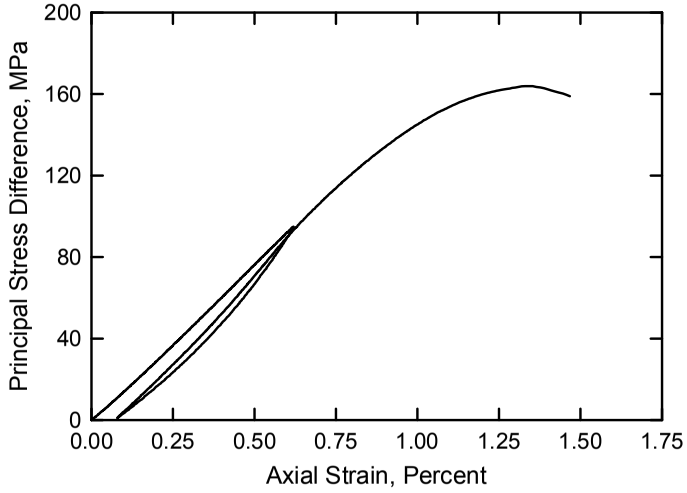

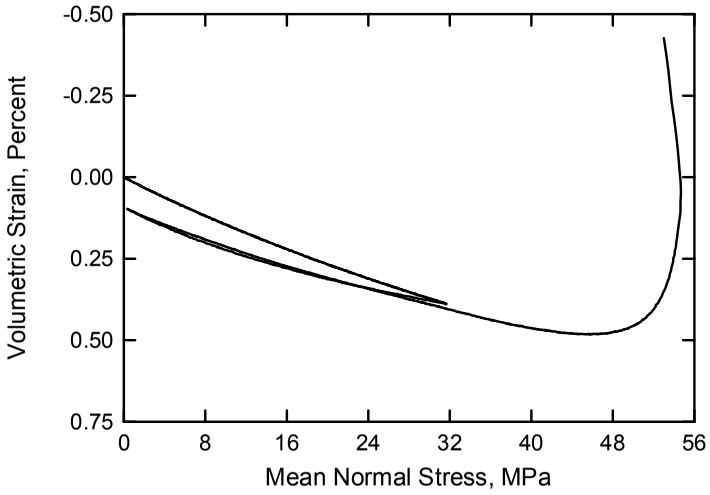

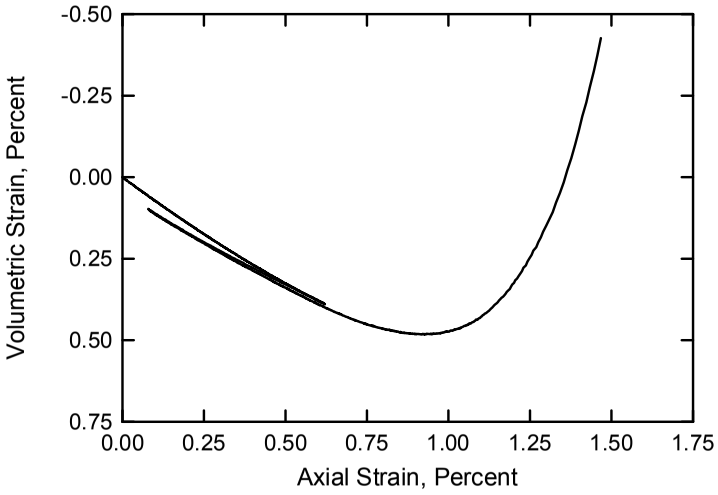

Solid Grade SW Brick
Test No. 13

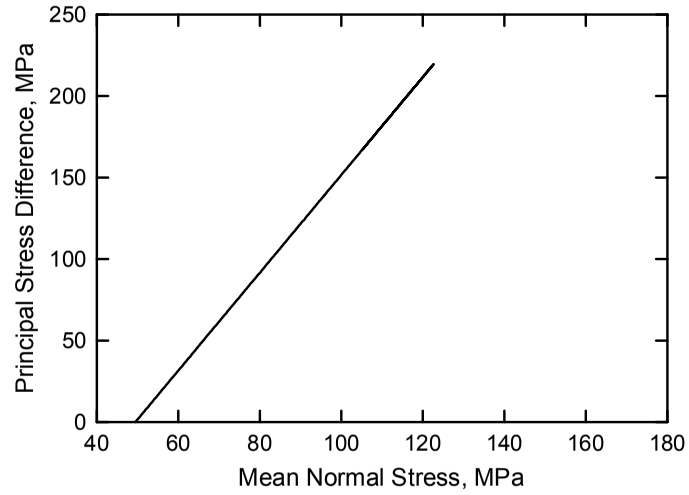

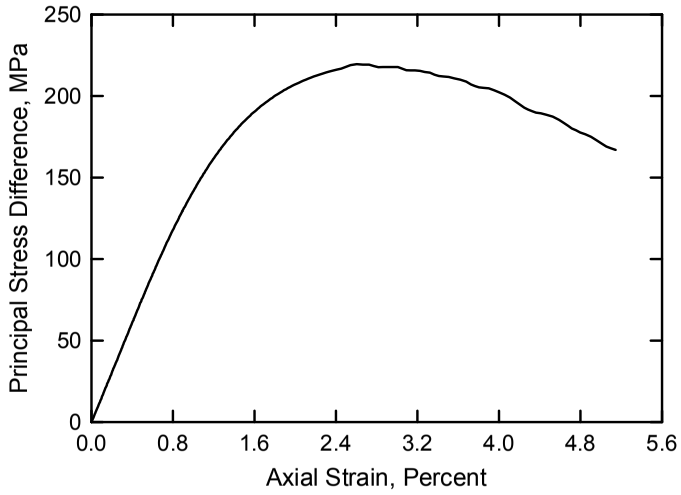

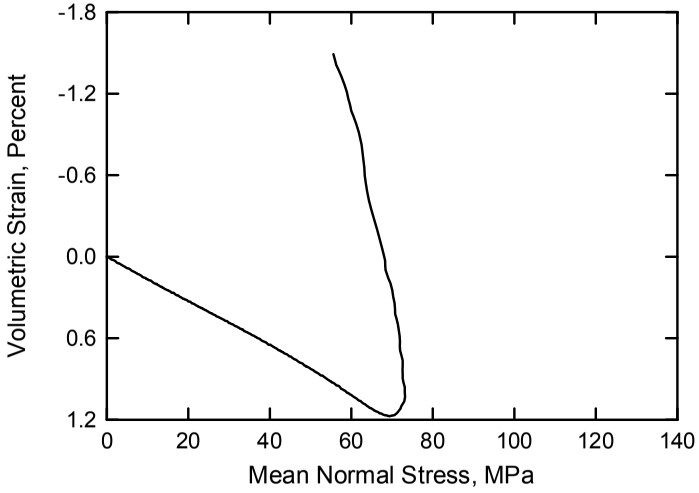

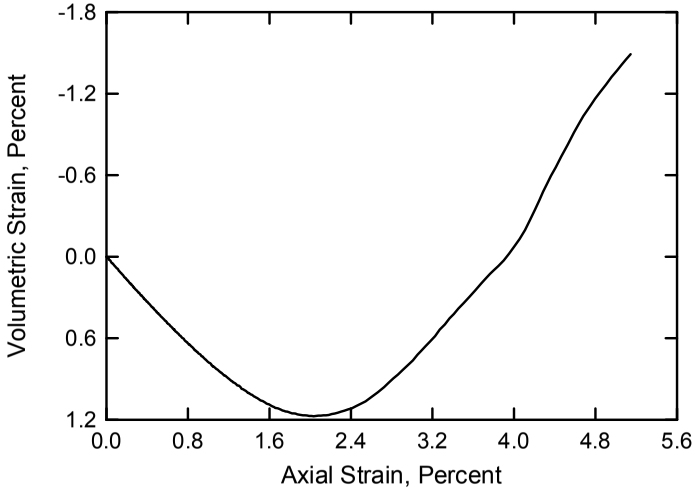

Solid Grade SW Brick
Test No. 14

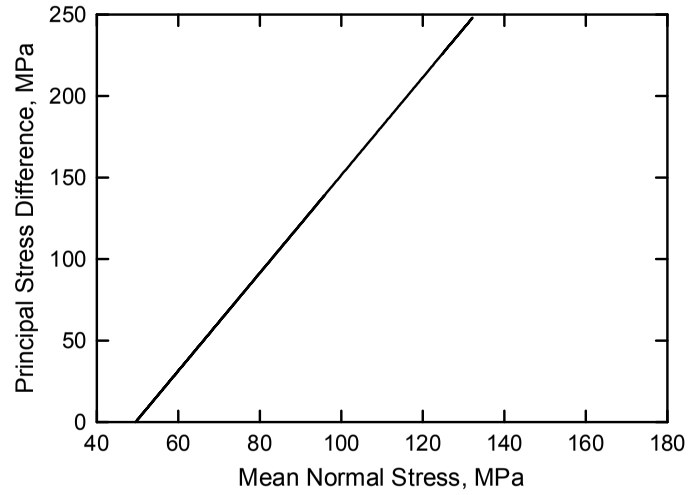

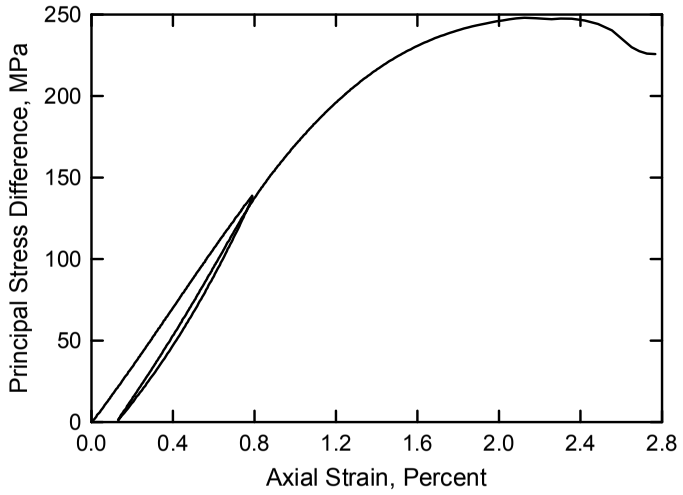

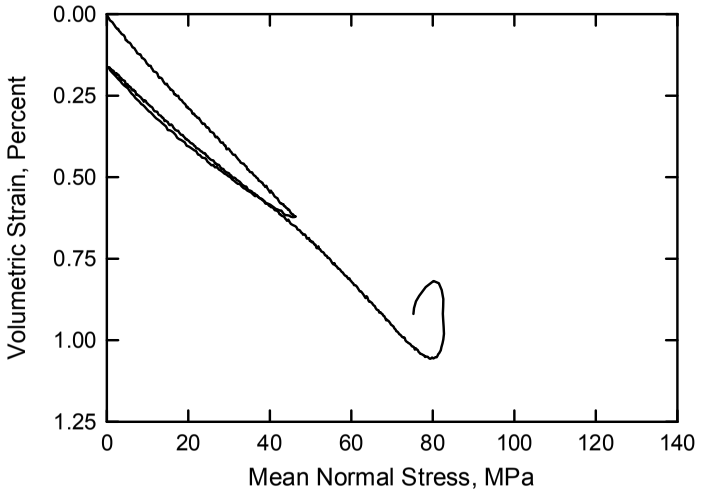

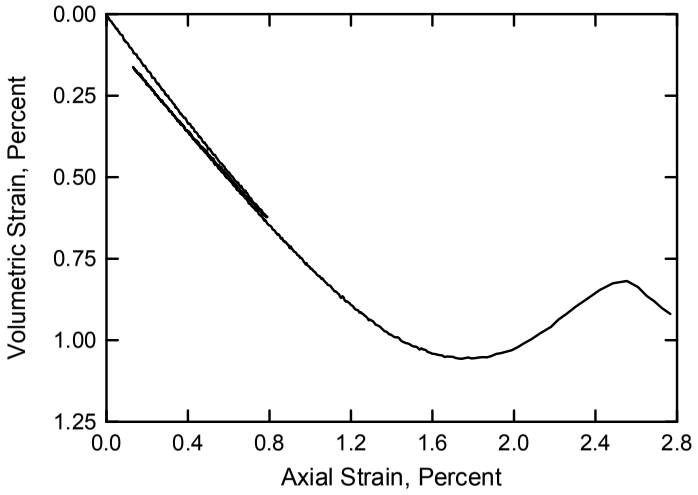

Solid Grade SW Brick
Test No. 16

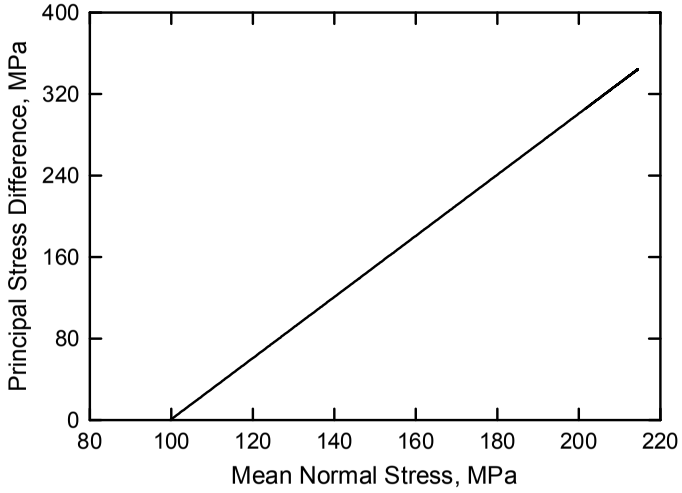

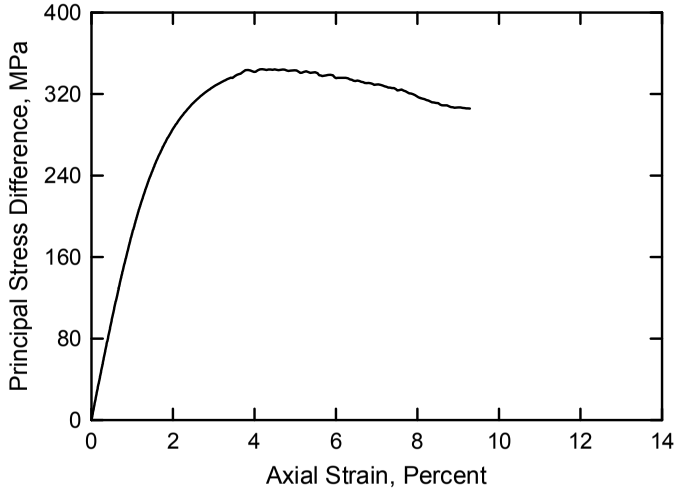

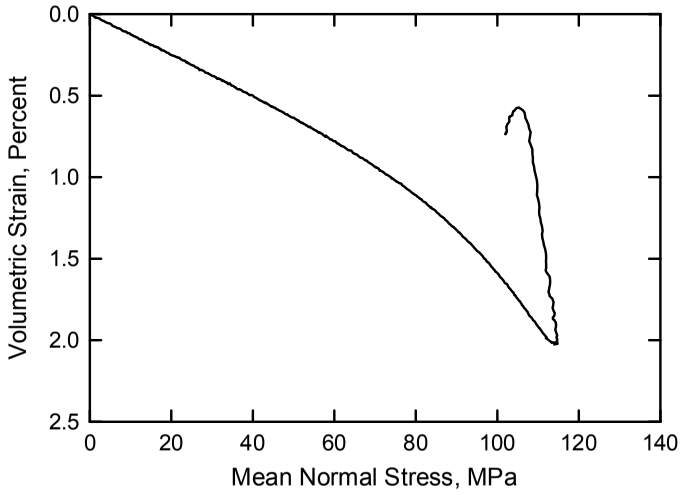

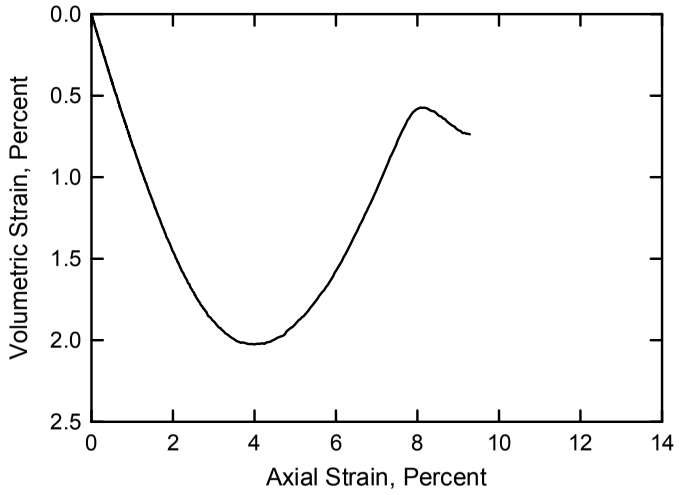

Solid Grade SW Brick
Test No. 17

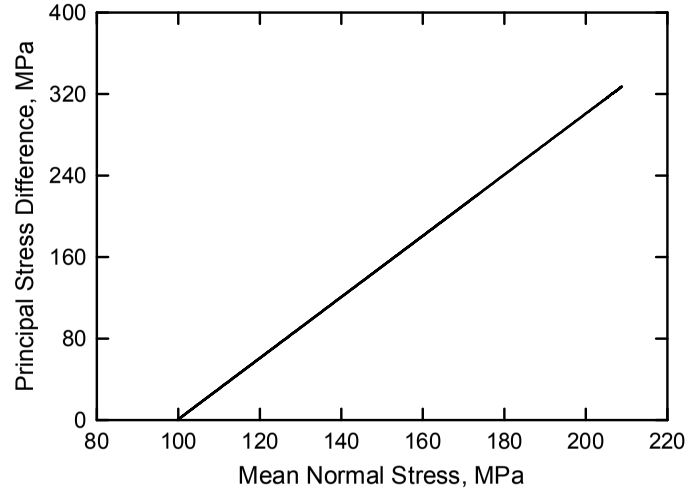

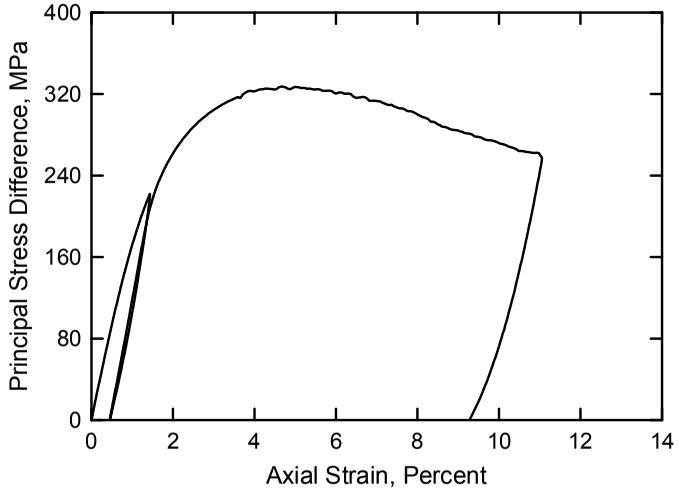

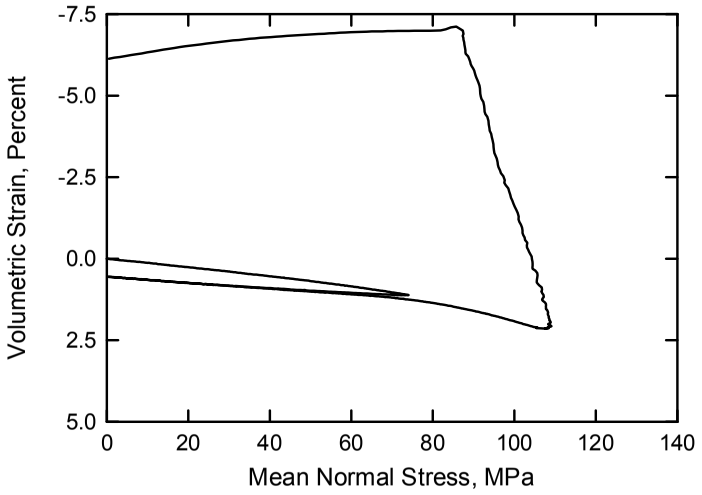

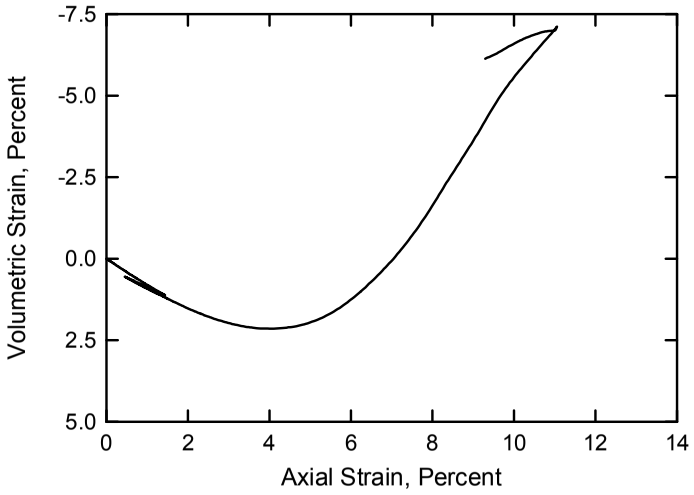

Plate 14

Solid Grade SW Brick
Test No. 15

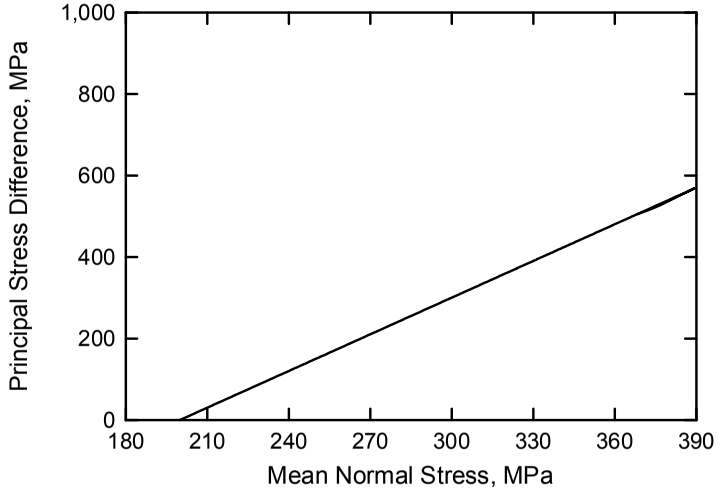

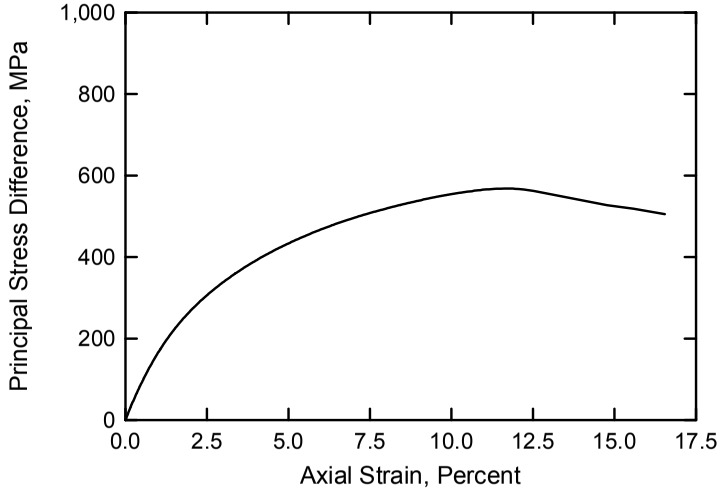

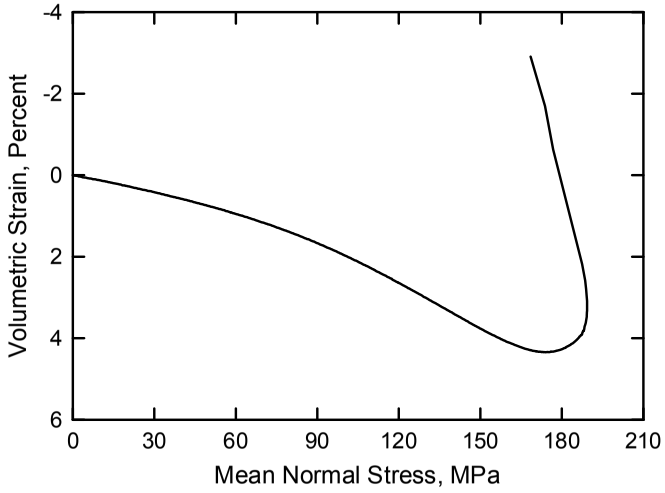

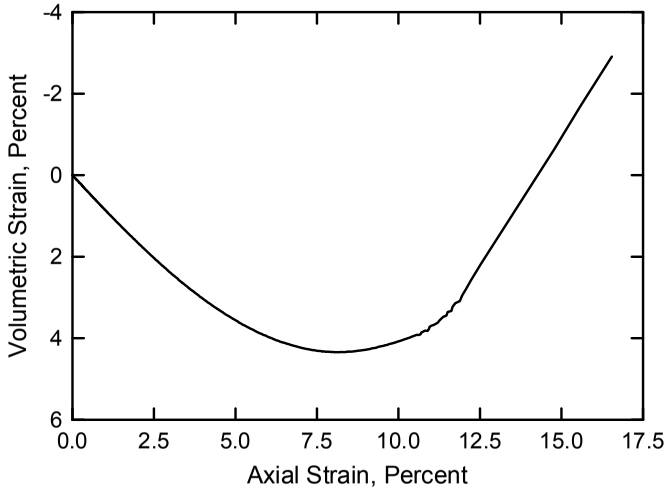

Solid Grade SW Brick
Test No. 18

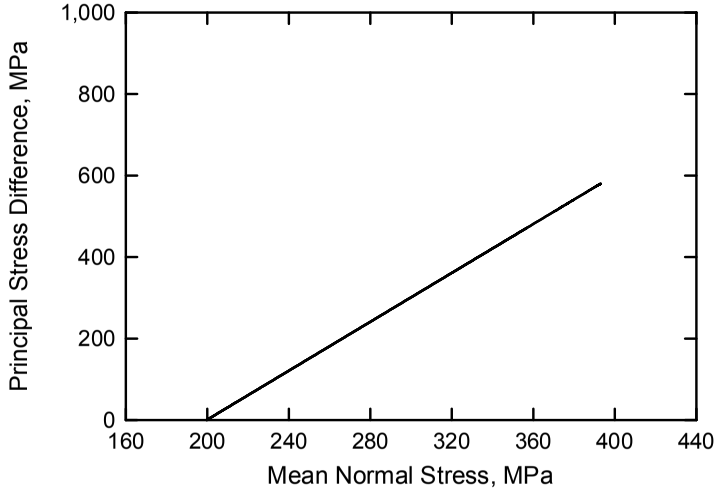

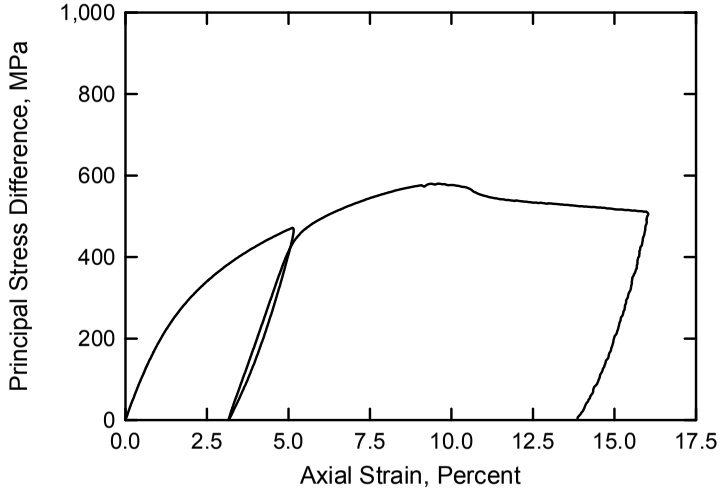

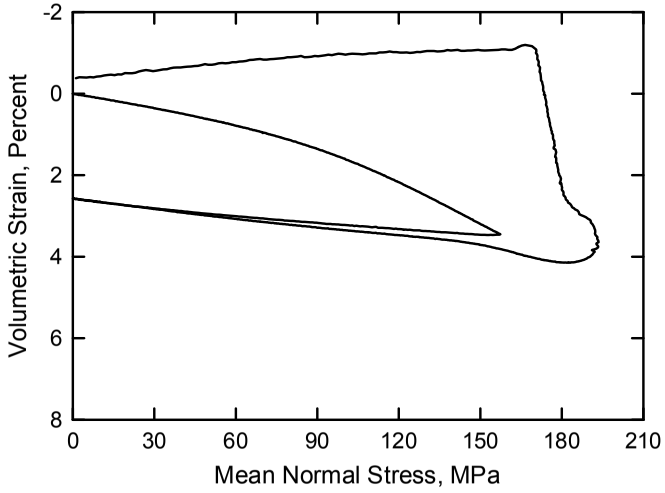

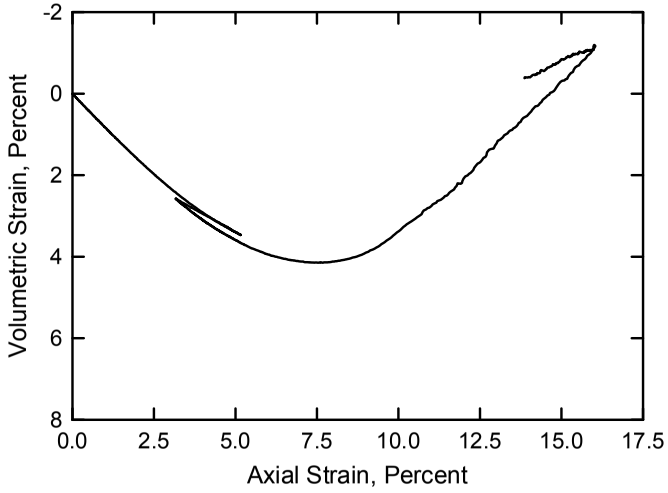

Plate 16

Solid Grade SW Brick
Test No. 20

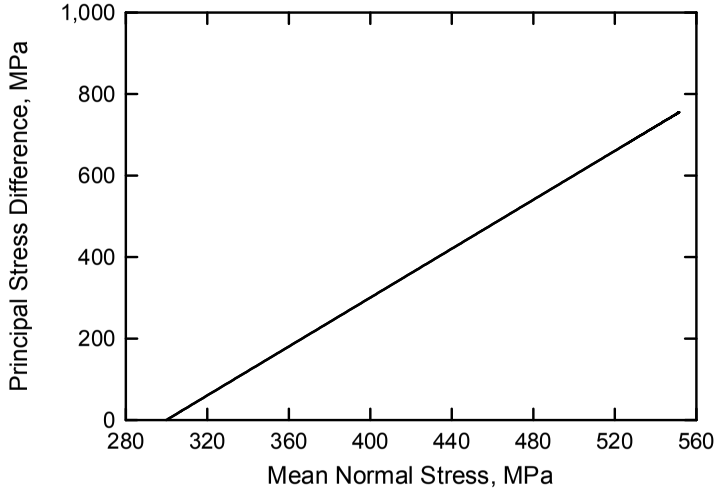

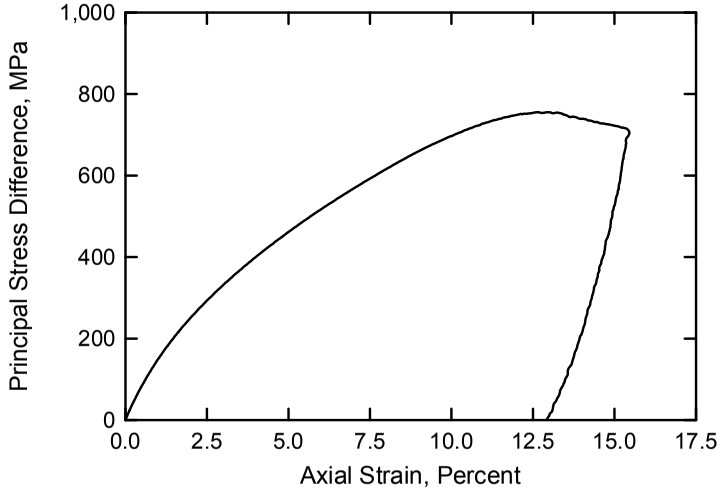

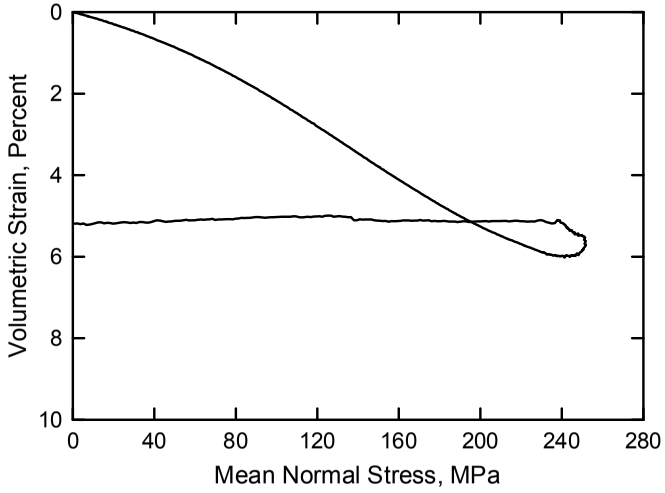

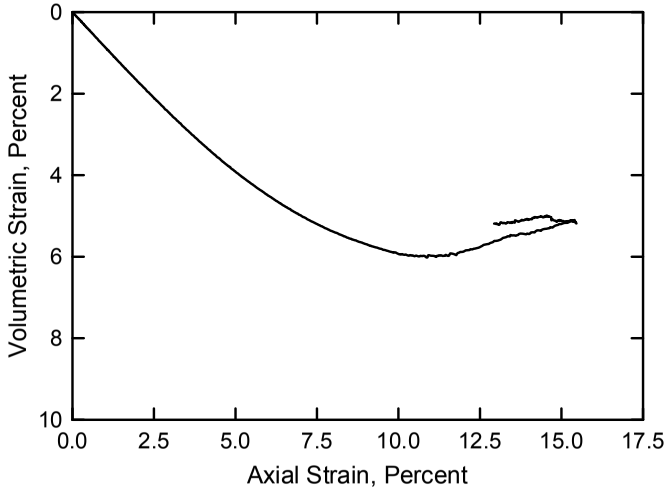

Solid Grade SW Brick
Test No. 35

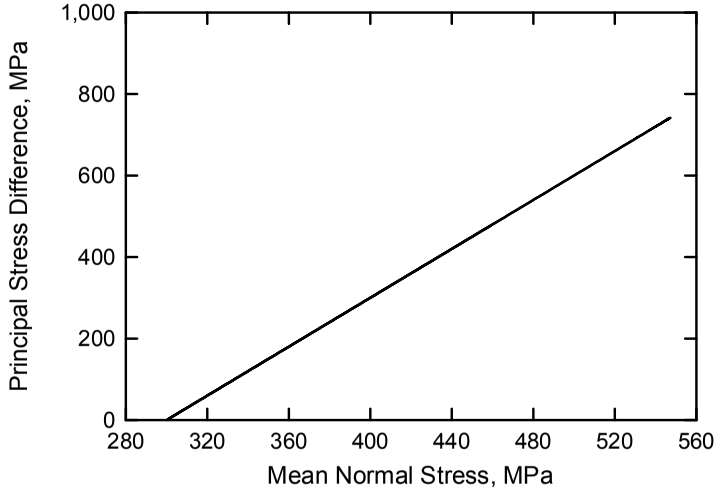

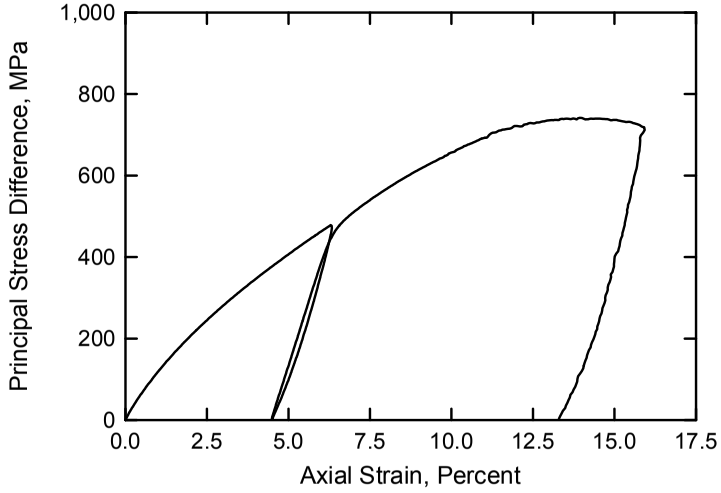

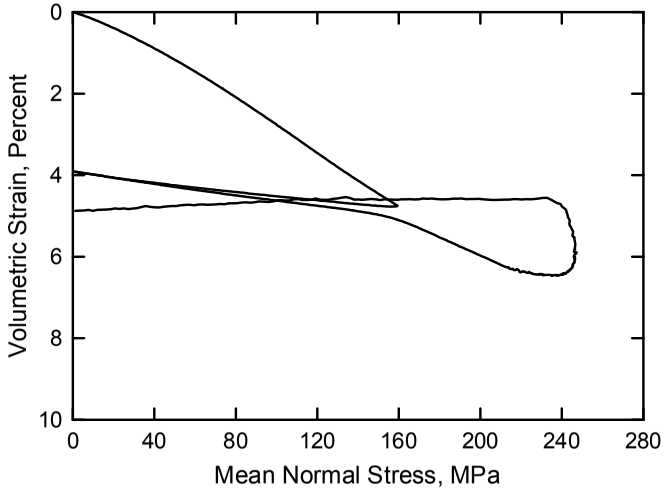

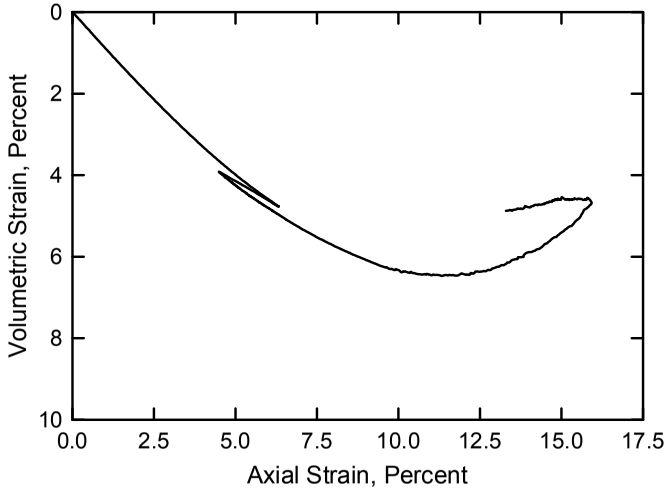

Solid Grade SW Brick
Test No. 40

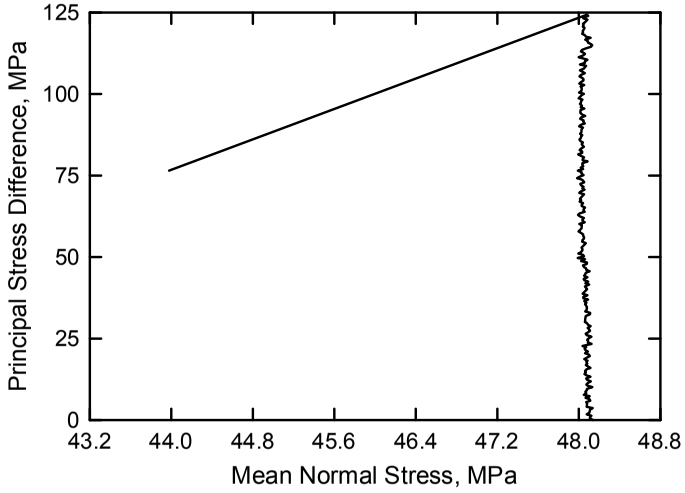

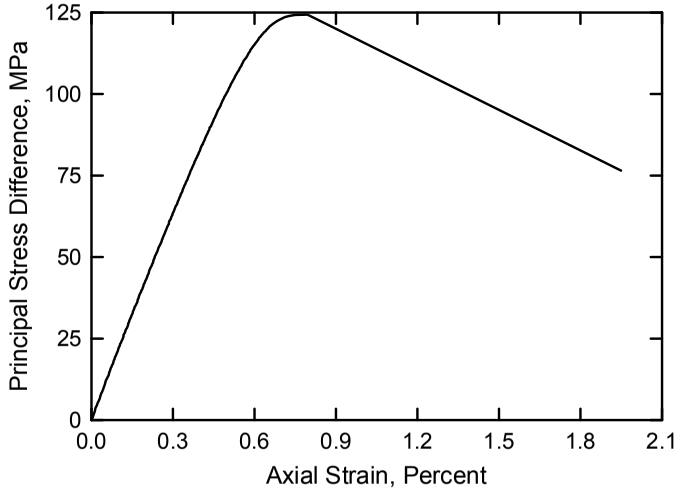

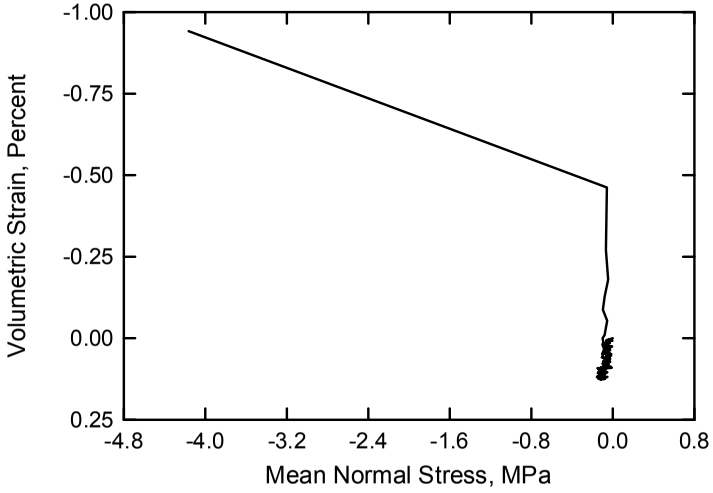

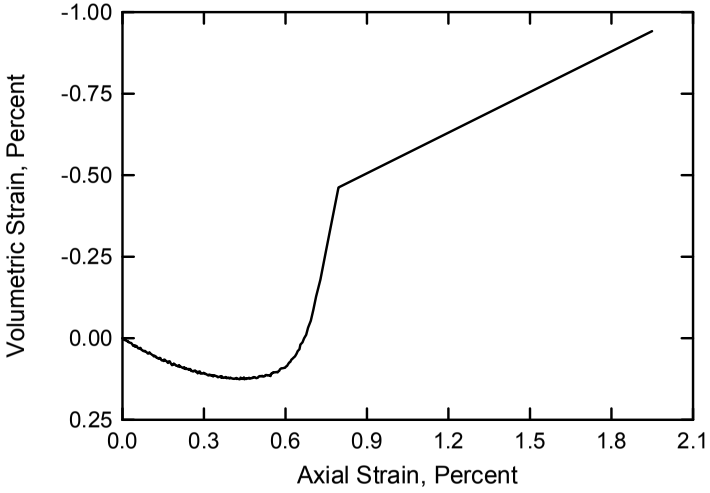

Solid Grade SW Brick
Test No. 41

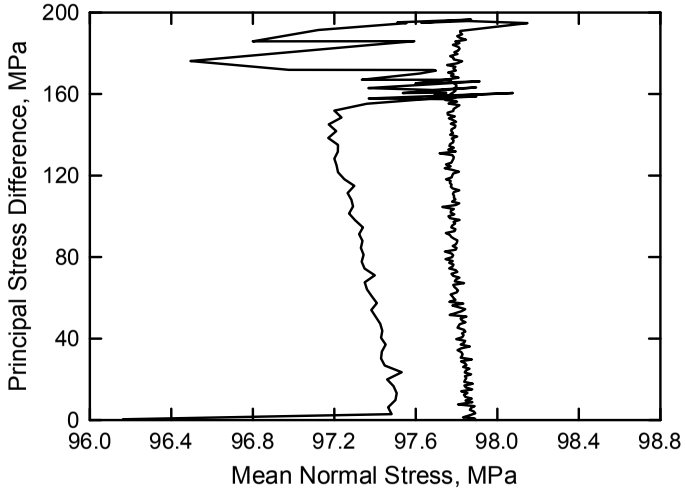

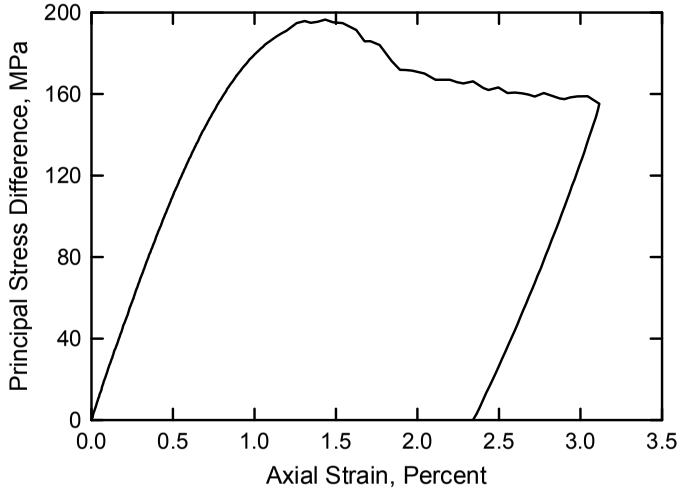

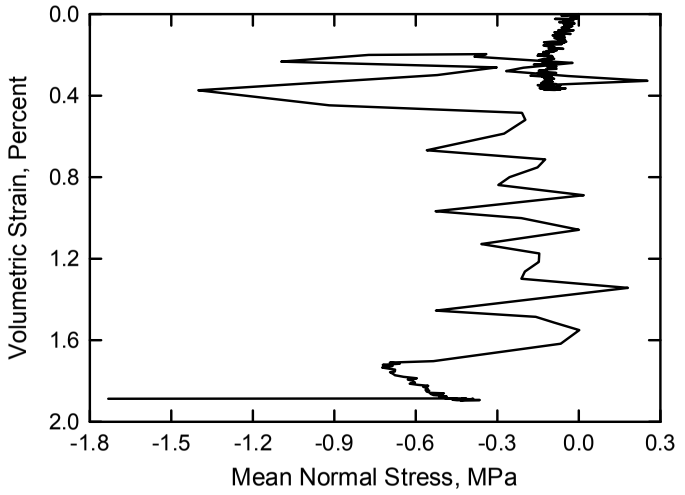

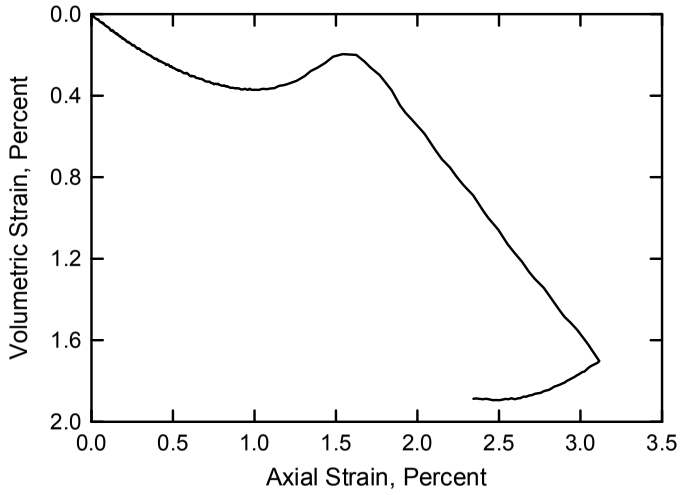

Solid Grade SW Brick
Test No. 07

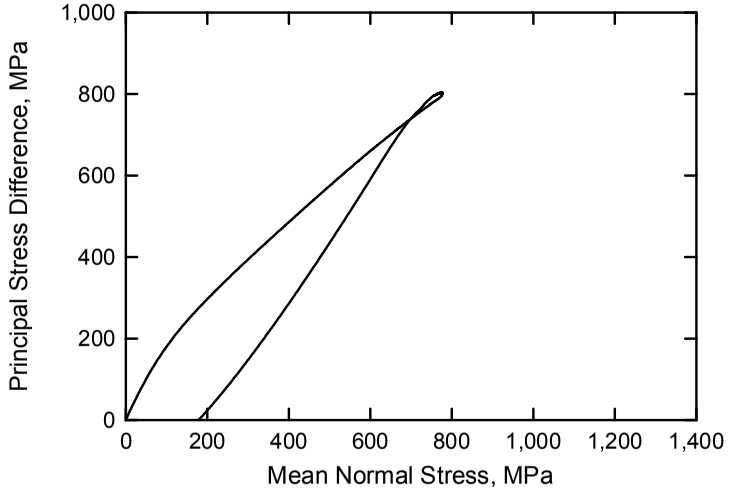

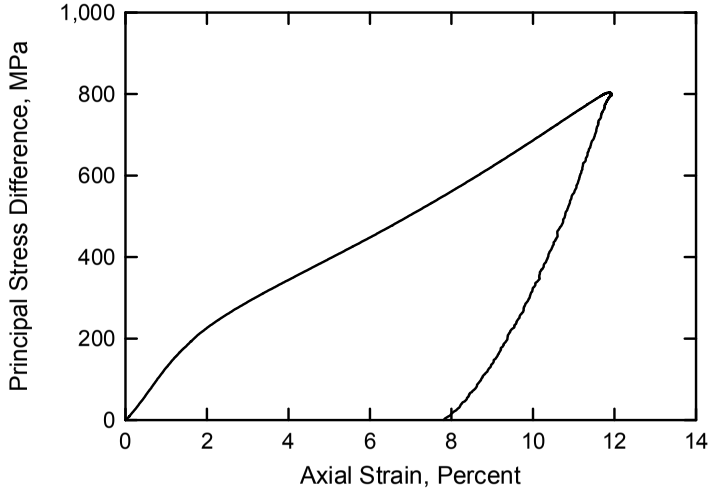

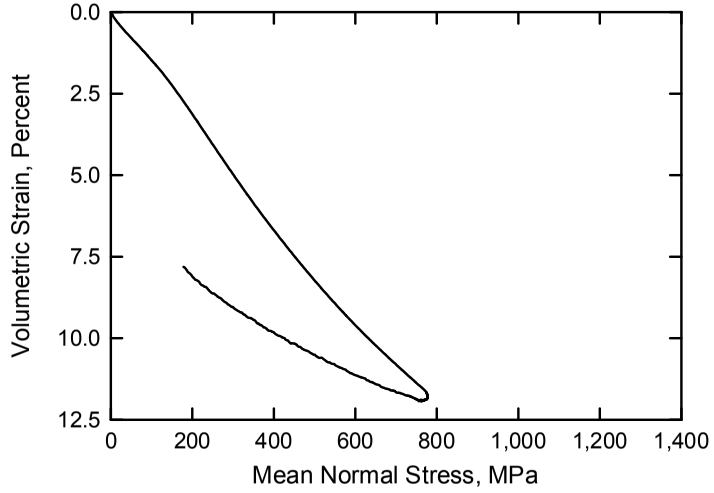

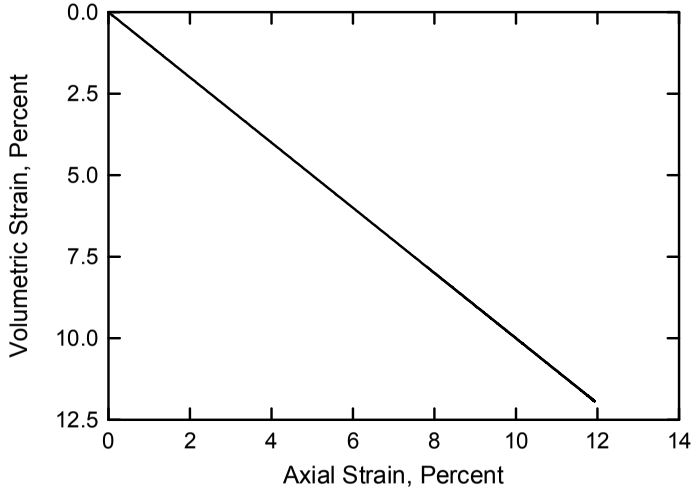

Solid Grade SW Brick
Test No. 08

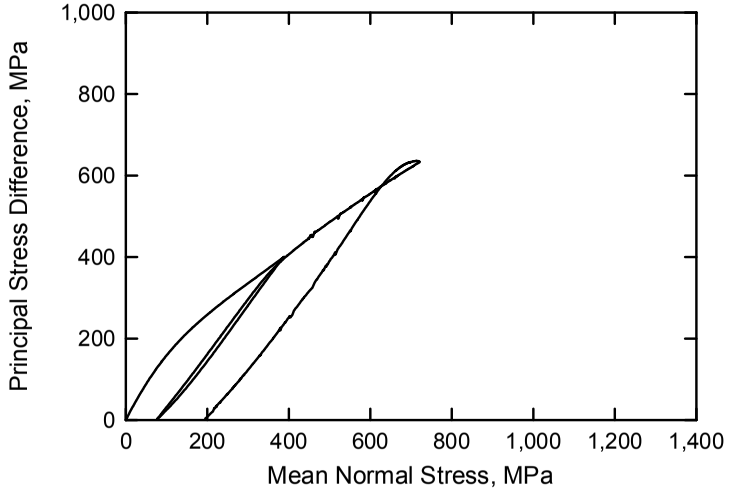

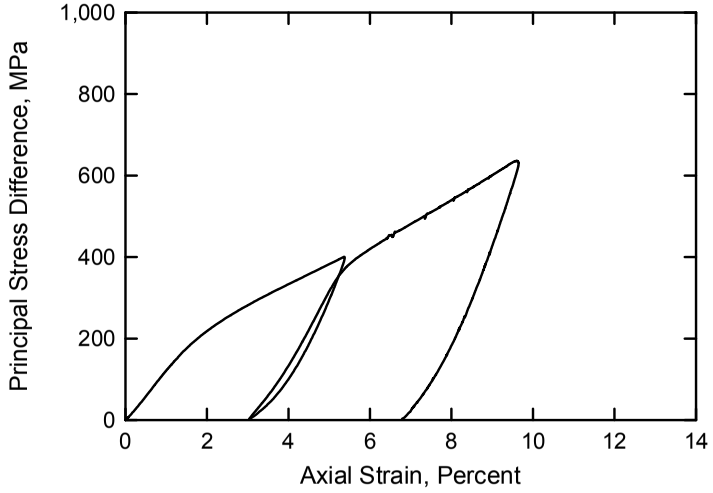

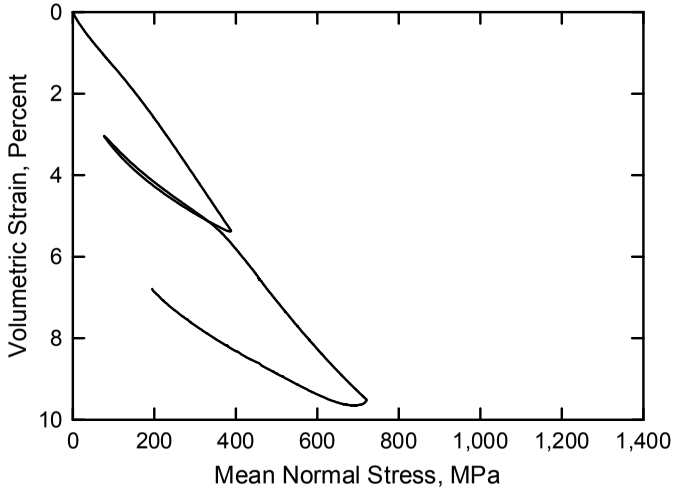

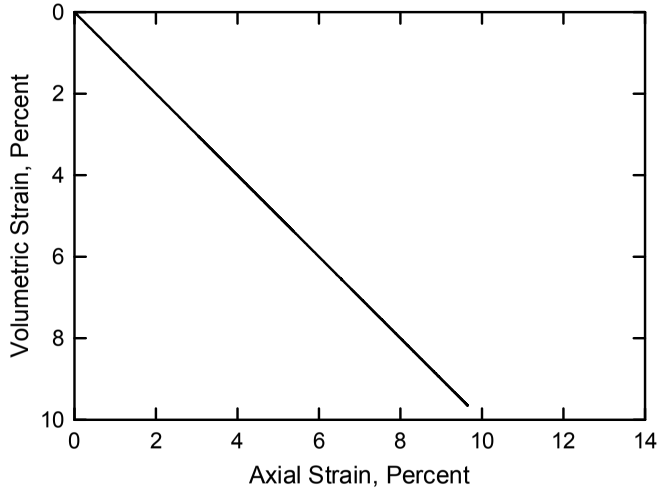

Solid Grade SW Brick
Test No. 23

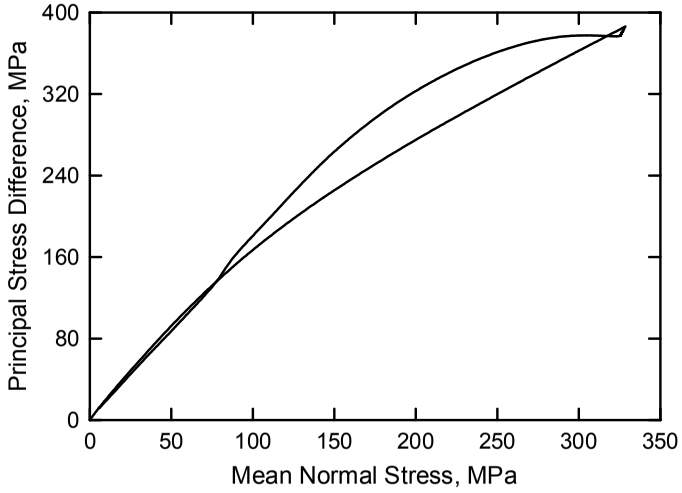

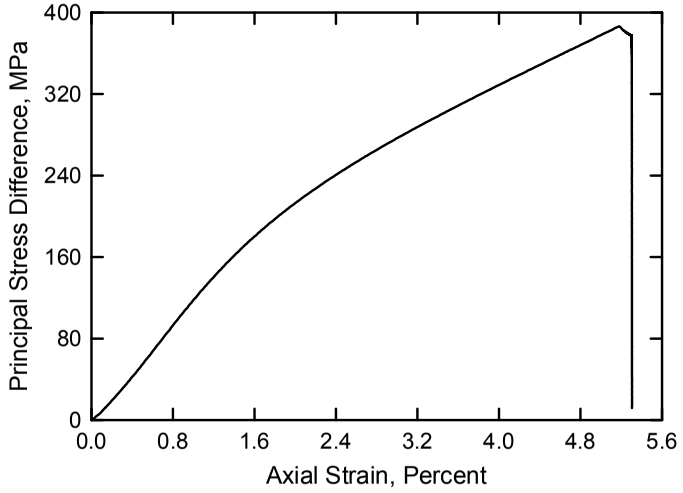

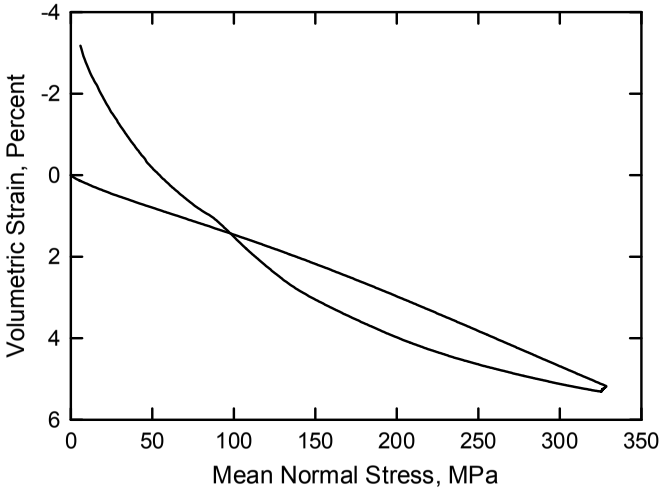

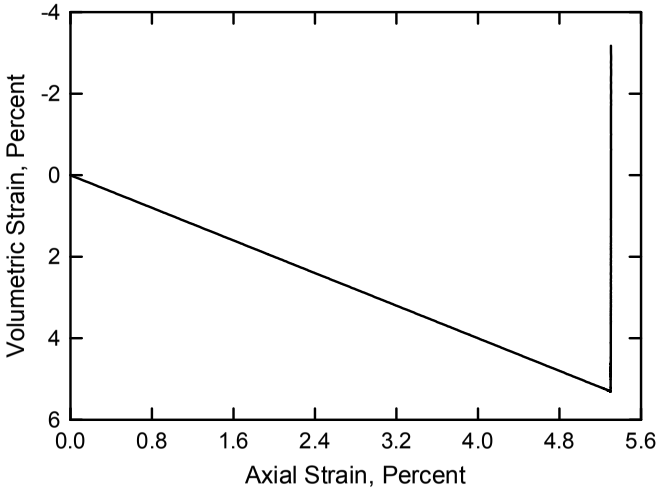

Solid Grade SW Brick
Test No. 24

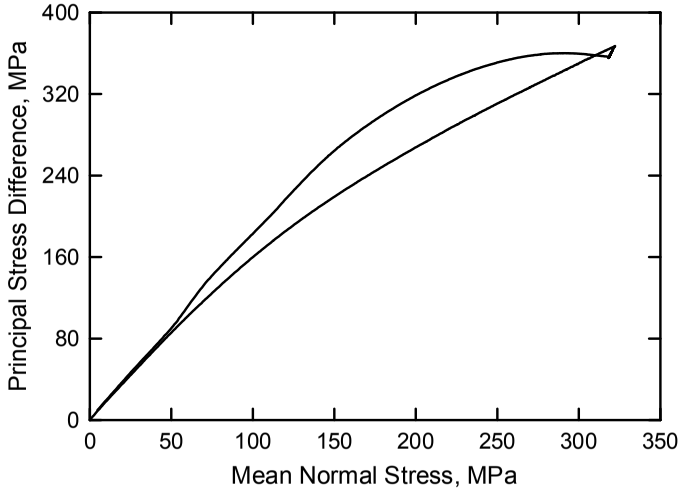

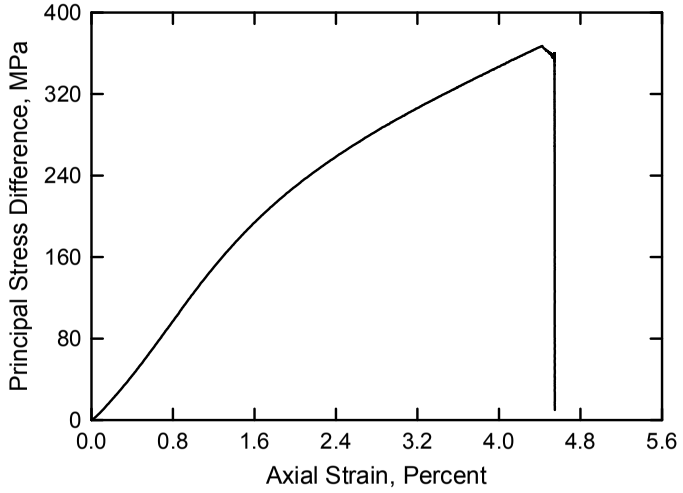

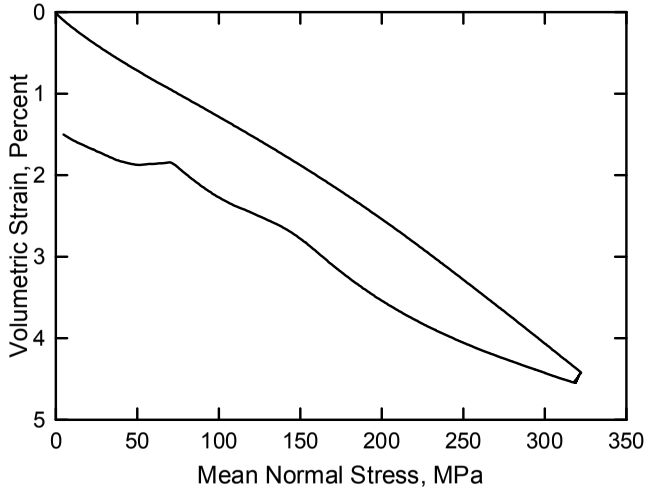

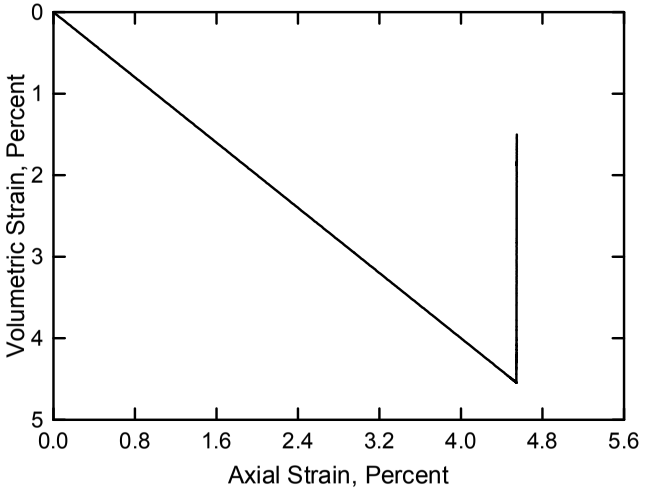

Solid Grade SW Brick
Test No. 25

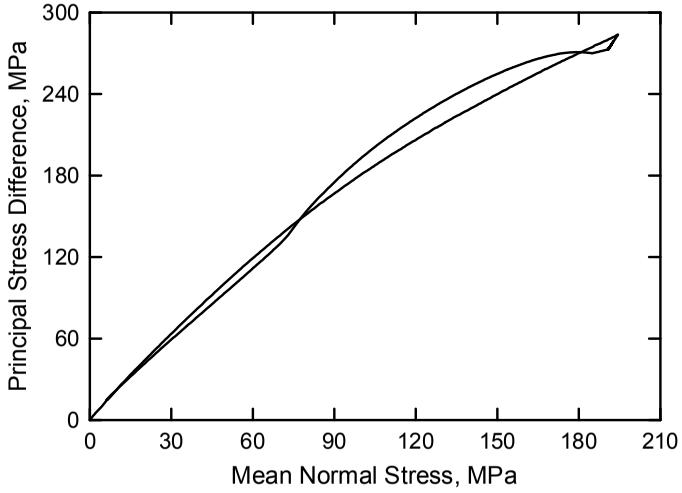

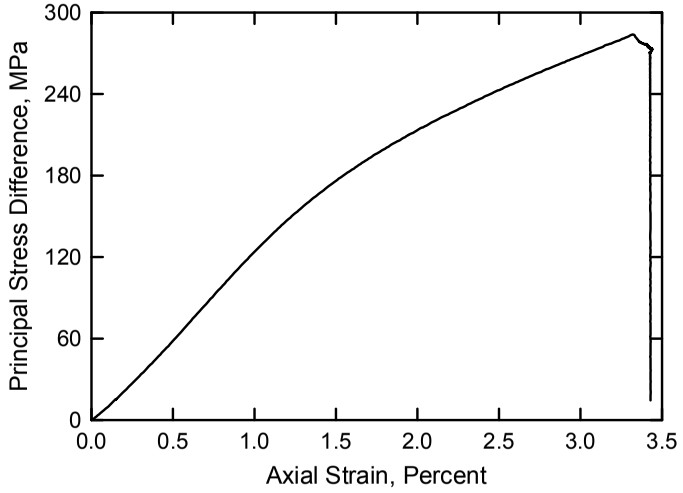

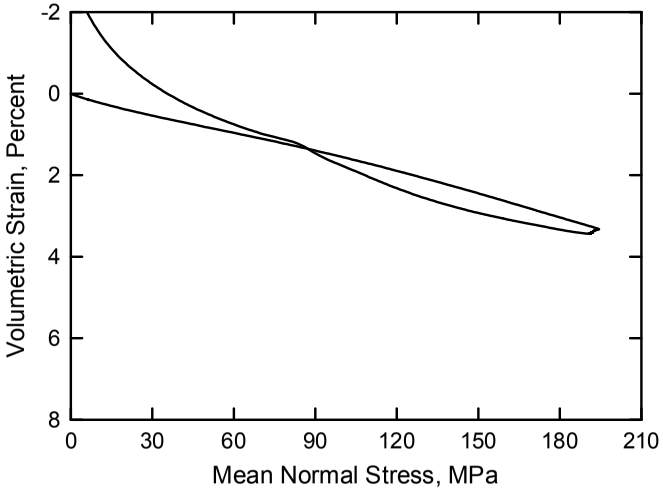

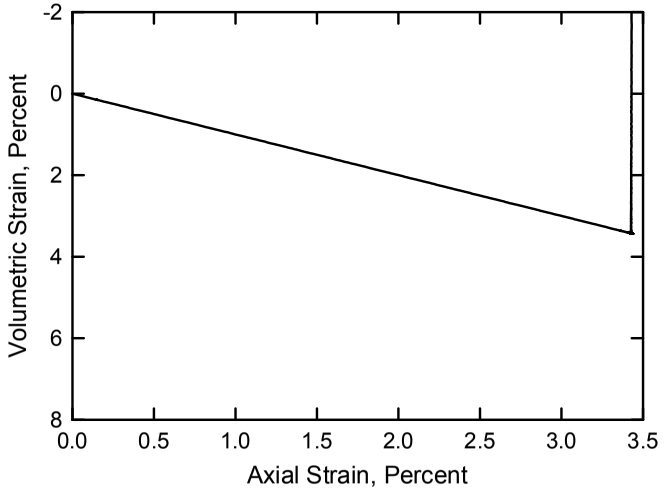

Solid Grade SW Brick
Test No. 26

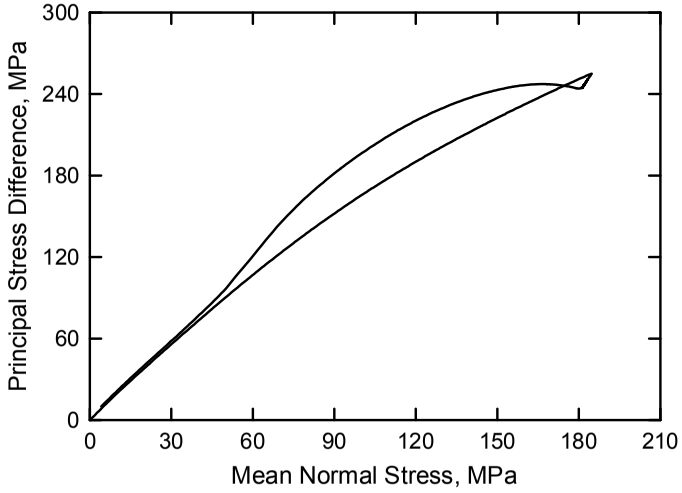

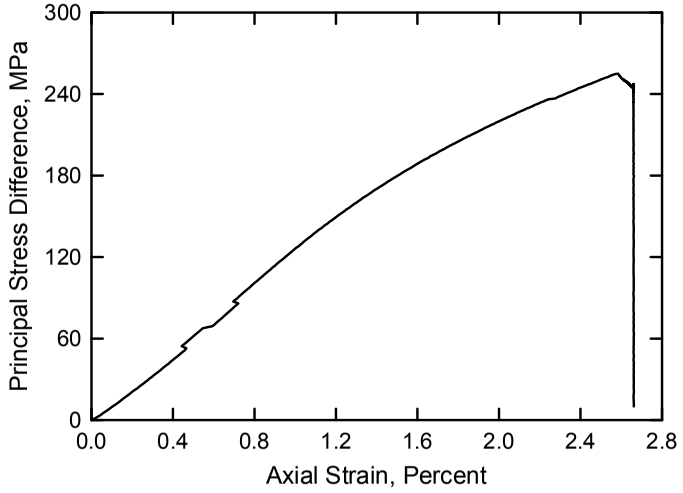

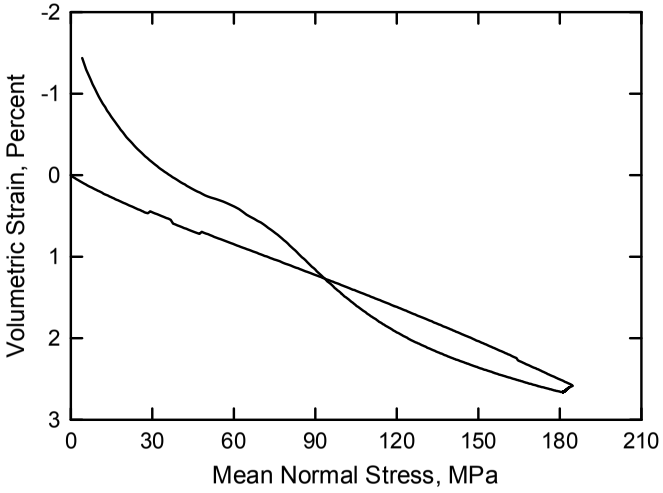

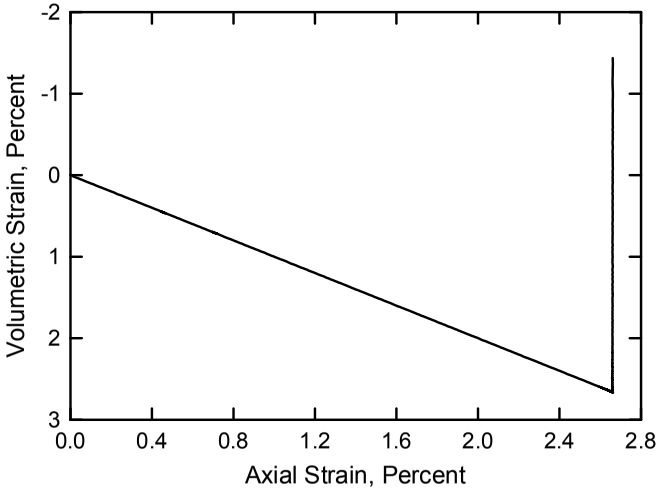

Solid Grade SW Brick
Test No. 27

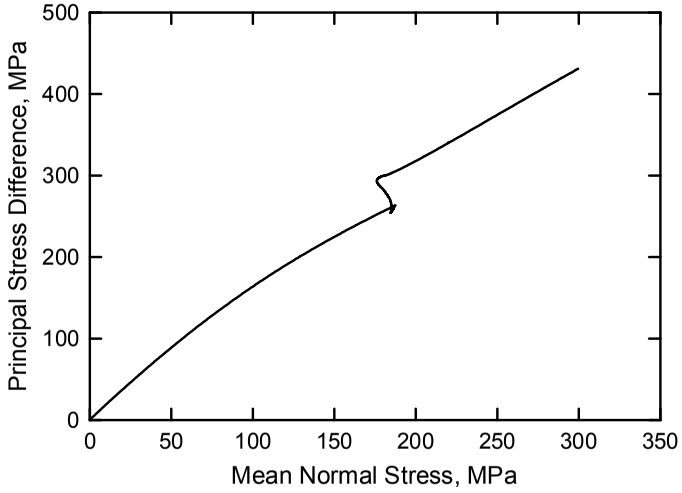

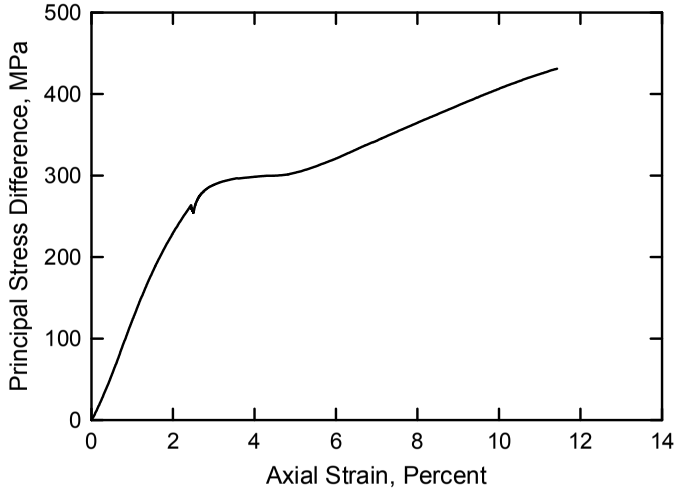

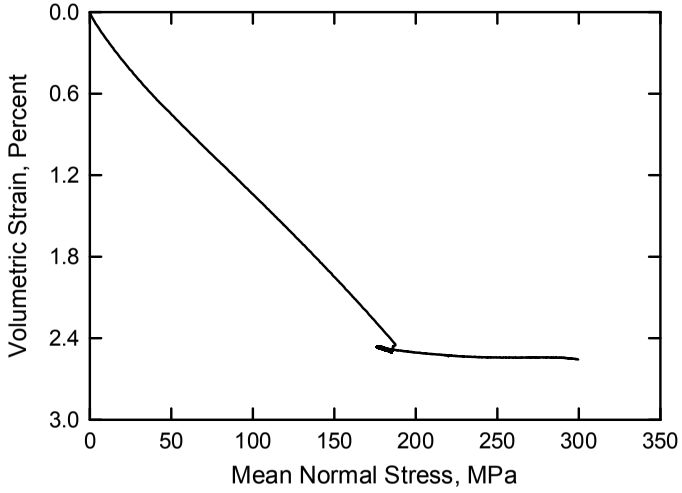

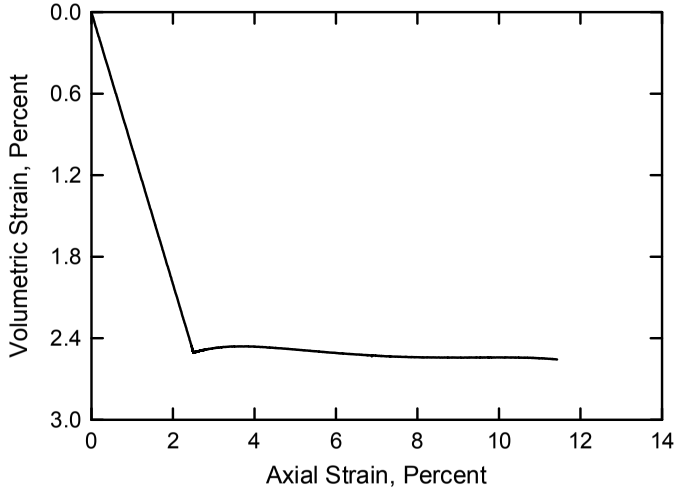

Solid Grade SW Brick
Test No. 28

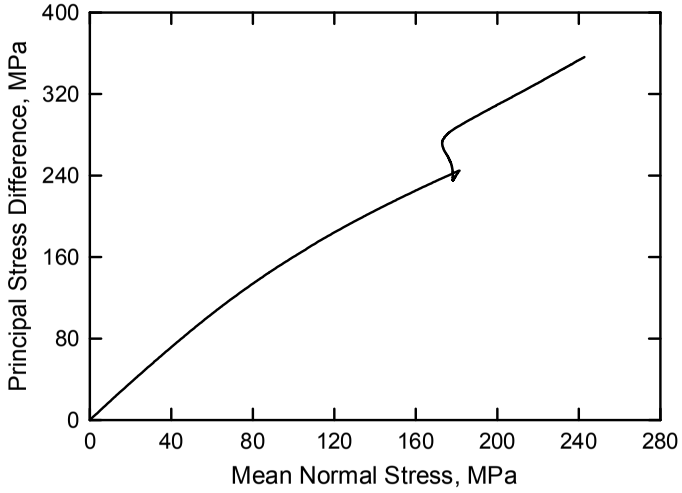

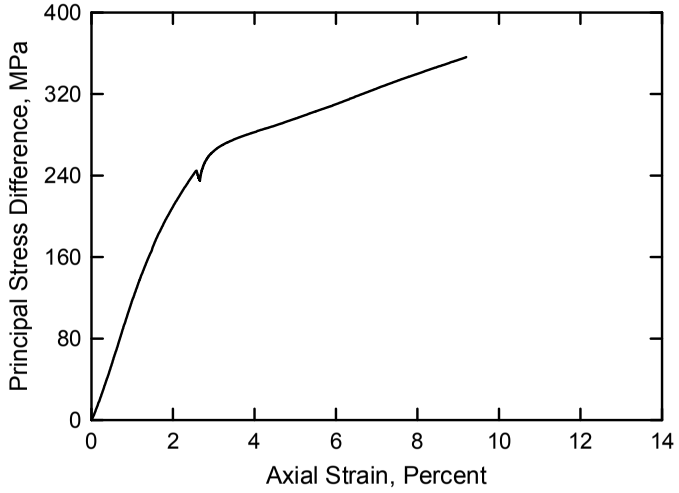

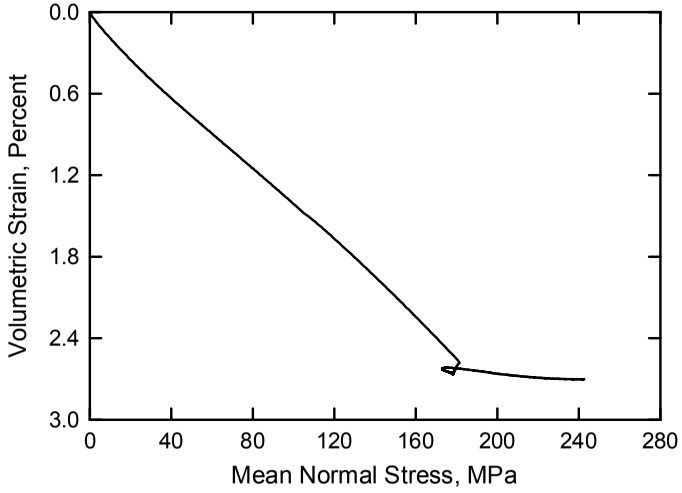

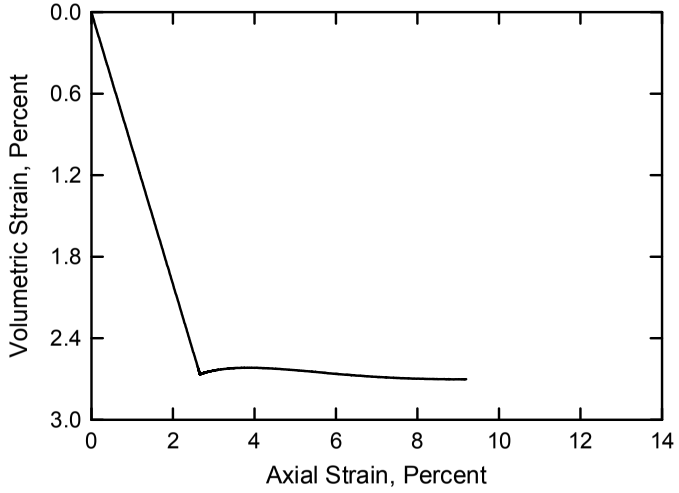

Solid Grade SW Brick
Test No. 29

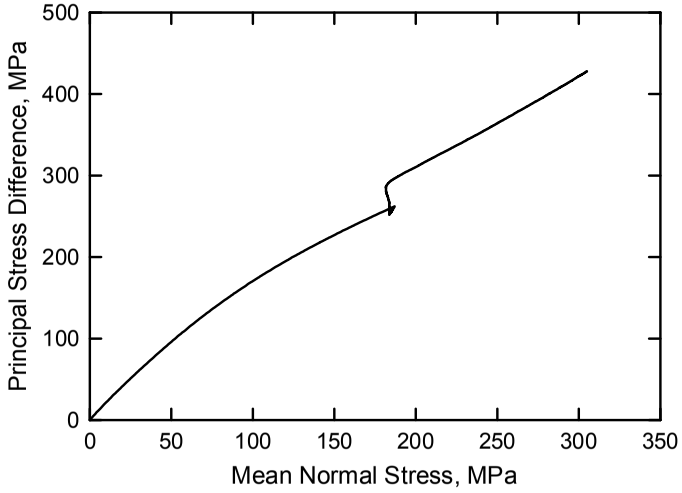

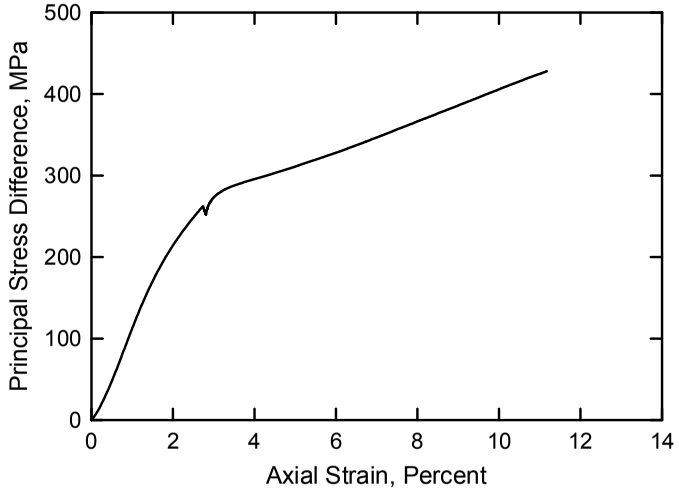

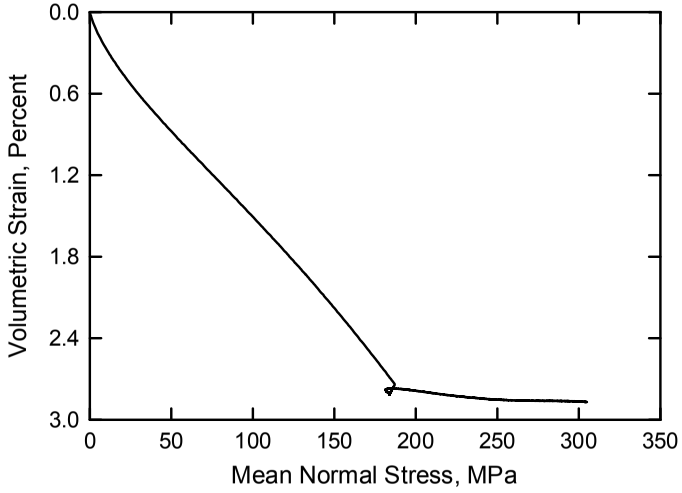

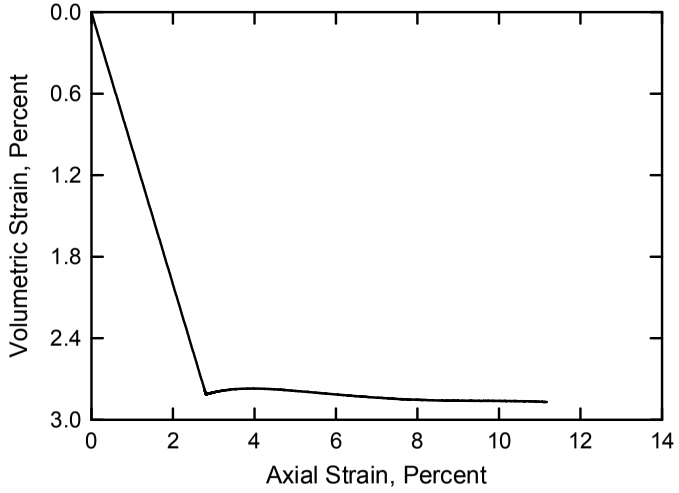

Solid Grade SW Brick
Test No. 31

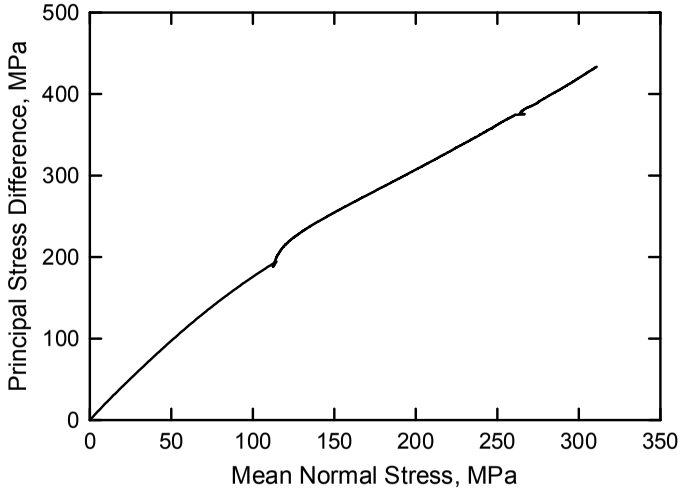

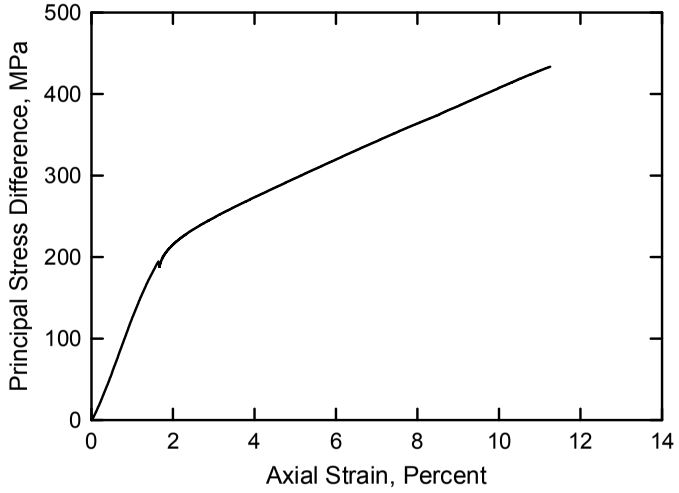

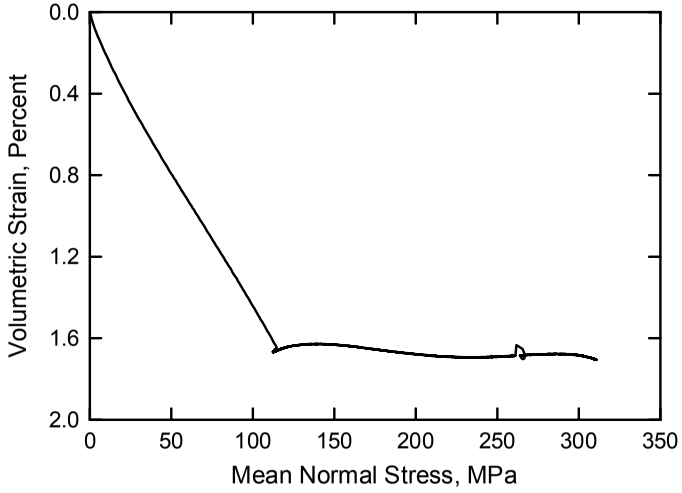

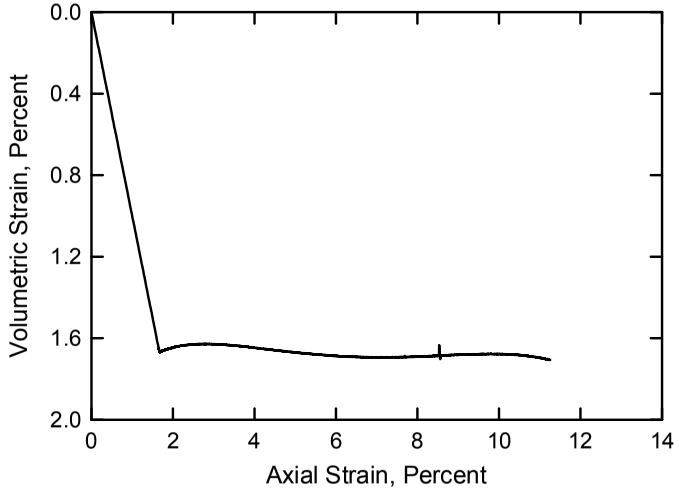

Solid Grade SW Brick
Test No. 32

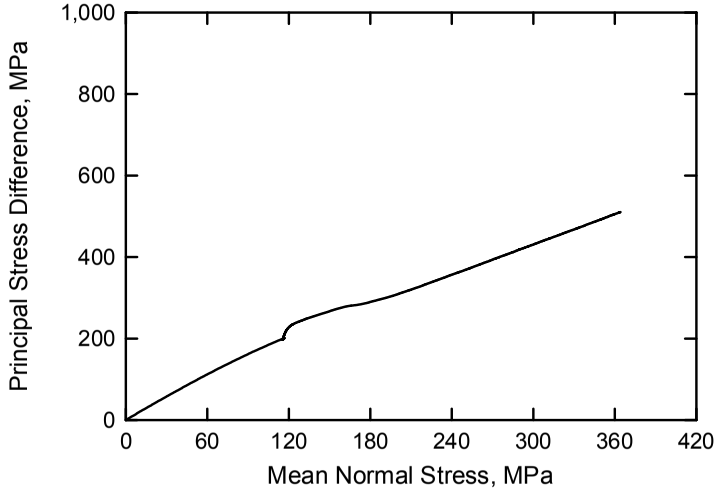

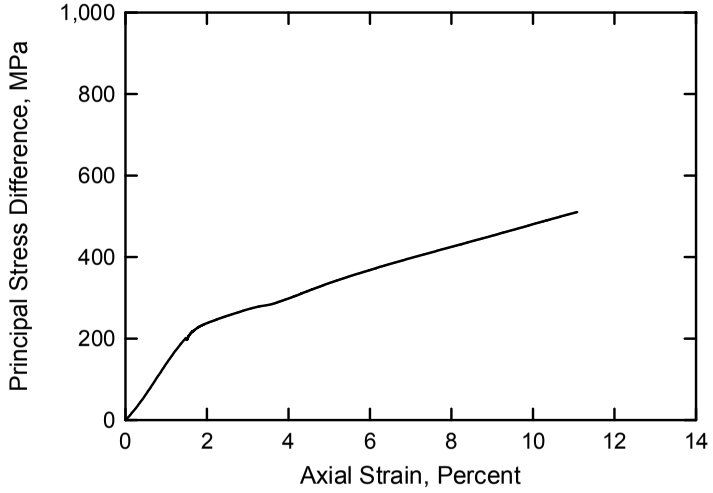

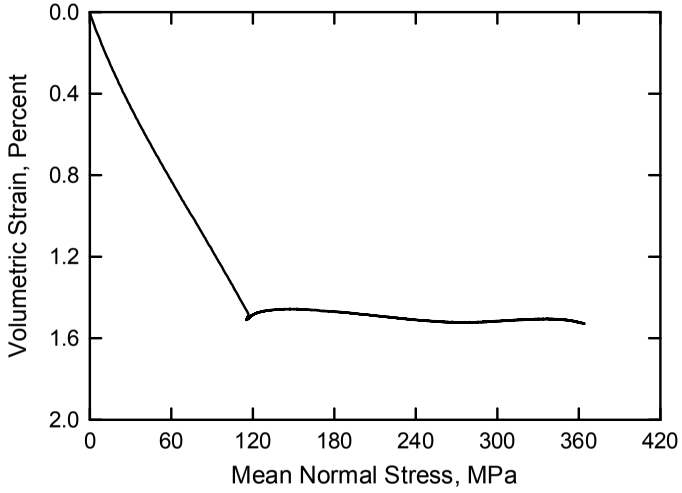

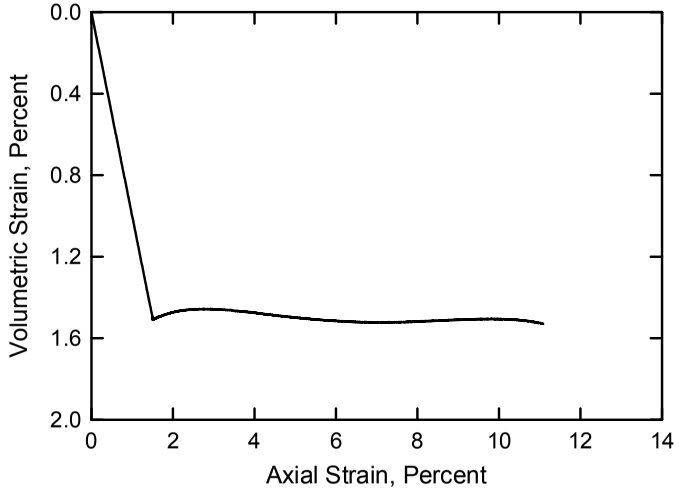

Solid Grade SW Brick
Test No. 33

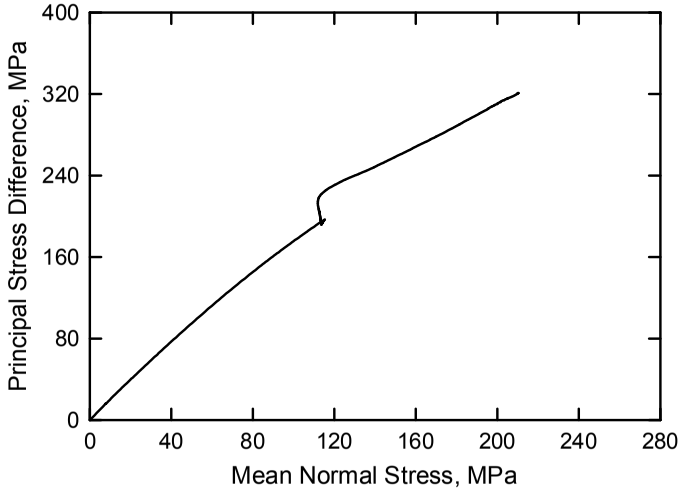

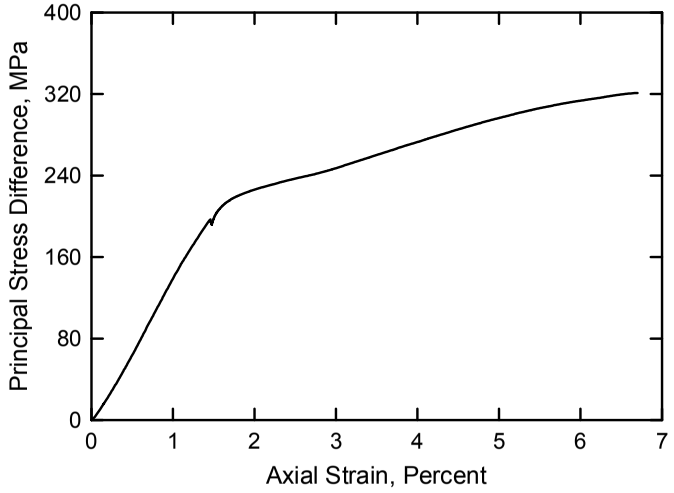

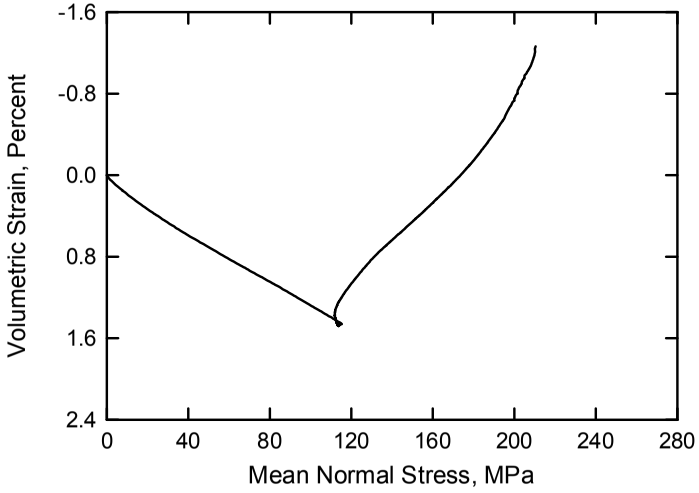

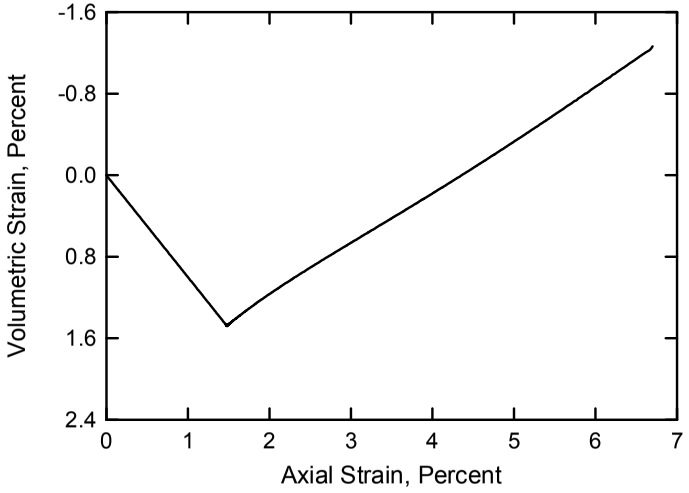

Solid Grade SW Brick
Test No. 34

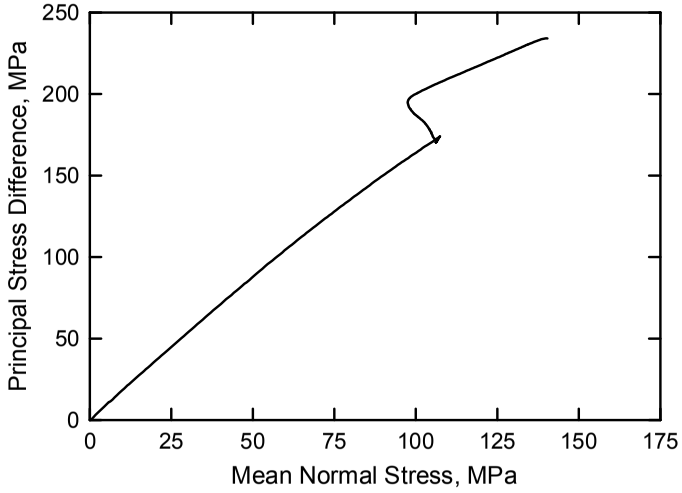

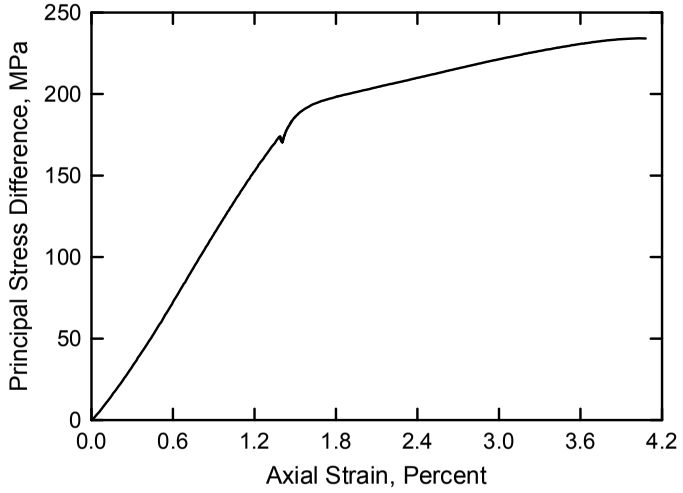

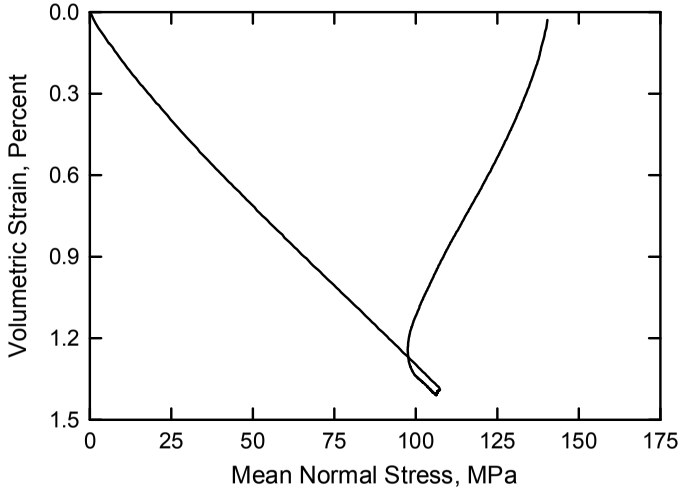

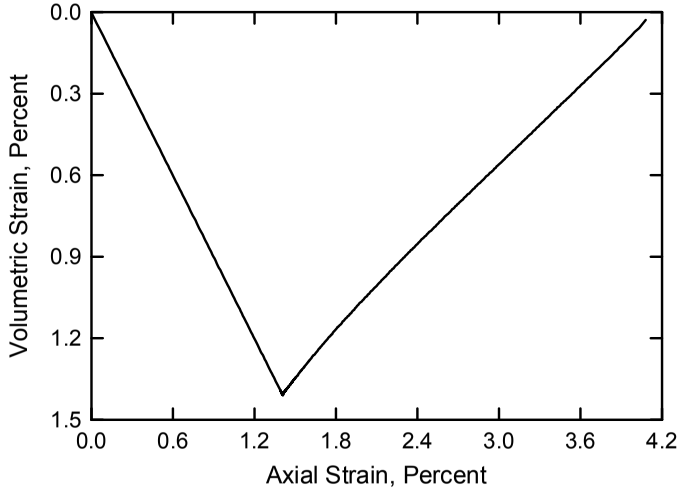

REPORT DOCUMENTATION PAGE

Form Approved
OMB No. 0704-0188

1. REPORT DATE *(DD-MM-YYYY)*	**2. REPORT TYPE**	**3. DATES COVERED** *(From - To)*
August 2007	Final report	

4. TITLE AND SUBTITLE

Laboratory Characterization of Solid Grade SW Brick

5a. CONTRACT NUMBER

5b. GRANT NUMBER

5c. PROGRAM ELEMENT NUMBER

6. AUTHOR(S)

Erin W. Williams, Stephen A. Akers, and Paul A. Reed

5d. PROJECT NUMBER

5e. TASK NUMBER

5f. WORK UNIT NUMBER

7. PERFORMING ORGANIZATION NAME(S) AND ADDRESS(ES)

U.S. Army Engineer Research and Development Center
Geotechnical and Structures Laboratory
3909 Halls Ferry Road
Vicksburg, MS 39180-6199

8. PERFORMING ORGANIZATION REPORT NUMBER

ERDC/GSL TR-07-24

9. SPONSORING / MONITORING AGENCY NAME(S) AND ADDRESS(ES)

Headquarters, U.S. Army Corps of Engineers
Washington, DC 20314-1000

10. SPONSOR/MONITOR'S ACRONYM(S)

11. SPONSOR/MONITOR'S REPORT NUMBER(S)

12. DISTRIBUTION / AVAILABILITY STATEMENT

Approved for public release; distribution is unlimited.

13. SUPPLEMENTARY NOTES

14. ABSTRACT

Personnel of the Geotechnical and Structures Laboratory, U.S. Army Engineer Research and Development Center, conducted a laboratory investigation to characterize the strength and constitutive property behavior of solid Grade SW brick. A total of 37 mechanical property tests were successfully completed, consisting of two hydrostatic compression tests, four unconfined compression (UC) tests, 12 triaxial compression tests (TXC), two constant mean normal stress tests, four direct pull (DP) tests, two uniaxial strain tests, four uniaxial strain load/biaxial strain unload (UX/BX) tests, five uniaxial strain load/constant volume strain loading (UX/CV) tests, and two uniaxial strain load/constant strain path (UX/SP) tests. In addition to the mechanical property tests, nondestructive pulse-velocity measurements were performed on each specimen. Results from the TXC tests exhibited a continuous increase in principal stress difference with increasing confining stress. A compression failure surface was developed from the TXC results at six levels of confining pressure and from the results of the UC tests. The results for the DP tests were used to evaluate the tensile strength of the brick. During UX/BX tests, stress relaxation was evident during the change from uniaxial strain loading to biaxial strain unloading. Good correlations were observed between the stress paths obtained from the UX/BX, UX/CV, and UX/SP strain path tests and the failure surface developed from the TXC tests.

15. SUBJECT TERMS

Brick
Compression tests
Extension tests
Material characterization
Material properties

16. SECURITY CLASSIFICATION OF:			**17. LIMITATION OF ABSTRACT**	**18. NUMBER OF PAGES**	**19a. NAME OF RESPONSIBLE PERSON**
a. REPORT	**b. ABSTRACT**	**c. THIS PAGE**			**19b. TELEPHONE NUMBER** *(include area code)*
UNCLASSIFED	UNCLASSIFED	UNCLASSIFED		88	